UNIVERSITY OF TECHNOLOGY SYDNEY
Faculty of Engineering and Information Technology

Resource Optimization for Communication and Radar Sensing in Vehicular Networks

by

Ping Chu

A Thesis Submitted
in Partial Fulfillment of the
Requirements for the Degree

Doctor of Philosophy

Sydney, Australia

2020

Certificate of Authorship/Originality

I, Ping Chu declare that this thesis, is submitted in fulfilment of the requirements for the award of Doctor of Philosophy, in the School of Electrical and Data Engineering at the University of Technology Sydney.

This thesis is wholly my own work unless otherwise reference or acknowledged. In addition, I certify that all information sources and literature used are indicated in the thesis. This document has not been submitted for qualifications at any other academic institution.

I certify that the work in this thesis has not previously been submitted for a degree nor has it been submitted as part of the requirements for a degree at any other academic institution except as fully acknowledged within the text.

This thesis is the result of a Collaborative Doctoral Research Degree program with Beijing University of Posts and Telecommunications.

This research is supported by the Australian Government Research Training Program.

Production Note:
Signature: Signature removed prior to publication.

Date: 10/09/2020

ABSTRACT

Resource Optimization for Communication and Radar Sensing in Vehicular Networks

by

Ping Chu

With a great increasing volume of vehicles and population, transportation systems are facing many challenges such as congestion, air pollution, crashes and noise. Vehicular communication and radar sensing technology is promising for realizing intelligent, faster, safer transportation. The rapidly increasing amount and mobility of vehicles require frequent resource allocation, which can cause network congestion , large signalling and processing delay. In addition, due to the limited available bandwidth, wide deployment of radar sensors on automotive vehicles can potentially lead to a severe interference problem. Therefore, resource optimization for vehicular communication and automotive radars becomes a key issue in future autonomous vehicular networks, to meet their performance requirements and improve the spectral efficiency.

In this thesis, we investigate the resource optimization algorithm for communication and radar sensing in vehicular networks, addressing the following three issues:

1. The resource allocation and optimization scheme for vehicular communications based on traffic prediction, considering both critical latency requirement and spectral efficiency;

2. The mode selection scheme for vehicle-to-everything (V2X) communications to optimize energy consumption, considering resource reusing between vehicular users and conventional users;

3. The power optimization and interference characterization for automotive radars,

including the modeling of vehicle distribution, the consideration of different types of radars and the assumption of radar antenna directivity.

Regarding the first issue, we propose a novel semi-persistent resource allocation scheme based on a two-tier heterogeneous network architecture including a central macro base station (MBS) and multiple roadside units (RSU). Considering the predictability of vehicular flows, we combine the traffic prediction with this resource allocation scheme. In the proposed semi-persistent scheme, the MBS pre-allocates persistent resources to RSUs based on predicted traffic, and then allocates dynamic resources upon real-time requests from RSUs while vehicles simultaneously communicate using the pre-allocated resources. Based on this scheme, we mainly study two classes of optimization problems: 1) minimizing the relative latency with the constraint of total bandwidth; 2) minimizing the total bandwidth with the constraint of transmission latency. Different algorithms are developed to address the problems.

Towards the second issue, we investigate a two-tier heterogeneous cellular network where the macro tier and small cell tier operate according to a dynamic time-division duplex (TDD). Based on dynamic TDD which can adjust UL and DL time configurations to accommodate to the traffic asymmetry, we propose a vehicular device-to-device (V-D2D) mode selection scheme jointing time allocation, power control to minimize the energy consumption of the vehicles and the whole network. The problem is formulated as a convex optimization problem, and a geometrical interpretation is provided.

For the third issue, we firstly study the mean power of effective echo signals and interference, by considering both front- and side- mounted automotive radars equipped with directional antennas. We employ the stochastic geometry method to characterize the randomness of vehicular location and hence radars in both two-lane and multi-lane scenarios, and derive closed-form expressions for the mean interference by approximating the radiation pattern by Gaussian waveforms. Based on the interference analysis, we aim to minimize the total transmission power of each vehicle with constraints on the required signal to interference and noise ratio. An optimal solution is obtained based on linear programming techniques.

Dedication

To my parents Meizhen Zhu and Guanghe Chu

To my husband, Xuewei Pan

Thank you for your love and support

Acknowledgements

The accomplishment of my PhD thesis is owed to the contributions and support of many people. First of all, I would like to express my deepest thanks to my supervisor Prof. Jian Andrew Zhang for his guidance and support throughout my PhD study years at UTS. I would like to thank Prof. Andrew for his encouragement and mentorship during discussions on doing research and paper writing. His guidance helped me in all the time of research and writing of this thesis. His systematic and accurate understanding of knowledge, creative ideas, and meticulous attitude towards technical details have taught me how to become a good researcher. The experience with Andrew is something that I will always cherish as it has greatly helped me to grow professionally and intellectually. I also want to thank my co-supervisor Dr. Gengfa Fang for his wonderful support and valuable advice for my research. From them, I have learned to be patient and dedicated to the work, which will undoubtedly influence my life.

I would like to thank my supervisor Prof. Xiaoxiang Wang from Beijing University of Posts and Telecommunications (BUPT) for her guidance in my early graduate years, from whom I have learned how to think rigorously and how to solve research problems. I would like to thank her for giving me the opportunity to do research. My skills to grab the crucial part of knowledge, basic logic of learning, and the way of thinking, have been deeply influenced by her. Her guidance and help always make me feel very comfortable and I have never felt that I was being pushed or forced during my Ph.D. study. She is also a generous superior and I will cherish and remember all her encouragement and support, with great appreciation.

I would like to thank all of my UTS and BUPT colleagues including Dongyu Wang, Zijia Huang, Wenrong Gong, Xianan Wang, Mingming Li, Yanyan Qi, Yingping Feng, Wei Wang, Yufang Zhang, Yibo Zhang, Yanwen Lan, Yuyue Luo,

Weiwei Zhou, Bai Yan, Xin Yuan, Md Lushanur Rahman, Lang Chen, Pengfei Cui, Chuan Qin, Zhenguo Shi, Qingqing Cheng, Qianwen Ye, and all the other friendly lab mates. It is always enjoyable to work with them.

I am also thankful for my incredibly supportive friends, including Ying Hu, Sixuan Chen, Yuanyuan Yao, Yi Zhong, Fangfang Yin, Yanbin Zhang, Kesen He, Delong Su and many other lovely companions. They have brought me a lot of encouragement, comfort, and happiness during my doctoral study. I feel so lucky to have friends like them in my life.

Finally, but most importantly, I would like to express my deepest gratitude to my parents Meizhen Zhu and Guanghe Chu for their unconditional love and confidence. They are my solid backing and never give me restrictions about my decisions. During my Ph.D study, I encountered many difficulties in my study and life. My parents have always encouraged me and made me feel very safe. In addition, I would like to express my gratitude to my beloved husband Xuewei Pan. He always stayed with me in my toughest times during the writing of this thesis and gave me encouragement. I am very grateful for the beautiful memories he brought me. I feel extremely fortunate to have him in my life.

List of Publications

0.1 Publications Related to This Thesis

Journal Papers

J-1. **P. Chu**, J. Andrew Zhang, X. Wang, Z. Fei, G. Fang and D. Wang, "Interference Characterization and Power Optimization for Automotive Radar with Directional Antenna," in *IEEE Trans. Veh. Technol.*, vol. 69, no. 4, pp. 3703-3716, 2020.

J-2. **P. Chu**, J. A. Zhang, X. Wang, G. Fang and D. Wang "Semi-Persistent Resource Allocation Based on Traffic Prediction for Vehicular Communications," in *IEEE Trans. Intell. Veh.*, vol. 5, no. 2, pp. 345-355, 2020.

Conference Papers

C-1. **P. Chu**, J. A. Zhang, X. Wang, G. Fang and D. Wang, "Semi-Persistent V2X Resource Allocation with Traffic Prediction in Two-Tier Cellular Networks," *in Proc. IEEE 89th Veh. Technol. Conf (VTC 2019-Spring)*, pp. 1-6, 28 April-1 May, 2019.

C-2. **P. Chu**, X. Wang, D. Wang and L. Yu, "A D2D Mode Selection Scheme with Energy Consumption Minimization Underlaying Two-tier Heterogeneous Cellular Networks," *in Proc. 28th Annu. Int. Symp. Pers., Indoor, Mobile Radio Commun. (PIMRC 2017)*, pp. 1-5, 8-13 Oct., 2017.

Contents

List of Figures

Abbreviation

3GPP - 3rd Generation Partnership Project

AWGN - Additive White Gaussian Noise

ANN - Artificial Neural Networks

ARIMA - Auto-Regressive-Integrated-Moving-Average

BS -Base Station

CDF - Cumulative Distribution Function

CRLB-Cramér-Rao Lower Bound

CSI - Channel State Information

CUEs -Cellular Users

D2D - Device-to-device

DS - Dynamic Resource Allocation Scheme

DSRC - Dedicated Short Range Communication

FMCW - Frequency Modulated Continuous Wave

FoVs - Field of Views

FR - Front-mounted Radar

ITS - Intelligent Transportation System

JCRS - Joint Communication and Radar Sensing

KKT - Karush-Kuhn-Tucker

kNN - k-Nearest Neighbour

LMMSE - Least Minimum Mean Square Error

LP - Linear Programming

LRR - Long Range Radar

LTE - Long-Term Evolution

LTE-V - Long-Term Evolution-Vehicle

MAPE - Mean Absolute Percent Error

MBS - Macro Base Station

MNAE - Mean Normalized Approximation Error

MIMO - Multi input multi output

MRR - Medium Range Radar

PPP - Poisson Point Process

PS - Persistent Resource Allocation Scheme

QoS - Quality-of-Service

RCS - Cross-Section Area

RSU - Roadside Unit

SINR - Signal-to-Interference-plus-Noise Ratio

SIR - signal-to-Interference Ratio

SNR - Signal-to-Noise Ratio

SPS - Semi-Persistent Resource Allocation Scheme

SR - Side-mounted Radar

SRR - Short Range Radar

TDD - Time Division Duplex

ULA - Uniform Linear Array

V2V - Vehicle-to-vehicle

V2I - Vehicle-to-everything

V2P - Vehicle-to-pedestrian

V2X - Vehicle-to-everything

V-D2D -Vehicular Device-to-device

VUEs -Vehicular Users

Nomenclature and Notation

Bold lower-case letters denote column vectors.

Bold Capital letters denote matrices.

$(\cdot)^{\dagger}$ denotes pseudo-inverse of a matrix.

$\overline{x}$ denotes the mean of x.

$\|\mathbf{x}\|$ denotes the norm of the vector $\mathbf{x}$.

$\mathbb{E}[\mathbf{x}]$ denotes the expectation of $\mathbf{x}$.

Chapter 1

Introduction

1.1 Research Background

With an increasing volume of vehicles over the past decades, traffic accidents and congestion have become important transport issues all around the world. Therefore, the concerns on improving roadway safety and relieving traffic congestion have been growing. Vehicular network is an enabling technology for realizing intelligent, faster, safer transportation [1, 2]. Future autonomous vehicular networks will be equipped with high-quality wireless services, which incorporate high-data-rate communications technology with intelligent vehicles and high-resolution radar sensing capabilities. Firstly, vehicles can exchange different kinds of information with roadside infrastructure or other vehicles with the assistance of wireless communication technology. In addition, automotive radar also is an essential configuration in smart transportation systems, which play a key role in estimating the position, speed, and feature signal of objects, activities, and events.

There are two main categories of services for vehicular communication, namely non-safety and safety services [3]. Targeting at decreasing traffic accidents, safety service has more stringent requirements on delay and reliability. System latency includes both signal transmission time and the delay caused by the associated signalling process, e.g., resource request and allocation. Therefore, resource management for vehicular communications based on its stringent requirements is an important and challenging problem. Device-to-device (D2D) communication has been widely recognized as a key component in 5G mobile networks from academia

and industry [4,5]. The use of D2D communication underlaying cellular network can significantly improve both spectrum and energy efficiency, coverage extension, and can decrease the delay and energy consumption. Moreover, using D2D communication also extends the battery lifetime of mobile terminals by facilitating the physical proximity of devices. D2D is an enabler for vehicular communication to meet its stringent reliability and latency requirements [6, 7]. There are different modes for vehicular communication in cellular networks, an efficient mode selection scheme is necessary to operate vehicular device-to-device (V-D2D) communication and optimize resources. The vehicles in the same cell within the possible range for direct communication have an opportunity to select the V-D2D mode. How to operate mode selection and optimize the resources for V-D2D is a challenge.

For automotive radar sensing, the main challenge also lies in the resource management. In the last few years, automotive radar systems have become common on the high-end vehicles and are now being installed on more electronic models, too. In the near future, we will see wide deployment and usage of automotive radar on the road. However, the increasing usage of automotive radar sensors potentially leads to increasing occurrence of radar-to-radar interference. The reception of unwanted signals from other automotive radar sensors is usually called mutual interference between automotive radar sensors [8]. Such interference happens when the sensors use the same frequency channel and are within the range of their respective coverage. The reception of interference signals can lead to problems such as ghost targets or a reduced signal-to-noise power ratio (SNR). Therefore, resource optimization is necessary to meet the performance requirements for automotive radar sensors with interference.

In this dissertation, we comprehensively investigate and develop the resource optimization for communication and radar sensing in vehicular networks, addressing the problems discussed above. Note that, in this dissertation, we study the resource

optimization for vehicular communication and automotive radar sensing separately to pave the way for future research on joint communication and radar sensing (JCRS) technology in autonomous vehicular networks.

1.2 Motivation and Objectives

1.2.1 Critical Delay and Reliability of Vehicular Communications

As a component of the intelligent transportation system (ITS), vehicular communication has attracted research attention from both academia and industry [9,10]. There are two main solutions to enable vehicular communications, i.e., IEEE 802.11p protocol dedicated short-range communication (DSRC) and cellular network standards. The IEEE 802.11p protocol is designed for vehicular communications based on dedicated infrastructure and licensed transmission bands. However, recent study [11] has revealed several inherent issues of the 802.11p-based technologies, including scalability, potentially unbounded channel access delay, lack of quality-of-service (QoS) guarantees. In addition, it is hard to know the communication status of neighboring vehicles due to the lack of a centralized control node [12].

Cellular networks provide an off-the-shelf potential solution for vehicular communications, which can make use of a high-capacity, large-cell-coverage-range, and widely deployed infrastructure. Vehicular communications have stringent requirements on delay and reliability considering safety service. However, current studies about resource management did not consider the limitations: (1) the existing resource management schemes in V-D2D communication rarely take the signalling latency into consideration when doing the latency analysis; (2) growing vehicular communications will greatly increase cellular load, which will cause signalling congestion and larger latency. Underlaying cellular network, we introduce a two-tier system framework to solve the potential network congestion problem and reduce the signalling delay.

1.2.2 Limited Resources for Vehicular Networks and Predictability of Traffic Flow

Dense vehicles and their high mobility require frequent and heavy resource allocation. For vehicular communication underlaying cellular networks, frequency resources are limited since they also need to be used by traditional cellular users. Considering the limited frequency resources, the most crucial problem needing to be solved is how to effectively allocate and use the resources based on different objectives (e.g., sum throughput capacity, latency, total rate). Therefore, resource optimization algorithms for improving resource efficiency are necessary and significant. In addition, vehicle flow is regular and predictable. It also denotes resource requirement for vehicular communications. Higher accuracy prediction for short-term traffic flow is an efficient way for resource management to improve resource efficiency. We conduct studies of a resource allocation scheme for vehicular communication combining traffic predictions.

Conventionally, radar sensing systems are often designed at mmWave or even higher frequency bands. Nowadays, both academia and industry have shown strong interest in mmWave wireless communications owing to the appealing features such as the very wide bandwidth and hence high communication capacity. This can further increase the congestion of the mmWave spectrum and also lead to the increasing occurrence of radar-to-radar interference. Based on a basal road system model, we introduce stochastic geometry methods to construct the system model and conduct studies of radar interference and resource optimization.

1.2.3 Green Transportation Systems

In conventional cellular networks, communication requests of all the vehicles have to be served by the base station (BS), which does not only put a heavy burden on the delay and capacity-constrained backhaul links, but it is also energy inefficient.

Aiming to reduce CO_2 emissions from vehicles and save non-renewable energy, a sustainable and green transportation system is therefore of crucial importance [13]. V-D2D communication can be applied to achieve very considerable energy efficiency and latency improvement by efficient data offloading via either single-hop or multi-hop transmissions. Underlaying the conventional cellular networks, we conduct studies of mode selection for V-D2D communication toward the goal of improving energy efficiency.

1.3 Approach and Contribution

In this dissertation, we first study the resource allocation scheme with traffic prediction for vehicular communications. We mainly propose a novel semi-persistent resource allocation scheme on top of a two-tier heterogeneous network for vehicular communications. The scheme can improve bandwidth efficiency, avoid network congestion, and reduce the processing latency significantly. We propose a simple and effective method for predicting the short-term traffic flow by considering the correlation window in both time and spatial domains according to the vehicle moving speed. Based on the total available bandwidth and the predicted resource needs mapped from the predicted vehicle traffic, an improved water-filling algorithm is proposed to optimally allocate the resource. By combining pre-allocation of persistent resource and dynamic resource allocation in real time, significant delay linked to resource allocation can be reduced, with negligible degradation on spectrum efficiency. The proposed semi-persistent scheme over the two-tier cellular architecture is effective and promising for vehicular communications. In addition, we also formulate another optimization problem based on this system framework, which shows significant improvement for the performance evaluation.

We then investigate the mode selection of V-D2D communications. We study the optimal mode selection with energy consumption minimization for V-D2D communi-

cation underlaying a two-tier heterogeneous cellular network considering a dynamic time-division duplex (TDD) scheme. In particular, we have discussed the problem with two optimal objectives: minimizing the energy cost of the overall network and the vehicular energy only. The analysis results show that V-D2D communication is preferable and energy-efficient in a large portion of the macro cell and small cell in some cases.

In the last part of our work, we study the interference characterization method and power optimization for automotive radar. We introduce a stochastic geometry method to model the location and density of vehicles and hence automotive radars. We consider both front- and side-mounted radars with directional antennas, and develop a framework for analytically calculating the mean interference power seen by each radar. Approximating the antenna radiation pattern with a Gaussian function, we derive closed-form expressions for the mean interference power. Based on the interference analysis, we then formulate the cost function for minimizing the total transmission power of radars on each vehicle. Our results provide important guidance for developing ad-hoc automotive radar networks and optimizing their frequency resource access and allocation.

1.4 Thesis Organization

This thesis is organized as follows:

- *Chapter 2*: As a literature review chapter, this chapter firstly presents a survey of vehicular networks, including vehicular communication networks and automotive radar sensing networks. Next, resource optimization for both vehicular communication and radar sensing is also reviewed.

- *Chapter 3*: In this chapter, based on the two-tier heterogeneous cellular networks, we propose a semi-persistent resource allocation scheme, which aims

to offload centralized traffic and support low-latency communications. Based on the system framework, a classical algorithm and an improved traffic prediction method are introduced for persistent resource allocation in advance. Next, with the formulation of different optimization problem, an improved water-filling algorithm and corresponding solution are proposed for dynamic resource allocation.

- *Chapter 4*: This chapter demonstrates a mode selection scheme for V-D2D communications with energy consumption minimization underlaying two-tier heterogeneous cellular networks. The formulation problem with two objectives are discussed and a geometrical interpretation of energy-optimal mode selection is given.

- *Chapter 5*: In this chapter, we develop a signal and interference power analysis framework for automotive radar, by applying the stochastic geometry model. First, we formulate the vehicular location distribution and derive the expressions for the mean power of the interference. Next, we investigate how to minimize the total transmission power while guaranteeing an average signal-to-interference-and-noise ratio (SINR) for radar sensing. Simulation results and performance analysis are also provided in this chapter.

- *Chapter 6*: A brief summary of the contents and contributions of this thesis is given in this chapter. Possible research directions for future work are also discussed.

Chapter 2

Literature Review

This chapter is devoted to reviewing works which is related to this thesis, including studies on cellular-based vehicular networks, automotive radar sensing, resource optimization for vehicular communications, prediction for vehicular traffic flow and resource management for automotive radars.

2.1 Communication and Radar Sensing in Vehicular Networks

Next-generation autonomous vehicular networks include not only automotive radar sensing but also vehicular communications. Vehicle-to-everything (V2X) communications, including vehicle-to-vehicle (V2V), vehicle-to-pedestrian (V2P), vehicle-to-infrastructure (V2I), and vehicle-to-network (V2N) communications has been defined by the 3rd Generation Partnership Project (3GPP) group [14]. A typical vehicular network in the urban environment is shown in Fig. 2.1. V2X communications technology together with existing automotive radar sensing capabilities in the modern smart vehicles have a great potential for enabling a variety of applications for optimizing traffic congestion, improving road safety, providing driver infotainment and manufacturer services. Examples of such advanced applications include road hazard warning, cooperative collision alert , point-of-interest notification, in-vehicle Internet access and remote vehicle diagnostics [15, 16]. Extensive work in the literature investigated the performance of vehicular communications, measured for example by routing, broadcasting, security and traffic management of vehicular

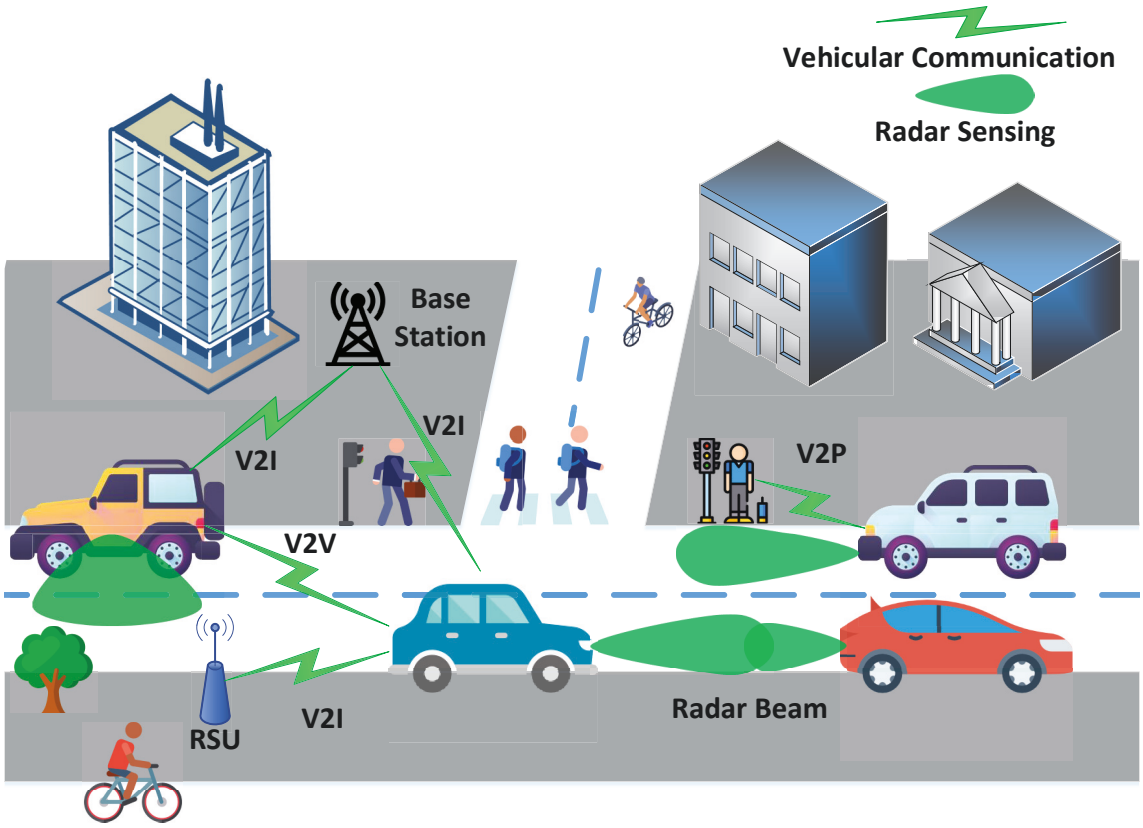

Figure 2.1 : An illustration of vehicular networks on an urban road.

ad-hoc networks [17–19], resource allocation and communication link quality [20,21]. Among the major techniques to enhance these performance measures, cellular networks are capable of providing wide coverage and flexible centralized control for network resources, which is critical for achieving reliable V2X communication for fast-moving vehicles. Simultaneously, a radar sensing system enables exact measurement of distance and relative velocity of objects in front, beside, or behind the car, which is required to improve driving safety and enable safe autonomous operations. Particularly, mm-Wave automotive radar is expected to be a key technology improving driving safety in the next-generation autonomous vehicular networks due to its unique advantages of detecting vehicles even under bad weather conditions like fog, spray, heavy rain, or snow [22, 23].

The following kinds of literature investigated cellular V2X communications [11, 24–27] and automotive radar sensing [28–31] in vehicular networks. [11] provided a survey on the state of the art of LTE, which discussed the related work and running standardization activities, analyzed strengths and weaknesses of long term evolution (LTE) as an enabling technology for vehicular communications. [24] provided a comprehensive overview of the long-term evolution-vehicle (LTE-V) standard supporting sidelink or V2V communications using LTE's direct interface named PC5 in LTE. In [25], the authors proposed a mobile-edge computing architecture for future cellular vehicular networks and demonstrate its potential advantages. In [26], enhanced design aspects to support LTE-based V2X services were presented, and a new demodulation reference signal sequence design was performed. [27] introduced the NOMA technique into the LTE-based vehicular network to support massive connectivity and reduce resource collision for multiple V2X applications via either power domain or code domain multiplexing. In [28], the authors proposed an automotive radar signal processing scheme for target detection, tracking, and classification. [29] proposed a novel way to cluster radar data points for radar signal processing, which has shown a good measurement on radar data. Different approaches which focused on the application of automotive radar were proposed to mitigate radar interference in [30, 31].

2.2 Resource Optimization for Vehicular Communications

Resource allocation for vehicular communication is one of the most important and challenging problems due to the highly dynamic mobility of vehicles, vast range of data services and congested frequency spectrum [32]. Numerous ideas and techniques have been emerging, aiming to allocate resource for V2X communications based on DSRC [33–36] and cellular networks. Considering the advantage of cellular networks, we mainly focus on the investigation of cellular V2X communications.

In the following, we review works on resource management in cellular vehicular networks, mode selection of V-D2D. In addition, we also do a literature survey on the prediction for vehicular flows with consideration of the relationship between resource requirements and traffic flows.

2.2.1 Resource Management for Cellular V2X Communications

The vehicular users (V-UEs) in cellular networks can operate either in the underlay or in the overlay modes [37, 38]. In the underlay modes, an important problem that needs to be addressed is the interference among traditional cellular users (CUEs) and VUEs. Numerous studies on resource allocation algorithms have been investigated.

Based on safety-critical requirements of vehicular communication, literatures [20, 39, 40] proposed radio resources and power allocation algorithms to maximize the sum rate of CUEs under the condition of fulfilling V-UEs' requirements. In [39], the authors proposed a two stages resource allocation algorithm. First, by problem transformation, the interference which is caused by resource reusing between the V2V and traditional cellular transmissions will be resolved. The eNB allocates resource blocks (RBs) to both VUEs and CUEs with the assumption of equal power allocation. Then, the transmission power is adjusted for each VUE and CUE by the eNB after completing the RB allocation in the first stage. In [20], the sum rate of the CUEs is maximized and the transmit power of the VUEs is minimized. In [40], authors first proposed a problem transformation method to transform the requirements of V2X communications into mathematical constraints which can be computed only using channel state information (CSI). Different from [20, 39], resource reusing can occur not only between cellular users and vehicles but also among different vehicles in this study. Then, a novel three-stage cluster-based RB sharing and power allocation scheme based on matching theory was proposed, which had not only better

cellular sum rate performance and availability, but also improved robustness to the number of VUEs as well as the required number of RBs per VUE compared to the existing schemes. In [41], Mei *et al.* investigated a radio resource, power allocation, and coding schemes for jointly optimizing V2V communications. This scheme aims to guarantee the latency and reliability requirements of VUEs and maximize the information rate of CUEs. In [42], Wei *et al.* proposed a resource allocation scheme for V2X communications in the heterogeneous networks to jointly address power control, frequency allocation and sharing. This scheme aims to achieve fairness among CUEs, WiFi-UEs, and VUEs. Based on different service needs, VUEs are classified into non-safety and safety ones. Then, to reduce computation complexity, the orginal optimization problem is decomposed into three steps to maximize the total throughput of CUEs and non-safety VUEs while guaranteeing the quality-of-service (QoS) demands of safety VUEs and WiFi-UEs.

The above methods mainly studied resource allocation schemes that allow users to share the same resources based on user pairing. Some works focused on investigating the resource allocation scheme allowing VUEs to reuse the same resources based on user clustering [43, 44] and user geographic location [45, 46]. In [43], the authors proposed a zone-based hybrid scheduling algorithm aiming to maximize the sum rate of cellular V2V while accounting for the link reliability in terms of the outage probability for all receiving VUEs. Depending on the geographical locations, the VUEs are divided into different communication groups. In the first, the eNB allocates resources for VUEs by a proposed hybrid scheduling. In the second, the reuse patterns are defined where resources are reused in each communication group. Then, specific resources are allocated to VUEs in each zone of one pattern. In [44], the authors studied and proposed a radio resource management scheme for D2D-based vehicular communications to maximize the sum V2I capacity while guaranteeing the reliability of all V2V links. The graph partitioning tools are used to

divide interfering V2V links into different clusters before formulating the spectrum sharing problem as a weighted 3-dimensional matching problem, which is then solved through adapting a high-performance approximation algorithm. In [45], a two-stage resource allocation scheme was proposed for V2X communications to minimize the latency of delay-sensitive services, meanwhile satisfying the corresponding reliability requirements and data rate requirements. In the first phase, based on the traffic density information, resources are allocated for each sub-region, where orthogonal resources are allocated in different sub-regions. In the second phase, resources that can be reused are used among sub-regions based on the channel state information. A novel proximity and load-aware resource allocation scheme for V2V communication was proposed in [46] to minimize the total network cost while satisfying QoS requirements of vehicles. Firstly, based on the proximity information and traffic patterns of vehicles, a dynamic clustering scheme is proposed to group the VUE pairs into sets of zones. Then, a matching game is proposed to allocate resources among VUEs in each zone. In contrast to the resource allocation algorithms in the underlaying mode, some works [47–49] focused on the study of cellular V2X communication in the overlaying scheme where the conventional cellular transmission and V2V are carried out in a separate frequency band. Thus, cellular users are well protected with overlay scheme, but in some cases, frequency efficiency may be relatively low because the frequency is not reused. However, despite the large amount of literature focused on resource allocation for cellular V2X communication with different modes, they rarely take the signalling latency and heavy loading into consideration when conducting the latency analysis. In addition, the papers for resource allocation based on geographic zone do not consider the connection between different zones caused by the directionality of the vehicle.

Heterogeneous vehicular network is efficient for offloading centralized traffic, improving the sum-rate capacity and supporting low-latency communications [50–54].

A heterogeneous vehicular network is typically a two-tier network with a central macro base station (MBS) and multiple distributed small cells. In [50, 51], network performance is characterized, with particular concern for frequent handoff between small cells. In [52], an analytical model based on clustering is proposed to characterize the network performance. In [53, 54], cognitive radio is proposed for sharing spectrum between macro cells and small cells. These studies demonstrate the feasibility and great potential of heterogeneous vehicular networks.

In D2D communication, the choice of cellular communication or direct communication defines the mode selection underlaying cellular networks and extensive research on mode selection of D2D has been conducted, e.g., [55–57]. An efficient mode selection scheme is a way for optimizing the resources. For cellular V2X, VUEs can also communicate using either direct link (i.e., V-D2D) or traditional cellular link. Focusing on the mode selection and resource allocation of cellular V2X communications, the authors in [58] designed a deep reinforcement learning-based mode selection and resource allocation scheme for cellular V2X to maximize the sum capacity of V2I while guaranteeing the latency and reliability requirement of V2V. In [59], the authors proposed a flexible mode selection scheme for cellular V2X to decide transmission mode (i.e., direct and network modes) of vehicular transmitter. Based on a stochastic geometry model, the expressions for success probabilities of different modes are derived. In [60], Li *et al.* proposed a novel joint power control and resource mode selection approach to support safety-related V2X services under different network load conditions. They considered different resource allocation modes and proposed power control strategies for different modes to maximize the information while mitigating the interference between VUEs and pedestrian user equipment. However, from the perspective of non-renewable resources and green transportation, minimizing the energy consumption of vehicles is not considered by these studies when conducting the mode selection for V2X.

2.2.2 Prediction for Vehicular Traffic Flow

Accurate short-term traffic prediction is important for efficient resource management [61,62]. Existing techniques can be classified into two main classes: parametric model-based and non-parametric based predictions [63]. The former adopts explicit mathematical models such as auto-regressive-integrated-moving-average (ARIMA) and its variants [64,65]. The latter does not assume a model, and it predicts the traffic using machine learning techniques such as artificial neural networks (ANN) [66] and k-Nearest Neighbour (kNN) [67–69]. Several works focused on the resource allocation scheme based on a prediction algorithm [70–73]. In [70], Asheralieva *et al.* proposed a predictive resource allocation strategy for cognitive wireless networks by employing adaptive algorithms to predict the network loading. These algorithms can detect changes in the traffic characteristics, and adapt automatically. A novel prediction-based resource allocation algorithm [71] was proposed in a heterogeneous wireless access medium. The developed scheme is decentralized and does not require a central resource manager to perform the resource allocation. In [72], the authors presented a solution that applied forecasting techniques to adjust the allocated slice resources based on different service classes to optimize the network utilization. In [73], the authors proposed a stacked long short term memory model to predict the historical traffic data of V2V communications to reveal the pattern of traffic volume, from which it was found that potential patterns may help implement resource allocation in large scale. However, for vehicular communications, there has been little work to combine resource allocation and vehicular traffic flow forecasting.

2.3 Resource Optimization for Automotive Radars

The reception of interference signals can lead to problems such as ghost targets or a reduced SNR. In the real road traffic situation, mutual interference between different automotive radars is unavoidable due to the resource reusing. For example,

forward- and sideward- looking radars interfere with their peers travelling in the opposition direction or crossroads. Backward-looking radars can interfere with the forward- and sideward- looking radars in the same direction.

There have been some studies on radar interference modelling. In [74], the mutual interference between FMCW radars was analysed and the effect of interference on radar performance was evaluated. In [75], interference was investigated for different types of radars under different conditions (e.g., weather condition and vehicular position). Detailed causes of mutual interference for two types of radar sensors were analyzed. In [76], a simulation-based predictor using ray-tracing was proposed for modelling the received power levels for useful echo and interference signals. In [77], a stochastic geometry method was adopted to analyze radar interference, where vehicle locations were assumed to follow two types of point models including a linear Poisson Point Process (PPP) and a fully regular lattice. It was shown that the mean interference is independent of the point models when the width of the road approaches zero.

To mitigate radar interference, techniques such as resource allocation [78, 79] and interference mitigation [80, 81] have been proposed. In [78], a power allocation strategy based on game theory was proposed for distributed multiple radars in a spectrum sharing environment. In [79], a game theoretic approach was introduced for joint beamforming and power allocation in a distributed radar network and a pricing mechanism was proposed to minimize the inter-radar interference. In [80], an adaptive beamforming approach was developed based on MIMO radar to mitigate wireless interference for radar-wireless spectrum sharing systems. In [81], a frequency-hopping random chirp FMCW technique was proposed to reduce mutual interference for FMCW radars. In [82], two power allocation schemes were proposed for distributed multiple-radar systems to meet a predetermined localization threshold. Optimal resource allocation schemes under various constraints were al-

so investigated for coexisting and integrated radar and communications systems in [83–86].

One major limitation of these works is that they do not take into consideration the impact of antenna radiation pattern on interference modelling and then mitigation. In [77], a directional antenna was considered but it was assumed that the gain in the main-lobe is the same and the side-lobe was disregarded. Using a flat main-lobe may cause exaggerated interference, while ignoring side-lobes leads to under-estimated interference, particularly when each signal for sensing is typically very small and can be comparable to the interference received through the side-lobes [75, 87]. Nevertheless, stochastic geometry is a powerful tool for characterizing the randomness of vehicular locations [77, 88, 89]. It has been widely used for modelling nodes in cellular networks [90], femtocells [91], and vehicular networks [92, 93]. It is particularly useful for vehicular networks where both transmitters and receivers are randomly located and moving. Random geometric graph [94] is also a useful tool for performance analysis and optimization of large wireless networks. Compared with random geometric graphs, stochastic geometry enables more flexible and tailored analysis, e.g., studying the average behavior over many spatial realizations of a network, where nodes are placed according to a specified probability distribution.

So far, we have reviewed the resource allocation for communication and radar sensing. In summary, all the above works on optimizing resources in vehicular networks either focused on interference management of cellular V2X and performance improvement based on vehicular reliability requirements, or focused on resource sharing of coexisting radar and communications systems, but rarely took the signalling latency into consideration when conducting the latency analysis, also did not consider the impact of antenna radiation pattern when modelling interference and allocating resources. In the following chapters, we will introduce our work that

brings new contributions to the existing research.

Chapter 3

Semi-Persistent Resource Allocation Based on Traffic Prediction for Vehicular Communication

In this chapter, based on the two-tier heterogeneous vehicular network, we propose a semi-persistent resource allocation scheme. This scheme aims to address the two aforementioned limitations in resource management, and can significantly reduce signalling latency while optimizing resource allocation. In the proposed scheme, the MBS provides centralized control over resource allocation for RSUs and each RSU provides direct short-range communication as well as resource allocation to vehicles within its coverage. The traffic of vehicles is regular and predictable, so is their resource requirement for communications. This scheme first pre-allocates persistent resources to each RSU based on predicted traffic, and then provides additional real-time dynamic resource allocation to RSUs with insufficiently allocated resources during pre-allocation. With pre-allocated resource, each RSU can directly provide initial resource allocation to vehicles when receiving their requests, without having to wait for the resource being assigned by the MBS. This can significantly reduce the signalling latency and mitigate congestion. By combining pre-allocation and real-time dynamic allocation, the proposed scheme is expected to achieve an excellent balance between spectrum efficiency and latency.

The rest of this chapter is organized as follows: Section 3.1 introduces the system model, the proposed semi-persistent resource allocation scheme, the problem formation, kNN prediction algorithm and the solution of the optimization problem. Simulation results are also given in this Section which validate the effectiveness of the proposed semi-persistent scheme in comparison with two benchmark schemes.

Another optimized problem based on the semi-persistent scheme are formulated in Section 3.2. The corresponding system model, solution of the problem and simulation results are also presented in this Section. Section 3.3 summarizes this chapter.

3.1 Bandwidth-Constrained Semi-persistent Resource Allocation Scheme in Two-tier Cellular Networks

Performance of the proposed scheme is closely related to the accuracy of predicted traffic, the ratio between allocated persistent and dynamic resources, and the actual resource optimization algorithm. In this section, we consider a segment-based road model, where a road is divided into multiple segments and the resource request and allocation are per-segment based. We first develop a cost function for the overall latency, including both communication and signalling latency, subject to the bandwidth constraints. We then develop a kNN algorithm for predicting the vehicle traffic and then the resource requirement, by assuming a linear relationship between them. Based on the predicted value, we then propose an improved water-filling algorithm to generate near-optimal solution to the constrained delay minimization problem. Extensive simulation results using practically measured traffic data demonstrate the superiority of our proposed scheme in latency reduction. Compared to benchmark schemes, our scheme is shown to achieve latency reduction up to 11.6%.

3.1.1 System Model for Semi-persitent Resource Allocation

In this section, we present the system model, propose the semi-persistent resource allocation scheme, and then formulate the cost function of delay that will be optimized later.

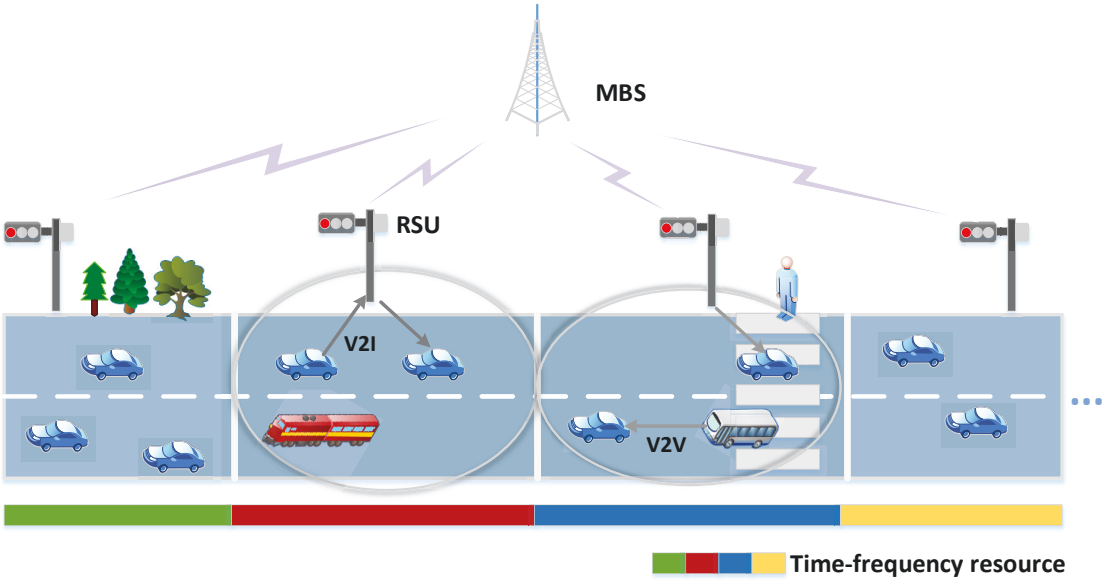

Figure 3.1 : RSU-cellular architecture and the segmented road model.

System Model

We consider an urban free-way fully covered by the LTE cellular network, as shown in Fig. 3.1, where a straight road with two lanes is exemplified. We assume that the road is equipped with RSUs, spaced at distances based on individual coverage. We divide the road of interest into N segments, where each RSU supports the communication of vehicles in each segment. Road segmentation enables efficient spectral resource allocation and management, and offers potential for low-latency communications. Denote the segment set as $\mathcal{N} = \{1, 2, ..., N\}$. Given two-way traffic, the density of vehicles in different segments can be different, and can also be correlated over space and time.

For vehicular communications, we consider a two-tier heterogeneous network, where a MBS provides centralized control on network resource for RSUs, and each RSU is directly responsible for providing access to vehicles in the V2I communication mode, and conducting local resource allocation for V2V and V2I communications within its segment. Since the communications between vehicles are mainly limited

to be within a segment, they are directly managed by the corresponding RSU. When resource allocation is needed, each RSU collects requests from vehicles and lodges a request to the MBS. Once the resource is allocated, the RSU will then confirm with the vehicles.

The required network resource for communications is assumed to be linearly proportional to the vehicle traffic within the segment. We represent the requested resource as bandwidth, but it can be easily extended to general time-frequency resource blocks. Hence for each segment, the required bandwidth is linearly proportional to the vehicle traffic with a scalar ε.

We do not consider frequency reuse here and the frequency channels being allocated across segments are different. For frequency reuse, in the considered road model we may divide the roads into blocks, each block containing a sequence of continuous segments. The same set of frequencies can then be allocated in an increasing order to the segments in each block, so that segments in different blocks using the same frequencies are sufficiently spaced with negligible interference. Our proposed scheme can then be applied to each block straightforwardly.

Semi-persitent Resource Allocation

In a conventional persistent resource allocation scheme, the MBS only allocates frequency resources to RSUs in advance based on traffic prediction. On the opposite, in a dynamic scheme, the MBS only allocates resources to RSUs upon their real-time requests, without doing pre-allocation. These two allocation schemes have respective advantages and disadvantages. For persistent allocation, its performance largely depends on the accuracy of predicted resource demands. Although it avoids the real-time signalling loading and delay, inaccurate and insufficient prediction and resource allocation can lead to low spectrum efficiency and even longer delay. For dynamic allocation, each request and confirmation for resource allocation incurs

delay, and it could also be impractical due to the instantaneous very-high loading resulting from fast-varying traffic flow.

Our semi-persistent scheme combines persistent and dynamic resource allocation, which can achieve an excellent balance between reducing the delay and improving the bandwidth efficiency. In the proposed semi-persistent scheme, the total available resource is divided into persistent and dynamic resource pools. Using predicted mean traffic and then the mean bandwidth needs, the MBS pre-allocates some resource to each RSU in a segment from the persistent pool in advance, as will be detailed in Section 3.1.2. In real-time, the MBS then further allocates resources to the segments that only need additional resources upon requests from the dynamic resource pool, as will be investigated in Section 3.1.3. Our scheme can be applied to either vehicle density based prediction by assuming a linear relationship between the bandwidth requirement and the number of vehicles in one segment, or the prediction for communication bandwidth/capacity directly.

Assume that we are at time tT_s where t is an integer and T_s is the observation interval, and we are now processing the resource allocation problem for the next time period from tT_s to $(t+1)T_s$. For simplicity, we use t to represent either the time tT_s or the period from $(t-1)T_s$ to tT_s hereafter. We define some symbols and rules as follows:

- The total available bandwidth, total allocated persistent bandwidth and total remained dynamic bandwidth are denoted as B, B^P, and B^D respectively. We have $B^D + B^P \leq B$, as there could be unallocated bandwidth due to constraints applied in our optimization problem. The current time is t;
- The persistent bandwidth allocated to the n-th segment for $(t+1)$ is $B_n^p(t+1), n \in \mathcal{N}$. Therefore $B^P = \sum_{n=1}^{N} B_n^p(t+1)$.
- When $B_n^p(t+1) < B_n^{\text{req}}(t+1)$, the n-th RSU will request dynamic resources

from the MBS. The dynamic bandwidth allocated to each segment for $(t+1)$ is $B_n^d(t+1)$, where $\sum_{n=1}^{N} B_n^d(t+1) \leq B^D$. In addition, the actual bandwidth requirement at $t+1$ is denoted as $B_n^{\text{req}}(t+1), n \in \mathcal{N}$ and $B_n^d(t+1)$ needs to satisfy $B_n^d(t+1) \leq B_n^{\text{req}}(t+1) - B_n^p(t+1)$.

- The total allocated bandwidth $B_n(t+1)$ to the n-th segment at $t+1$ is then given by $B_n(t+1) = B_n^p(t+1) + B_n^d(t+1)$.

- Let the signalling and processing delay for the dynamic resource request and allocation be t^s. We assume that t^s is a constant for all segments.

- The ground-truth delay $\tau_n^{\text{exp}}(t+1)$ denotes the "true" delay if the requested bandwidth $B_n^{\text{req}}(t+1)$ is fully allocated.

Referring to Fig. 3.2, the system operation and the actual latency in the proposed scheme are described as follows. We divide the communication process within each segment into two stages. In the first stage, a RSU schedules vehicle communications using the pre-allocated persistent bandwidth meanwhile it will start a new resource request with the MBS upon receiving the actual bandwidth requests from vehicles. After communication for a period t^s that corresponds to the signalling and processing delay for the new bandwidth request, the RSU receives updated bandwidth allocation and the second stage starts. The RSU now schedules the communication with the combined persistent and dynamic bandwidth. If no dynamic bandwidth is allocated, the segment continues using only the persistent bandwidth. We ignore the signalling delay within a segment during this process because it has little impact on our proposed scheme. Note that the prediction and persistent bandwidth allocation is assumed to be done in a relatively long interval of tens to hundreds of timeslots, while dynamic allocation is done within each timeslot, with a period of typically 100 ms. For vehicle density based prediction, the interval can be tens of

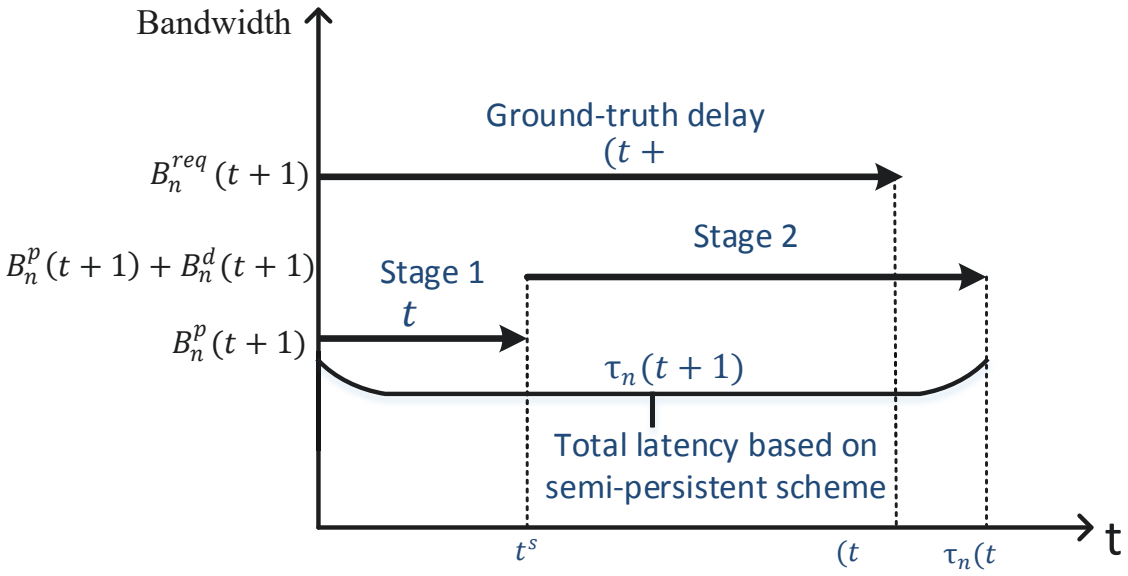

Figure 3.2 : Illustration of latency for each timeslot in the n-th segment for the period $(t, t+1)T_s$. Each period contains tens to hundreds of such timeslots.

seconds as the density will not change significantly during a short period; and for network-bandwidth-demand based prediction, it can be smaller.

Formulation of the Cost Function

We now formulate an average relative latency as the cost function for our optimization problem. We aim to minimize the average relative latency by optimizing the allocation of persistent and dynamic bandwidth.

Based on Shannon's capacity formula, the data rate is linearly proportional to the bandwidth. Here, we approximate the data rate as the product of the bandwidth and a segment-dependent constant c_n accounting for possibly different signal-to-noise ratios in different segments. Let the total number of bits to be transmitted be $S_n(t+1)$ in time $t+1$ and in the n-th segment. Then the bits being transmitted during the first stage will be $c_n B_n^p(t+1)t^s$ and the transmission latency in the second

stage will be

$$\tau_n^a(t+1) = \frac{S_n(t+1) - c_n B_n^p(t+1) t^s}{c_n (B_n^p(t+1) + B_n^d(t+1))}. \tag{3.1}$$

The total latency is then given by

$$\tau_n(t+1) = \tau_n^a(t+1) + t^s. \tag{3.2}$$

Therefore, the ground-truth expected latency that corresponds to the actually required bandwidth is

$$\tau_n^{\exp}(t+1) = \frac{S_n(t+1)}{c_n B_n^{\text{req}}(t+1)}. \tag{3.3}$$

Note that $\tau_n^{\exp}(t+1)$ is typically specified in a standard, for example, $\tau_n^{\exp}(t+1) = 100$ ms according to 3GPP TR 36.885 [14].

If the allocated persistent bandwidth exceeds the actually required bandwidth in one segment, i.e., $B_n^p(t+1) \geq B_n^{\text{req}}(t+1)$, the RSU does not need to request more bandwidth from MBS. Hence, we let $\mathcal{U}$ and $\mathcal{V}$ denote the index sets of the RSUs that do not and do request dynamic bandwidth, respectively. The size of the sets are U and V. We can then define the averaged total relative latency $T(t+1)$ as

$$\begin{aligned} T(t+1) &= \frac{1}{N} \sum_{n=1}^{N} \frac{\tau_n(t+1)}{\tau_n^{\exp}(t+1)} \\ &= \frac{1}{N} \left\{ \sum_{u \in \mathcal{U}} \frac{B_u^{\text{req}}(t+1)}{\min\left\{B_u^p(t+1), B_u^{\text{req}}(t+1)\right\}} + \sum_{v \in \mathcal{V}} \left[\frac{B_v^{\text{req}}(t+1) - B_v^p(t+1) t_v^s}{B_v^p(t+1) + B_v^d(t+1)} + t_v^s \right] \right\} \\ &= \frac{1}{N} \left\{ U + \sum_{v \in \mathcal{V}} \left[\frac{B_v^{\text{req}}(t+1) - B_v^p(t+1) t_v^s}{B_v^p(t+1) + B_v^d(t+1)} + t_v^s \right] \right\}, \end{aligned} \tag{3.4}$$

where $N = U + V$ and $t_v^s = t^s / \tau_v^{\exp}(t+1)$ is the relative signalling latency. Note

that both U and V depend on the allocated persistent resource.

Our objective is to determine optimal allocations for persistent and dynamic resources so that $T(t+1)$ is minimized. The optimization problem is formulated as

$$\min_{\left\{B_v^d(t+1)\right\}_{v=1}^{V}} \quad T(t+1) \tag{3.5a}$$

$$\text{subject to} \quad 0 < \sum_{v=1}^{V} B_v^d(t+1) \leq B^D; \tag{3.5b}$$

$$0 \leq B_v^d(t+1) \leq B_v^{d_u}(t+1), \ \forall v; \tag{3.5c}$$

where

$$B_v^{d_u}(t+1) = B_v^{\text{req}}(t+1) - B_v^p(t+1) \tag{3.6}$$

is the upper bound of $B_v^d(t+1)$. Equation (3.5b) represents a general constraint on the total available bandwidth for dynamic allocation. The constraint in (3.5c) ensures that no more bandwidth than that actually needed will be allocated to one RSU. It guarantees the fairness during resource allocation and enables the overall optimality attained.

3.1.2 Vehicular Traffic Prediction Based on kNN

In this section, we choose kNN for traffic prediction for its simplicity and efficiency in solving non-linear problems which typically exist in traffic prediction [95]. Its efficiency can be seen from our simulation results using practically measured traffic data as will be presented in Section 3.1.4. It is noted that although our prediction scheme is presented by referring to the vehicular traffic prediction, it can be readily extended to direct network traffic prediction.

We focus on short time traffic prediction (30 seconds) using a space-time kNN

(ST-kNN) algorithm. Previous works on the kNN method mainly focused on the whole road, which did not consider the difference and correlation between different parts on the road. In order to apply it into our problem where the traffic for each segment needs to be predicted, we introduce a space-time windowing method to exploit the data correlation, which can achieve better prediction performance. Our proposed kNN method predicts the future traffic using a weighted prediction function based on latest and historical data sets in both windowed space and time domains.

Fig. 3.3 depicts the processing flow of the proposed kNN method. The search procedure finds the nearest neighbours of each segment in the time and spatial domains from historical observations that are most similar to the current conditions. The nearest neighbors are then used as the input to a linear function to generate the prediction. The main process of our improved ST-kNN algorithm is summarized below and described in detail next.

1. Define an appropriate state space;
2. Decide the window size;
3. Define a distance metric to determine nearness of historical data to the current conditions;
4. Select a prediction method given a collection of nearest neighbours.

State Space

State vector is a standard for comparing the current data and the historical database. It can have a significant impact on the prediction accuracy. Here the state vector contains the traffic values measured over a continuous period $(t, t-1, ..., t-q)$, where q needs to be selected carefully to avoid resulting in excessive similar values

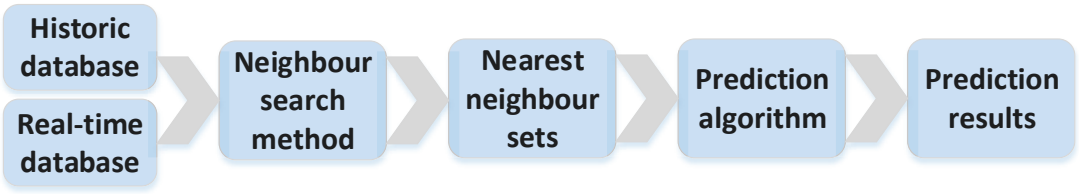

Figure 3.3 : Processing flow of the ST-kNN algorithm.

when comparing the current observation data and the historical database. We will show the impact of the value q on system performance in Section 3.1.4. For Segment $n(n \in \mathcal{N})$, the current traffic state vector is given by

$$\mathbf{v}_n(t) = [V_n(t),\ V_n(t-1),\ V_n(t-2), ...,\ V_n(t-q)] \tag{3.7}$$

where $V_n(t)$ is the traffic value at time t.

The state vector $\mathbf{v}_n(t)$ is then compared with neighbouring blocks in both space and time domains from the historical database. Selection of these blocks will be discussed in the next subsection.

Choice of the Window Size ν

Considering one traffic direction on the road, the traffic flow in different segments can be highly correlated over both the spatial and temporal domains. Fig. 3.4. illustrates the correlation of the traffic volume between different segments. The same color stands for the mostly correlated traffic, e.g., $V_3(t)$ in Segment 3 at time t is strongly correlated with $V_1(t-2)$, $V_2(t-1)$, $V_4(t+1)$, and $V_5(t+2)$.

Here, the window size is selected according to the correlation between different segments dependent on the movement speed of vehicles. The vehicle speeds could vary significantly between different time periods of a day such as peak and off-peak time. The time periods can be classified according to the variation of the speed or

the average speed using for example an unsupervised classification algorithm [96]. Here, we use the average speed $\overline{v}$.

For predicting the traffic in Segment n, we apply windowing across segments of distance $L = \overline{v}T_p$ in the spatial domain and over a period of T_p in the time domain, where T_p is the prediction interval. During this period, vehicles at Segment m, the furthest to Segment n, will travel to Segment n. In other words, the current traffic flow rate at time t in Segment n is strongly correlated with those up to Segment m at time $t - T_p$. The actual number of blocks will be the quantized values for L and T_p with respect to the length of segments and T_s, respectively. Let ν_{nm} be the relative index of samples and $0 < \nu_{nm} \leq \lceil T_p/T_s \rceil$ where $\lceil T_p/T_s \rceil$ denotes the least integer larger than T_p/T_s. Note that the selected state vector in the neighbouring blocks can be represented as

$$\begin{cases} \mathbf{v}_m(t+\nu_{nm}) = [V_m(t+\nu_{nm}),\ V_m(t+\nu_{nm}-1), \ldots, V_m(t+\nu_{nm}-q)]\,, \text{ when } m > n, \\ \mathbf{v}_m(t-\nu_{nm}) = [V_m(t-\nu_{nm}),\ V_m(t-\nu_{nm}-1), \ldots, V_m(t-\nu_{nm}-q)]\,, \text{ when } m < n. \end{cases} \tag{3.8}$$

When $m = n$, then $\nu_{nm} = 0$. Here, the window size ν based on speed and distance is only suitable for a one-way road.

Distance Metric of Traffic Data

Learning a good distance metric in feature space is crucial in real-world application [97]. Here we use Euclidean distance, a common distance metric between real-time and historical traffic data used in kNN prediction [67, 98]. It is given by

$$l_i = \frac{\sum_{i_q=1}^{q} \sqrt{(V_n(t-i_q) - V_m(t \pm \nu_{nm} - i_q))^2}}{q}, \tag{3.9}$$

where $V_n(t - i_q)$ is the traffic flow of segment n at the time $(t-i_q)$ and $V_m(t \pm \nu_{nm} - i_q)$ is the traffic volume of segment m which is strongly correlated with $V_n(t - i_q)$ in

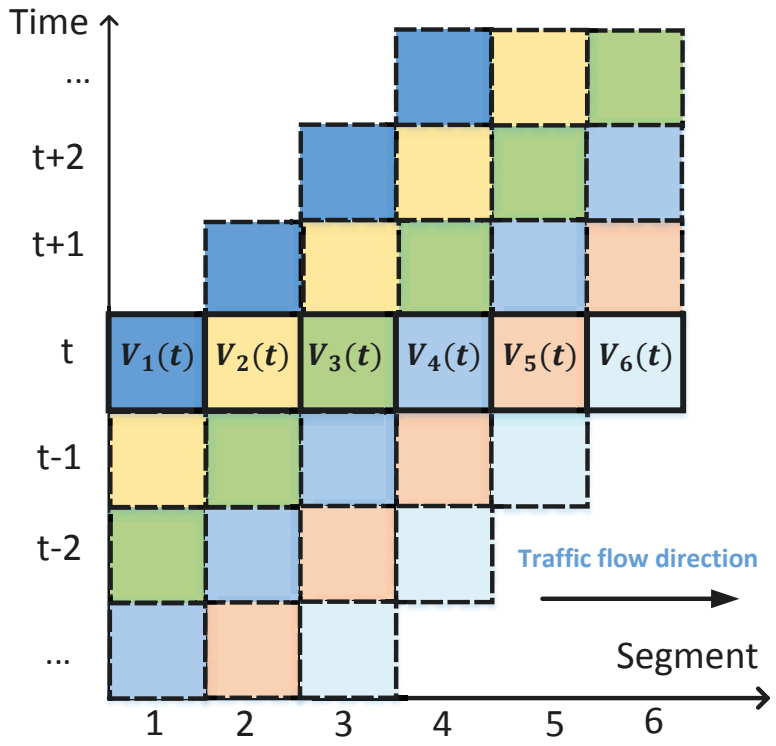

Figure 3.4 : Illustration of traffic correlation and the windowing concept.

the historical database, l_i represents the Euclidean distance of the two traffic state vectors.

Prediction Function

Based on the Euclidean distance values computed for the blocks in the windowed spatial and temporal domains, k nearest neighbours with the least distance values are found from the historical database. We then use a weighted linear function [99] [page 2-3] to predict the traffic. The predicted traffic flow $V_n(t+1)$ in segment n at time $(t+1)$ is given by

$$V_n(t+1) = \sum_{i=1}^{k} a_i V_m(i, t \pm \nu_{nm} + 1), \tag{3.10}$$

where the weight a_i is defined as

$$a_i = \frac{l_i^{-1}}{\sum_{i=1}^{k} l_i^{-1}}. \tag{3.11}$$

Assuming a linear relationship between the vehicular and network traffic, the predicted bandwidth for time $t+1$ can be obtained as $\hat{b}_n^p(t+1) = \varepsilon V_n(t+1), n \in \mathcal{N}$, where ε is the mapping coefficient.

Application of a Scaling Coefficient

Instead of directly using the predicted value to allocate the bandwidth to segments, we apply a scaling factor θ to it and the pre-allocated persistent bandwidth for the n-th segment is given by

$$B_n^p(t+1) = \theta \hat{b}_n^p(t+1), \tag{3.12}$$

with

$$0 < \theta \leq \frac{B}{\sum_{n=1}^{N} \hat{b}_n^p(t+1)}. \tag{3.13}$$

There are two reasons that we introduce θ here. Firstly, the total available bandwidth could be smaller than the sum of the predicted bandwidth for all segments, and hence we need to do a scaling. Secondly, even when the total bandwidth is sufficient, allocating less resource than the predicted value may achieve overall better performance given the fluctuation of the instantaneous traffic. We will investigate and propose a rule-of-thumb for selecting the values of θ for a given ratio between the total available bandwidth and the statistical mean of the required bandwidth in Section 3.1.4.

3.1.3 Minimization of Average Relative Latency

Assume that the total available bandwidth B is known. After allocating the persistent bandwidth using (3.12), we now get the remaining bandwidth $B^D(t+1)$ as

$$B^D(t+1) = B - \theta \sum_{n=1}^{N} \hat{b}_n^p(t+1), \tag{3.14}$$

which is available for dynamic allocation based on the actual requests $B_n^{\text{req}}(t+1)$ from RSUs.

Our goal is now to find the optimal dynamic allocation $B_n^d(t+1)$ for (3.5), with a given θ. Note that strictly speaking, an optimal solution will require optimization for both θ and $B_n^d(t+1)$. Since there exists no closed-form statistical distribution for the required bandwidth, it is hardly possible to find a closed-form expression for the optimal θ. Therefore, we only test a series of values for θ in the simulation in Section 3.1.4, and disclose the optimal range of θ based on practically measured channels. Note that in the case of $B_n^p(t+1) \geq B_n^{\text{req}}(t+1)$ when the allocated persistent bandwidth is sufficient, a RSU will not make a request for for dynamic bandwidth.

For the optimization problem in (3.5), we can separately consider two situations. In the first situation, $B^D \geq \sum_{v=1}^{V} B_v^{d_u}(t+1)$, which means there is sufficient bandwidth that can satisfy every RSU's request. In this case, the MBS can just allocate the bandwidth to each RSU as being requested. In the second situation, $B^D < \sum_{v=1}^{V} B_v^{d_u}(t+1)$, which implies that $\sum_{v=1}^{V} B_v^d(t+1) = B^D$ and not all requests can be satisfied. An optimization algorithm is needed for allocating the dynamic bandwidth in this situation.

It is easy to verify that $T(t+1)$ in (3.5) is a convex function of $B_v^d(t+1)$. Hence

the optimization problem meets the Karush-Kuhn-Tucker (KKT) conditions and can be generally solved by convex optimization algorithms such as linear programming. To provide a closed-form solution and shed more insights on the design, we propose a bandwidth-constrained water-filling algorithm (BC-WFA) next.

Algorithm 1 BC-WFA Algorithm.

Require: vector $\{p_v\}$, $\{w_v\}$,$\left\{B_v^{d_u}\right\}$ for $v = 1, 2, ..., V$, the set $E = \{1, 2, ..., V\}$, and B^D.
Ensure: $\left\{B_v^d\right\}$
1: **while** $E \neq \emptyset$ **do**
2: Use (3.18)-(3.20) to compute $\left\{B_v^d\right\}$.
3: $\Lambda \leftarrow \left\{v \mid B_v^d > B_v^{d_u}, v \in E\right\}$.
4: **if** $\Lambda \neq \emptyset$ **then**
5: **if** $v \in \Lambda$ **then**
6: $B_v^d = B_v^{d_u}$.
7: **end if**
8: $E \leftarrow E \backslash \Lambda$, $B^D = B^D - \sum_{v \in \Lambda} B_v^{d_u}$.
9: **else**
10: Output $\left\{B_v^d\right\}$ as $v \in E$.
11: **end if**
12: **end while**

Under the conditions of $B^D < \sum_{v=1}^{V} B_v^{d_u}(t+1)$, and $\sum_{v=1}^{V} B_v^d(t+1) = B^D$, the BC-WFA algorithm optimizes the dynamic bandwidth allocation, in order to minimize the relative latency in (3.5). The algorithm is developed based on the geometric water-filling method in [100]. The detailed steps are presented in Algorithm 1, with the concept illustrated in Fig. 3.5, where the dashed line denotes the water level.

Firstly, let $\{B_v^p(t+1)\}_{v=1}^{V}$ be a sorted sequence, which is positive and monotonically increasing. Let p_v denote the "step depth" of the vth stair and w_v represents

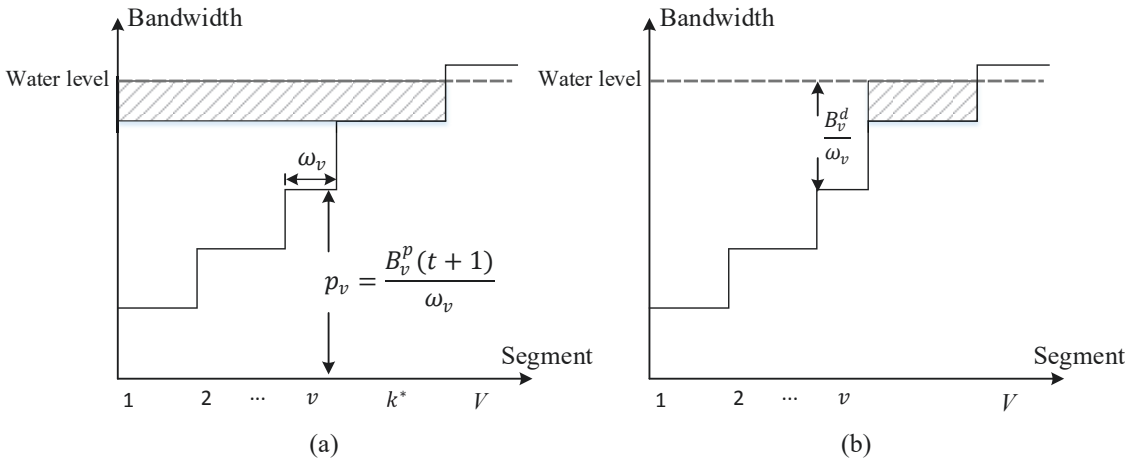

Figure 3.5 : Illustration of the BC-WFA water-filling for dynamic resource allocation.

the weighted coefficient as shown in Fig. 3.5(a). They are given by

$$w_v = \sqrt{B_v^{\text{req}}(t+1) - B_v^p(t+1)t_v^s}, \text{ for } v = 1, 2, ..., V. \tag{3.15}$$

$$p_v = \frac{B_v^p(t+1)}{w_v}, \text{for } v = 1, 2, ..., V. \tag{3.16}$$

Let $B_2^D(k)$ represent the water volume (dynamic bandwidth) above the kth step, as shown in the shadowed area in Fig. 3.5(a). It is given by

$$B_2^D(k) = \left[B^D - \sum_{v=1}^{k-1} (p_k - p_v) w_v \right]^+, \text{for } k = 1, ..., V \tag{3.17}$$

where $(x)^+ = \max\{0, x\}$.

According to the GWF algorithm without the individual upper bound constraint (3.5c) in [100], the explicit solution to (3.5) is given by

$$\begin{cases} B_v^d = \left[\dfrac{B_{k^*}^d}{w_{k^*}} + (p_{k^*} - p_v) \right] w_v, 1 \le v \le k^*, \\ B_v^d = 0, k^* < v \le V, \end{cases} \tag{3.18}$$

where

$$k^* = \max\left\{k \mid B_2^D(k) > 0, 1 \leq k \leq V\right\}. \tag{3.19}$$

Here k^* can be treated as the highest step under water. The allocated dynamic bandwidth for this step is

$$B_{k^*}^d = \frac{w_{k^*}}{\sum_{v=1}^{k^*} w_v} B_2^D(k^*), \tag{3.20}$$

which is illustrated by the shadowed area in Fig. 3.5(b).

In Algorithm 1, the constraints (3.5c) are checked in Steps 4-7. Allocations which do not satisfy the constraints are set as the individual upper bound and then removed in Step 8. The process repeats until all allocations are completed with constraints satisfied.

3.1.4 Simulation Results

In this section, we present simulation results for the proposed BC-WFA semi-persistent resource allocation scheme. As mentioned before, we would like to use real data for the simulation. Since the network model for vehicular communications is not available yet, we base our simulation on real vehicle traffic, and assume a linear mapping with $\varepsilon = 1$ between the network traffic (required bandwidth) and the vehicle traffic. Actually, we can see that ε does not have a direct impact on the objective function in (3.4) only if the linear mapping holds. In the case when this relationship does not hold, for example, when there are a burst of bandwidth requests, the proposed semi-persistent scheme can still cope with this via dynamically allocating bandwidth in real time using the proposed water-filling algorithm. This is because the vehicular traffic prediction is only used for allocating persistent bandwidth. However, the burst will translate into increased variance and the overall performance may be degraded.

We use the vehicular traffic dataset collected from a section of Interstate 80 (I-80) freeway located in Emeryville, California [101]. The dataset includes both traffic density and average vehicle speed. The study area was approximately 500 meters (1,640 feet) in length and consisted of six freeway lanes, including a high-occupancy vehicle (HOV) lane. The section includes six traffic stations and the time interval of the collected data is 30s within 10 days. Traffic flow data from the first nine days is selected as the historic database and data collected from the last day is used as the test data, assuming that RSUs co-locate with these traffic stations. The road is accordingly divided into six segments numbered as 1 to 6. We consider a one-way traffic with direction from Segment 1 to 6. With such data, we are capable of doing prediction every 30s. As discussed before, there is no particular requirement on the interval of prediction, and hence the interval here is indicative only.

Our simulation is based on a setup where the 30s interval is divided into many timeslots (200 in this chapter). During the interval, the required bandwidth in each time-slot in each segment could be varying and is assumed to follow a Gaussian distribution. Let the measured real free-way traffic over the 30s interval in [101] be the average of this distribution, denoted as $\overline{B}_n^{\text{req}}(t+1)$ for the time interval $[tTs, (t+1)T_s]$, with $T_s = 30$s. The actual bandwidth requirement is then assumed to follow the Gaussian distribution with mean $\overline{B}_n^{\text{req}}(t+1)$ and variance $0.2\overline{B}_n^{\text{req}}(t+1)$, i.e., $f(B_n^{\text{req}}(t+1)) \rightarrow \mathcal{N}\left(\overline{B}_n^{\text{req}}(t+1), 0.2\overline{B}_n^{\text{req}}(t+1)\right)$. Based on the predicted average traffic, persistent bandwidth will be requested and pre-allocated; the actually required bandwidth in each timeslot is then generated following the Gaussian distribution, and dynamic bandwidth is then allocated if requested. Note that our scheme does not exploit and hence does not rely on the actual traffic models. However its performance may be affected by the models indirectly. For example, a distribution with larger variance can lead to lower efficiency of the proposed scheme.

Prediction Performance

In order to evaluate the performance of the proposed prediction algorithm, we define and use Mean Absolute Percent Error (MAPE) [102] as a performance metric

$$\text{MAPE} = \frac{1}{n}\sum_{j=1}^{n}|\frac{V_j^p - V_j^r}{V_j^r}|, \tag{3.21}$$

where V_j^p is the predicted traffic flow and V_j^r is the real traffic flow. n is the number of predictions. Larger MAPE means worse prediction performance.

We first look for the best parameter values for the ST-kNN algorithm. To determine a proper window size ν_{nm} which is related to the moving speed, we adopt an ISODATA algorithm and classify a day into off-peak and peak time periods based on vehicle moving speed [96]. Fig. 3.6 shows the cumulative distribution function (CDF) of the average traffic for peak and off-peak periods using the real traffic data. The window size ν_{nm} can then be calculated for different time periods, and may vary across segments. Using segment 5 as an example at peak time (6:30-10 am), we get $\nu_{56} = 1, \nu_{54} = 1, \nu_{53} = 2, \nu_{52} = 3, \nu_{51} = 4$, based on the average speed and distance between segments [101].

We then determine the values for k and p. Fig. 3.7 shows the MAPE value of the prediction for Segment 5 using ST-kNN with different k and q values. When $k = 15$ and $q = 5$, the algorithm is found to achieve the best accuracy, with the averaged MAPE of 0.098 for the whole day. The best values for parameters k and q for all segments are shown in Table I. In practical implementation, a trial-and-update process can be applied regularly to decide their best values for the next time period. Since the characteristics of the traffic flow in a certain area vary slowly, such updates can be done slowly and at a low computational cost due to the simplicity of the ST-kNN algorithm.

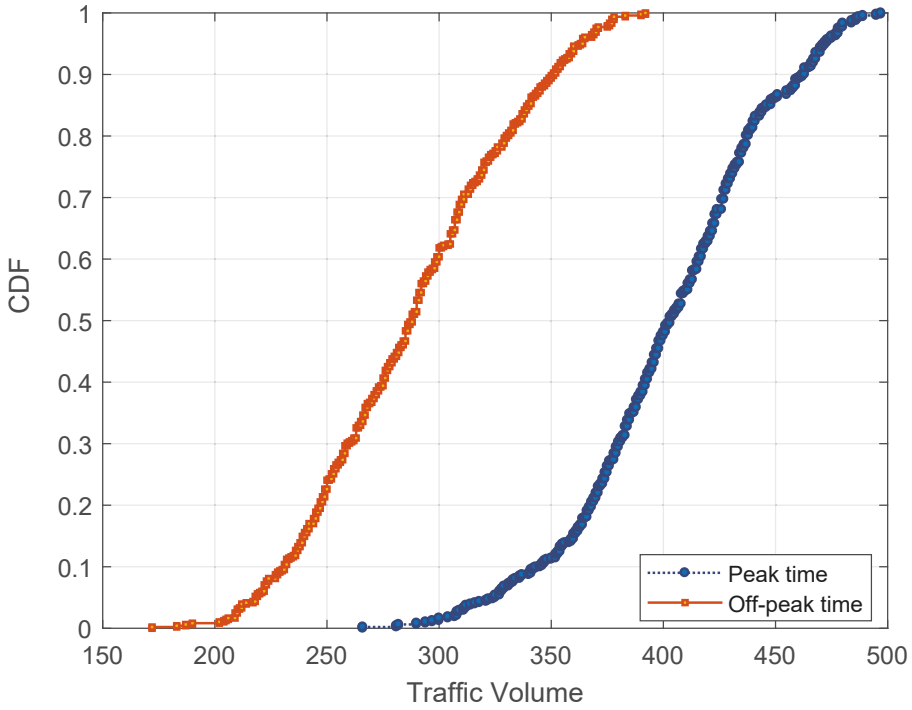

Figure 3.6 : The traffic volume during off-peak and peak time period, respectively.

Table 3.1 : Obtained best values for parameters k and q.

Segment n	1	2	3	4	5	6
k	15	15	18	15	15	15
q	5	5	4	5	5	5

The predicted traffic flow, as well as the actual data, are shown in Fig. 3.8(a). For comparison, we also presented the prediction results in Fig. 3.8(b) for *the least minimum mean square error (LMMSE)* algorithm, which is widely used for channel and traffic prediction [103,104]. The size of the adopted prediction correlation matrix in LMMSE is 10×10, and its complexity is much higher than the proposed ST-kNN due to the matrix inversion operation. For LMMSE, the averaged MAPE is 0.1063, comparable to that of the ST-kNN algorithm. The accuracy of LMMSE predictor can be improved with increasing the size of the prediction correlation matrix, at a higher complexity. The figure shows that LMMSE also tends to smooth the output of prediction, and hence is not as accurate as ST-kNN for predicting small-scale

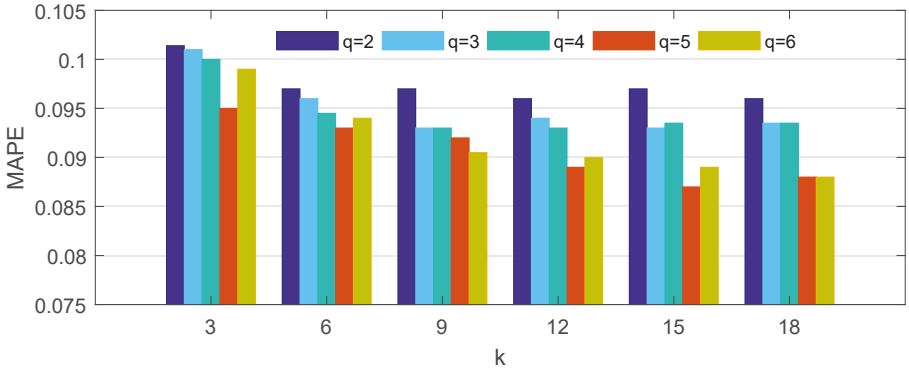

Figure 3.7 : Prediction results with different k and q values in Segment 5.

fluctuations.

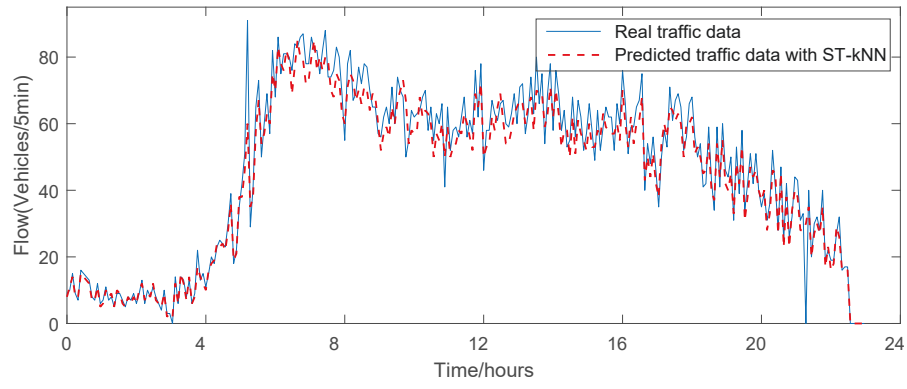

(a)

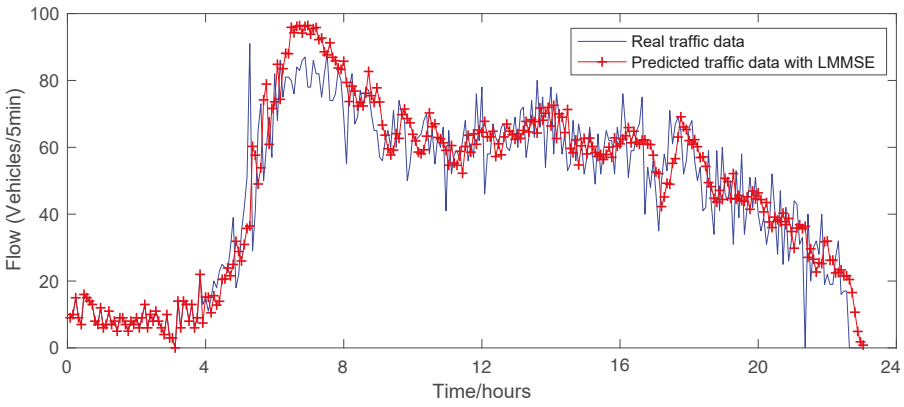

(b)

Figure 3.8 : Predicted and real traffic flow in a day in Segment 5 using (a) ST-kNN and (b) LMMSE algorithm. Time interval between the plotted samples is 5 minutes. The average MAPE values for ST-kNN and LMMSE are 0.098 and 0.1063, respectively.

Latency and Bandwidth Efficiency

Based on requirements specified by 3GPP TR 36.885 [14], we adopt $\tau_n^{\exp}(t+1) = 100$ ms and the signalling delay t^s is set to vary from 5ms to 25ms. Note that different latency values can be set for different segments in our scheme; for example, more stringent latency values such as $\tau_n^{\exp}(t+1) = 20$ ms can be used in certain safety critical cases like truck platooning. The relative latency $T(t+1)$ is obtained for each timeslot and is then averaged over all timeslots.

For comparison, we use the following two benchmark schemes. One is the conventional purely dynamic allocation scheme (DS) where the water-filling algorithm is used to allocate the total available bandwidth to each RSU in real time, with the goal of minimizing average relative latency. This corresponds to the case of $\theta = 0$ in the proposed semi-persistent scheme (SPS) and we can denote the delay as $T(t+1)|_{\theta=0,n\in\mathcal{N}}$. The other one is a purely persistent scheme (PS) where the total bandwidth is all allocated to RSUs based on predicted traffic without the following dynamic allocation. The optimal relative latency for the persistent scheme is given by

$$T(t+1) = \frac{1}{N}\sum_{n=1}^{N} \frac{B_n^{\text{req}}(t+1)}{\min\left\{\theta_{\max}\hat{b}_n^p(t+1), B_n^{\text{req}}(t+1)\right\}}, \tag{3.22}$$

where $\theta_{\max} = \dfrac{B}{\sum_{n=1}^{N}\hat{b}_n^p(t+1)}$.

The total bandwidth B may also be optimized, which is beyond the scope of this study. Here, we simply set it as a scaled value of the statistical mean of the total requested bandwidth, i.e., $B = a\mathrm{E}_t(\sum_n B_n^{\text{req}}(t))$, where a is the scalar close to 1, and $\mathrm{E}_t(\cdot)$ denotes the averaging operation over time. We will study its impact on the performance of the proposed scheme and on the coefficient θ shortly.

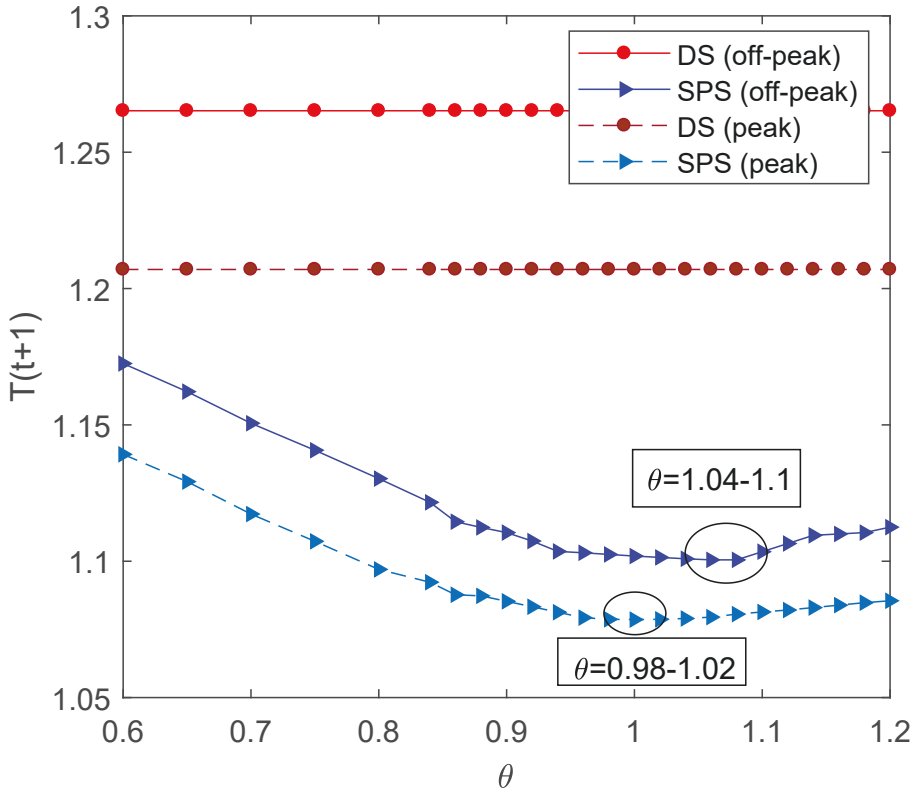

Figure 3.9 : Average relative latency versus θ for DS and SPS during off-peak and peak time. For PS, the averaged latencies are 1.1650 and 1.1404, respectively. Signalling latency is $t^s = 15$ms and $a = 0.9$.

We also define another performance metric, the bandwidth efficiency as

$$\rho = \frac{\sum_{n=1}^{N} \min\left\{B_n^p(t+1) + B_n^d(t+1), B_n^{\text{req}}(t+1)\right\}}{B}, \tag{3.23}$$

which characterizes the efficiency of bandwidth usage.

We first study whether there is an optimal θ that minimizes the overall latency for the proposed scheme. Figs. 3.9 and 3.10 present the average relative latency and bandwidth efficiency for the proposed SPS and DS, respectively, with $a = 0.9$ and $t^s = 15$ms. Note that the curves for DS are level straight lines as the scheme is unrelated to θ. For PS, the value of $\theta_{\max}$ is fixed in each segment. Hence we directly provide the averaged values across segments, which are 1.1650 and 1.1404 for the relative latency and 85.45% and 87.91% for the bandwidth efficiency, for off-peak

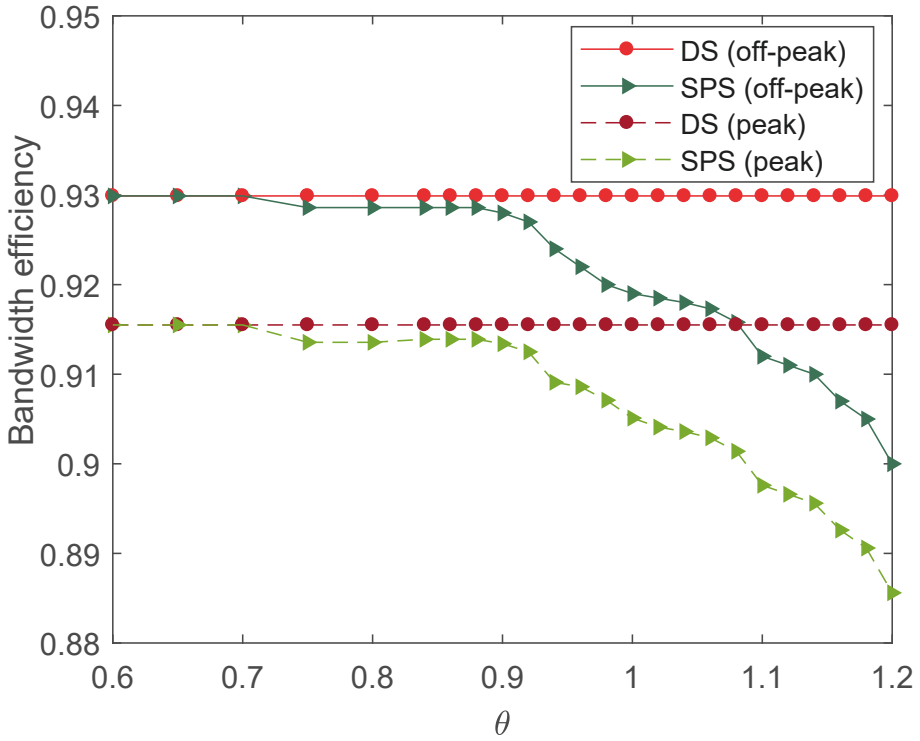

Figure 3.10 : Bandwidth efficiency versus θ for DS and SPS during off-peak and peak time. The averaged bandwidth efficiencies for PS are 85.45% and 87.91%, respectively.

and peak time respectively. We can see that the proposed SPS provides the lowest latency in the three schemes for most of the θ values ($\theta > 0.7$). Its bandwidth efficiency is always better than PS, and is close to DS when $\theta < 0.9$ and then the gap increases after that. The increased gap is due to the fact that in the proposed scheme, the allocated persistent bandwidth grows with θ increasing, which causes $B_n^p(t+1) > B_n^{\text{req}}(t+1)$ for some segments. We can also observe that the latency curves for the proposed scheme are somewhat convex, with optimal values of θ in the range of approximately $[1.04, 1.1]$ and $[0.98, 1.2]$, respectively.

In Fig. 3.11, we further show the bar-plot for the optimal values of θ for different values of B through varying the scalar a. It is clear that the ranges of optimal θ increase consistently with a increasing.

In Fig. 3.12, we demonstrate how the average relative delay varies with the

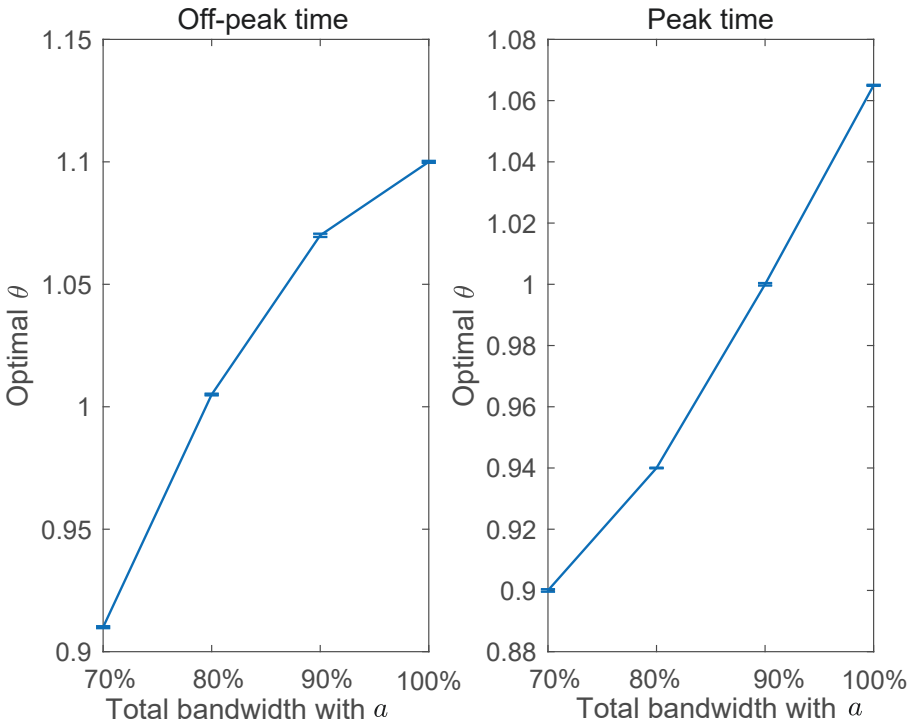

Figure 3.11 : Optimal θ values for different total bandwidth $B = a\mathrm{E}_t(\sum_n B_n^{\mathrm{req}}(t))$ for SPS.

total bandwidth. For the proposed semi-persistent scheme, we present the results for the cases where both the optimal θ and $\theta = a$ are used. The proposed SPS achieves consistently lower latency than the two benchmark schemes. With $a = 1$, the achieved average latency is only 5% more than the expected one. The latency gaps between the two values of θ are also small, which indicates that $\theta = a$ can be simply used as a rule-of-thumb for the proposed scheme.

Finally, we evaluate how the latency varies with the relative signalling delay t_n^s for the three schemes. The simulation results are presented in Fig. 3.13, where the optimal value of θ is used in the SPS. As expected, the relative latency increases linearly with t_n^s for the DS and it remains as a constant for the PS. Across the simulated range of t_n^s, the proposed SPS grows slowly with t_n^s increasing, and always achieves the lowest latency. The bandwidth efficiency is unrelated to the signalling delay and therefore is not presented.

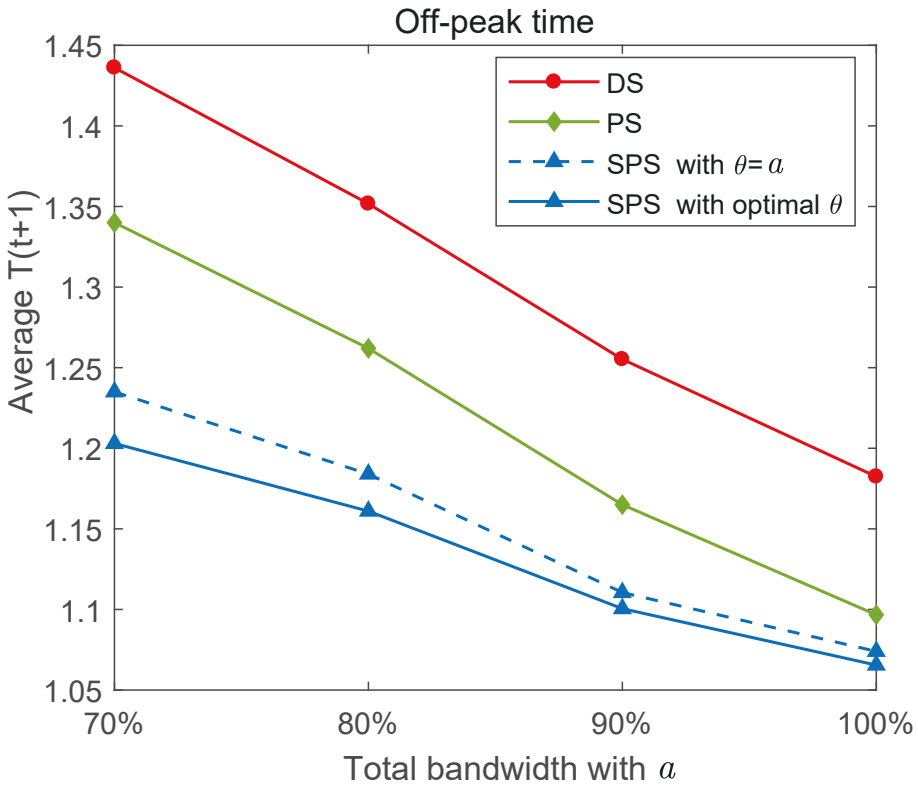

(a)

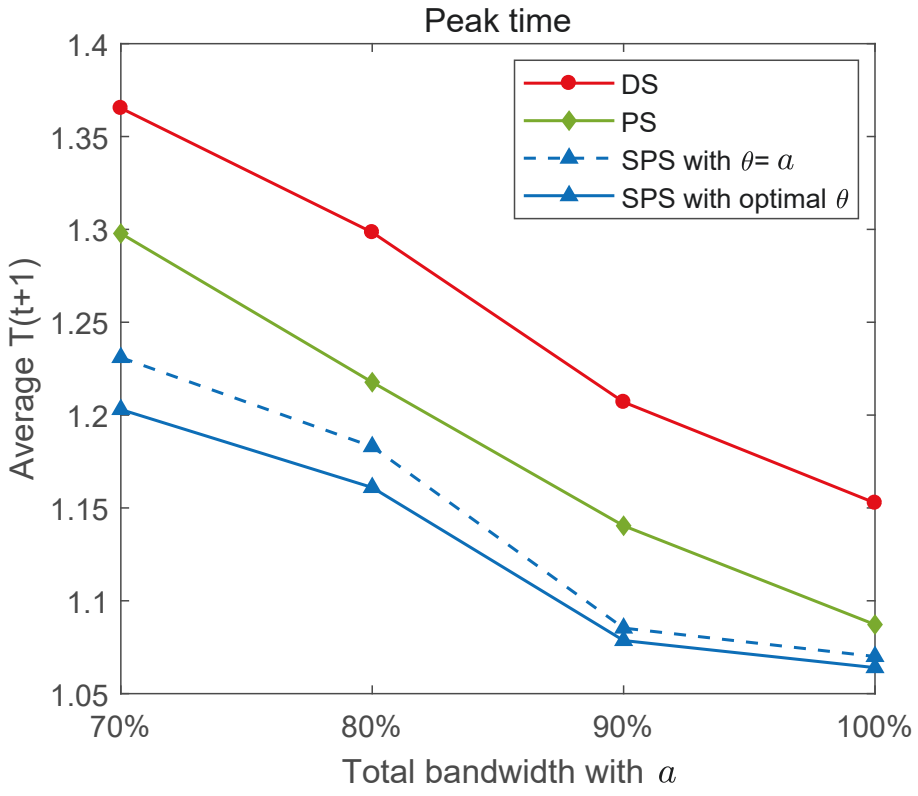

(b)

Figure 3.12 : Variation of average relative latency with the total bandwidth. Signalling delay is set as 15 ms.

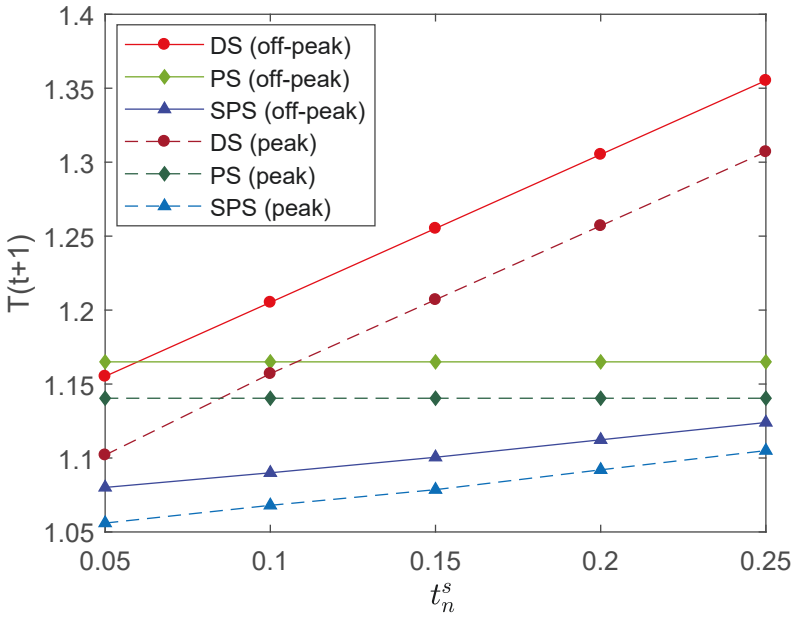

Figure 3.13 : The average relative time with varying relative signalling delay for three resource allocation schemes, where $\theta = 1.06$ and $\theta = 0.98$ for off-peak and peak time, respectively.

3.2 Latency-Constrained Semi-persistent Resource Allocation Scheme in Two-tier Cellular Networks

In this section, considering another system model, We introduce a non-model-based LMMSE predictor for predicting vehicular network traffic and use the semi-persistent resource allocation scheme for V2X communications with strict latency requirements. A cost function for the total bandwidth for the area of interest is developed under latency constraints for resource allocation.

3.2.1 System Model and Problem Formation

In this part, we present the system model, and then formulate the cost function of the total bandwidth.

System Model

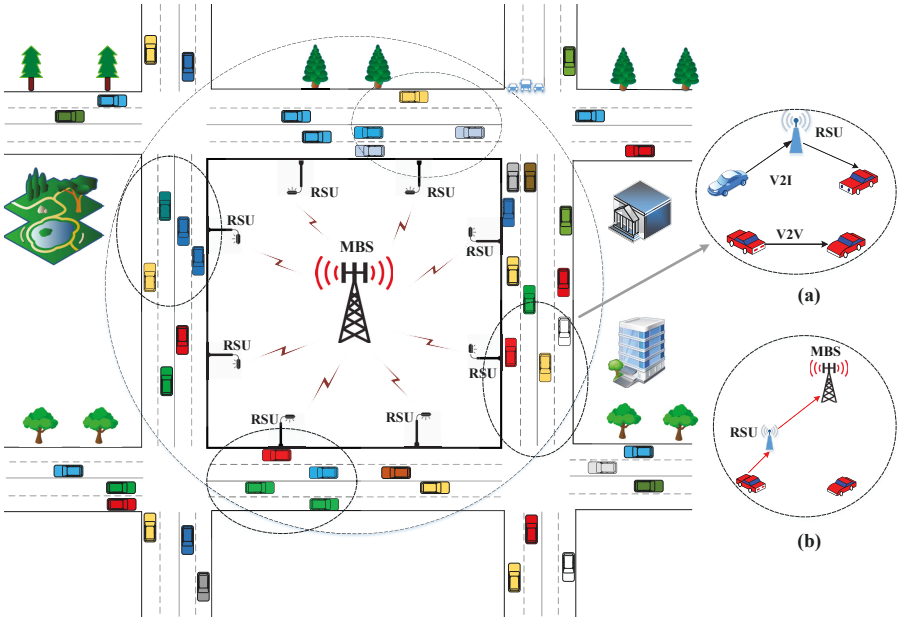

Figure 3.14 : Two-tier cellular architecture and the segmented road model.

As shown in Fig. 3.14, we consider an urban cellular V2X network with a two-tier architecture where a MBS is in the first tier and several RSUs are in the second tier. We divide the area of interest into N segments, where each RSU supports the communication of vehicles in each segment. Denote the segment set as $\mathcal{N} = \{1, 2, ..., N\}$. Assume that MBS provides centralized control over network resource for RSUs, and each RSU is directly responsible for providing access to vehicles in the V2I communication mode, or do local resource allocation for vehicles in the mode of direct V2V communications within its segment as shown in the subfigure Fig. 3.14 (a). In the two-tier heterogeneous network, purely dynamic resource allocation will incur delay due to resource requests and confirmation from all vehicular users. As shown in Fig. 3.14 (b), each vehicle user who wants to communicate with others needs to send a request to MBS via RSU.

In this part, we mainly investigate bandwidth allocation across segments by using

the proposed semi-persistent scheme in the area. Assume that there is no frequency reuse and orthogonal frequency channels are allocated across segments.

Note that our prediction is only for the mean traffic for one time period of T_s, and hence the resource pre-allocation is applied every T_s seconds. Real-time traffic request and dynamic allocation then happens many times during the T_s seconds. Assume that we are at time tT_s, and are now processing the resource allocation problem for the next time period from tT_s to $(t+1)T_s$. For simplicity, we use $t+1$ to represent this period. We now define some symbols and rules as follows:

- The dynamic bandwidth allocated to n-th segment for $t+1$ is $B_n^d(t+1)$, where $B^D = \sum_{n=1}^{N} B_n^d(t+1)$.
- When $B_n^p(t+1) < B_n^{\text{req}}(t+1)$, some vehicle users in the n-th segment will request dynamic resources from the MBS via RSU.
- The transmission latency requirements of vehicular users in the n-th segment at time $t+1$ is t_n^r and a signalling latency t_n^s will be introduced for vehicular users who need dynamic allocation.

Formulation of the Cost Function

Now, we formulate a cost function for the total required bandwidth in the area of interest. Our main objective is to minimize the total bandwidth under the transmission latency constraints of vehicular users. Based on the proposed semi-persistent scheme, the total required bandwidth can be expressed as

$$B(t+1) = \sum_{n=1}^{N} [B_n^p(t+1) + B_n^d(t+1)]. \tag{3.24}$$

Therefore, the cost funtion can be defined by

$$\begin{aligned} \min_{\{t_n\}_{n=1}^{N}} \quad & B(t+1) \\ \text{subject to} \quad & 0 < t_n^r \leq T_n^r, \end{aligned} \tag{3.25}$$

where T_n^r is the threshold of latency for vehicular communications in the n-th segment.

3.2.2 LMMSE Predictor for Network Traffic and Optimization of Cost Function

LMMSE Predictor for Persistent Allocation

Network traffic exhibits high correlation in short timescales and long-range dependence over segments, and such correlation and dependence can be well exploited for traffic prediction. Here, we introduce an LMMSE predictor, which is widely used for channel estimation and traffic prediction [103, 104].

Let $b(t)$ be the average network traffic in the $[(t-1)T_s, tT_s]$ time period, where T_s is the interval of observations. We propose the following M-coefficients linear predictor

$$\hat{b}(t+1) = \sum_{k=0}^{M-1} a(k) b(t-k) \tag{3.26}$$

for predicting the mean network traffic one sample ahead of the current one, where

$a_0, a_1, ..., a_{M-1}$ are the LMMSE coefficients. These coefficients can be obtained as

$$[a(0)\ a(1)\ ...\ a(M-1)] = [R(1)\ R(2)\ ...\ R(L)]\ \mathbf{R}_t^{\dagger},$$

$$\mathbf{R}_t = \begin{bmatrix} R(0) & R(1) & ... & R(L-1) \\ R(1) & R(0) & ... & R(L-2) \\ ... & ... & ... & ... \\ R(M-1) & R(M-2) & ... & R(L-M) \end{bmatrix}, \tag{3.27}$$

where $L \geq M$, the superscript † denotes the pseudo-inverse of a matrix, $\mathbf{R}_t$ is the autocorrelation matrix at time t with

$$R(i) = \frac{1}{M} \sum_{t=i+1}^{M+i} b(t)b(t-i), 0 \leq i \leq M-1. \tag{3.28}$$

According to the predicted network traffic, the MBS allocates persistent bandwidth to each segment. Here, we introduce a scaling factor θ instead of directly using the predicted value to allocate the bandwidth to segments, and the pre-allocated persistent bandwidth for the n-th segment is given by

$$B_n^p(t+1) = \theta \hat{b}_n(t+1). \tag{3.29}$$

The reason we introduce θ here is that there will be gaps between the predicted and real values. Therefore, an appropriate θ is helpful for minimizing the total bandwidth for the area of interest. In Section 3.2.3, we will investigate the optimal θ numerically.

Minimization of Total Bandwidth

After allocating the persistent bandwidth, we now need to complete dynamic allocation in real time. With a given θ, our goal is to find the optimal dynamic

allocation $B_n^d(t+1)$ based on the actually requested bandwidth $B_n^{\text{req}}(t+1)$ and the latency threshold. Note that, in the case of $B_n^p(t+1) \geq B_n^{\text{req}}(t+1)$, the allocated persistent bandwidth can already meet the latency requirement of vehicular communications. Let $\mathcal{V}$ denote the index sets of the segments where $B_n^p(t+1) < B_n^{\text{req}}(t+1)$. The size of the sets is denoted as V. Then we can rewrite (3.24) as

$$B(t+1) = \theta \sum_{n=1}^{N} \hat{b}_n(t+1) + \sum_{v=1}^{V} B_v^d(t+1) \tag{3.30}$$

According to the Shannon's capacity formula, the transmission rate of a vehicular communication link is $r = B\log(1+\text{SNR})$, where B denotes the channel bandwidth. Assume that b^{req} bits need to be transmitted over one link. Thus, the transmission delay can be expressed by $t = \dfrac{b^{\text{req}}}{B\log(1+SNR)}$. It is obvious that the transmission delay is inversely proportional to the bandwidth. Therefore, we define the relationship between transmission delay and bandwidth as $t_n = \dfrac{c_n}{B_n}$. Thus, we can obtain

$$t_v^r = \frac{c_v}{B_v^{req}(t+1) - B_v^p(t+1)}, \forall v \in V. \tag{3.31}$$

For the v-th segment, the transmission time needs to meet the following relationship based on the constraints of the latency

$$t_v^r - t_v^s = \frac{c_v}{B_v^d(t+1)}. \tag{3.32}$$

By substituting (3.31) into (3.32), the allocated dynamic bandwidth can be expressed by $B_v^d(t+1) = \dfrac{t_v^r}{t_v^r - t_v^s}[B_v^{req}(t+1) - B_v^p(t+1)]$. We then rewrite (3.30) as

$$B(t+1) = \theta \sum_{n=1}^{N} \hat{b}_n(t+1) + \sum_{v=1}^{V} \frac{t_v^r}{t_v^r - t_v^s}[B_v^{\text{req}}(t+1) - B_v^p(t+1)]. \tag{3.33}$$

With a given θ and the constraint $0 < t_v^r \leq T_v^r$, $B_v^d(t+1)$ obtains its minimum

value when $t_v^r = T_v^r$. The minimum is given by

$$B_{op}(t+1) = \theta \sum_{n=1}^{N} \hat{b}_n(t+1) + \sum_{v=1}^{V} \frac{T_v^r}{T_v^r - t_v^s}[B_v^{req}(t+1) - B_v^p(t+1)]. \tag{3.34}$$

3.2.3 Simulation Results

In this section, we present simulation results for the proposed semi-persistent resource allocation scheme (SPS) and demonstrate its performance based on two types of data sets. One data set is generated from simulated Autoregressive (AR) process, and the other is from real measured traffic flow data.

For comparison, we also provide results for the conventional purely dynamic resource allocation scheme (DS), which allocates bandwidth based on the latency requirements in real time. The minimum total bandwidth for DS is given by

$$B_{op}^D(t+1) = \sum_{n=1}^{N} \frac{T_n^r}{T_n^r - t_n^s} B_n^{req}(t+1). \tag{3.35}$$

In order to evaluate the performance of proposed prediction model LMMSE, we define and use Mean Absolute Percent Error (MAPE) as a performance metric

$$\text{MAPE} = \frac{1}{n} \sum_{j=1}^{n} \left| \frac{\hat{b}_j - b_j}{b_j} \right|. \tag{3.36}$$

Larger MAPE means worse prediction performance.

Simulation Results based on AR Model

Firstly, we generate the average bandwidth needs using an AR model with coefficients $a_i = \exp(r * i), i = 1, 2, 3$ and Gaussian noise with variance 10^{-4}. Let the prediction interval be $T_s = 5$s. Denote the generated average bandwidth for $[tT_s, (t+1)T_s]$ as $\overline{B}_n^{req}(t+1)$. We generate 8 sets of data (i.e., $N = 8$) based on

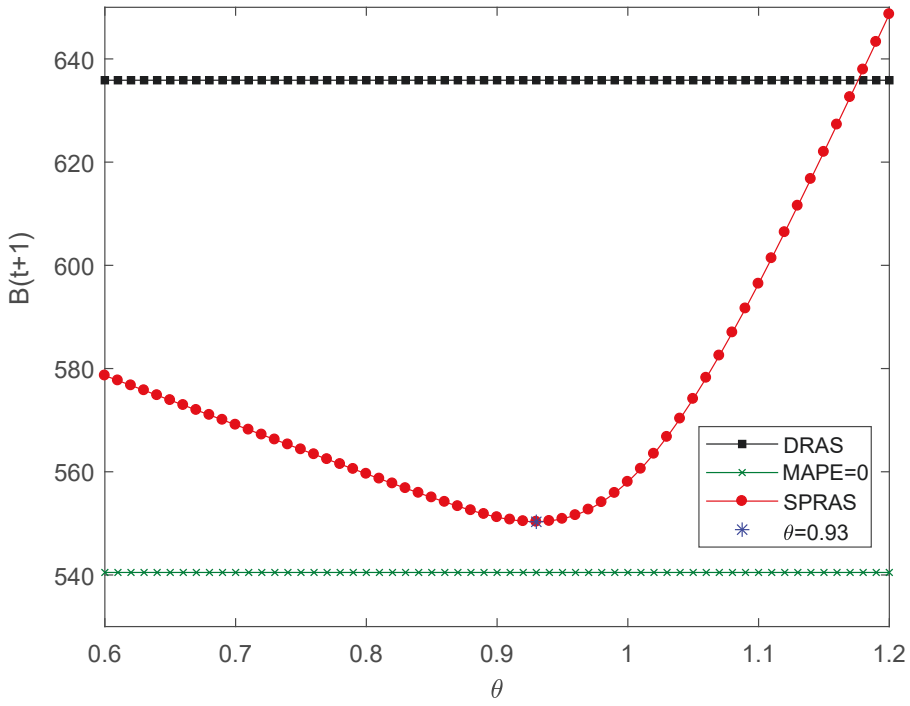

Figure 3.15 : Minimum total bandwidth versus θ for dynamic and semi-persistent schemes; MAPE=5.63%; $t^s = 15$ms.

different values of r ($r = -0.95, -1, -1.05, -1.1, -1.15, -1.2, -1.25, 1.3$). Each set includes 500 data samples. Using the LMMSE predictor, we can obtain the predicted bandwidth requirement for each segment, i.e., $\hat{b}(t+1)$. Based on the predicted average traffic, persistent bandwidth will be requested and pre-allocated in advance.

On the assumption that the actual bandwidth requirement in each 2s period follows the Gaussian distribution with mean $\overline{B}_n^{req}(t+1)$ and variance $0.2\overline{B}_n^{req}(t+1)$. In this study, each $5s$ interval is divided into 20 timeslots. In each timeslot, dynamic bandwidth is then requested and allocated.

According to the requirement specified by 3GPP TR 36.885 [14], we adopt 100ms as the latency threshold of vehicular communication in the simulation, i.e., $T_n^r = 100ms$ and the signalling delay t_n^s is set to vary from $5ms$ to $25ms$.

We first study whether there is an optimal θ for the proposed scheme. Fig. 3.15 presents the optimal total bandwidth for SPS and DS, respectively, with $t^s = 15$ms.

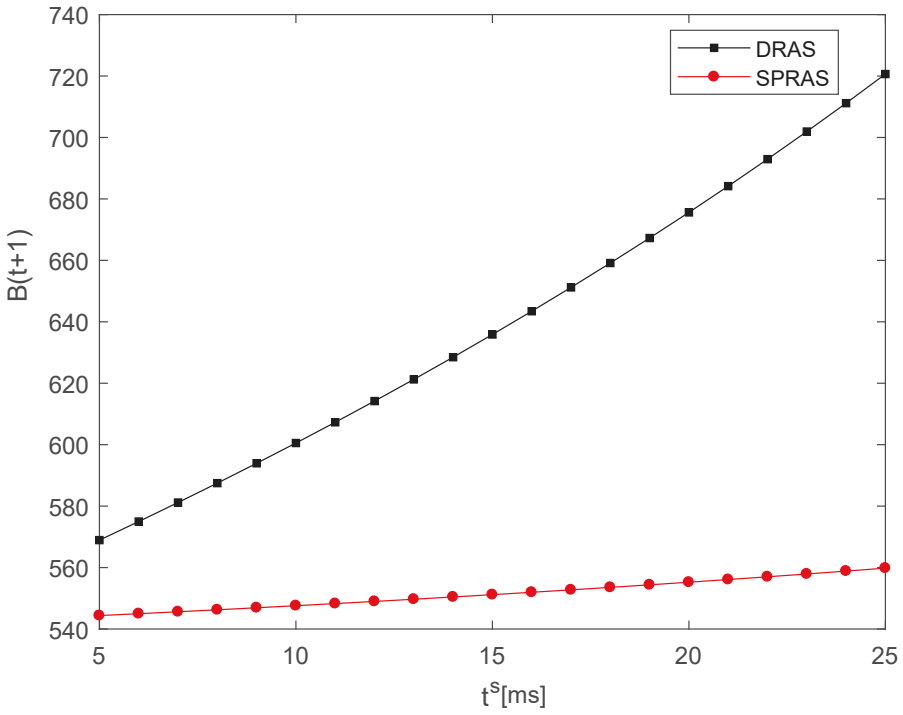

Figure 3.16 : Achieved total bandwidth versus signalling latency t^s for DS and SPS.

Note that the curve for the dynamic scheme is a level straight line as it is unrelated to θ. We can see that SPS provides smaller total bandwidth compared with DS for all of the θ values. Moreover, there exists an optimal θ ($\theta = 0.93$ in this example). The green curve is for the ideal situation (denoted as $B_{ideal}(t+1)$) where the accuracy of traffic prediction equals to 100%. When $\theta = 0.93$, the gap between $B_{op}(t+1)$ and $B_{ideal}(t+1)$ reaches the minimum value.

In Fig. 3.16, we show how the total bandwidth varies with the signalling latency t^s, where $\theta = 0.93$. As expected, the total bandwidth increases linearly with t^s for DS. Across the simulated range of t^s, the proposed SPS grows slowly with t^s increasing, and always achieves the lower total bandwidth.

In Fig. 3.17, we present the optimal values of θ for different signalling latencies for SPS. The optimal θ increases with t^s growing. The range of the optimal θ is [0.894 0.952].

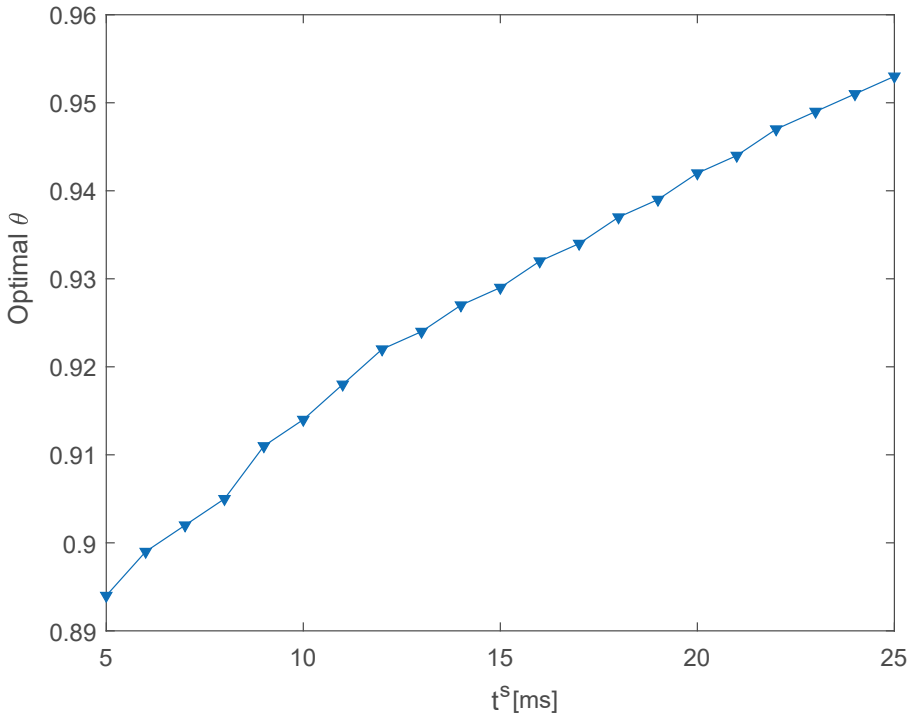

Figure 3.17 : Optimal θ with varying signalling latency t^s.

Simulation Results based on Real Traffic Flow Data

Assume there is a direct mapping between vehicle density and the network bandwidth requirements, we test the performance of the proposed scheme using real vehicle density data collected from a section of Interstate 80 (I-80) freeway located in Emeryville, California [101]. There are six traffic stations collecting the data, resembling six RSUs (i.e., $N = 6$). The record is for 10 days and the traffic flow data from the eighth day (8:00am-12am) is selected for testing. The time interval of the collected data is 30s, and hence $T_s = 30$s. Similarly, we divide T_s into 100 timeslots, and real-time bandwidth requirement in each timeslot is simulated using the same Gaussian distribution based on AR Model.

Firstly, for the prediction correlation matrix $\mathbf{R}_t$, we fix the product of the number of its rows M and the number of columns L ($M * L = 48$) to be 48, and we test the prediction performance of the LMMSE predictor. In Fig. 3.18, we compare the

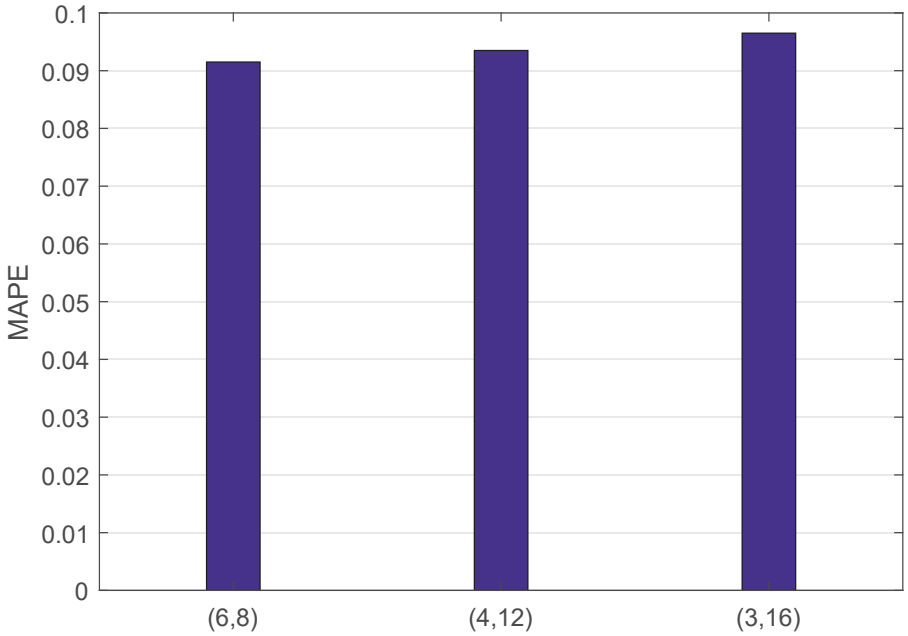

Figure 3.18 : Prediction results with different M and L values in segment 5.

MAPE values for different pairs of (M, L). The algorithm is found to achieve the best accuracy when $M = 6$ and $L = 8$.

Fig. 3.19, Fig. 3.20 and Fig. 3.21 show the simulation results for the real traffic data, in parallel to those for the artificially generated ones in Fig. 2, 3 and 4. Both of these results demonstrate the effectiveness of the proposed semi-persistent resource allocation scheme in minimizing the bandwidth usage under given time delay constraints.

3.3 Summary

In this chapter, we proposed a novel semi-persistent resource allocation scheme on top of a two-tier heterogeneous network for vehicular communications. The scheme can improve bandwidth efficiency, avoid network congestion, and reduce the processing latency significantly. Based on this scheme, we mainly study two classes of optimization problems: 1) minimizing the relative latency with the constraint of total bandwidth; 2) minimizing the total bandwidth with the constraint of trans-

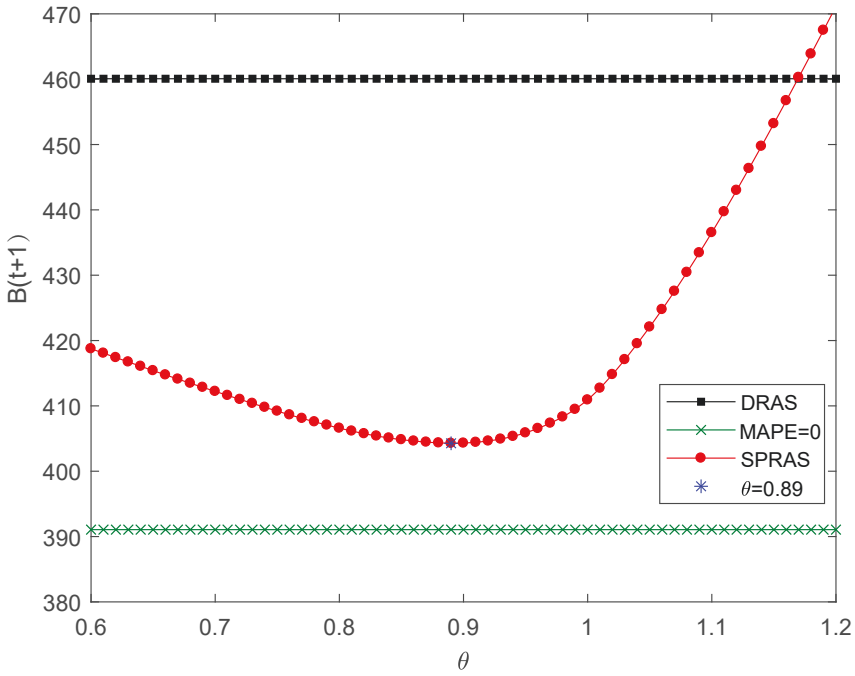

Figure 3.19 : Total bandwidth versus θ for DS and SPS using real vehicle density data; MAPE=9.15%; $t^s = 15$ms.

mission latency. For the first problems, we proposed a simple and effective ST-kNN method for predicting the short-term traffic flow by considering the correlation window in both time and spatial domains according to the vehicle moving speed. Based on the total available bandwidth and the predicted resource needs mapped from the predicted vehicle traffic, an improved water-filling algorithm is proposed to optimally allocate the resource to each RSU. By combining pre-allocation of persistent resource and dynamic resource allocation in real time, significant delay linked to resource allocation can be reduced, with negligible degradation on spectrum efficiency. Supported by simulation results with real traffic data, the proposed semi-persistent scheme over the RSU-cellular architecture is effective and promising for vehicular communications. For the second optimization problem, we use LMMSE for traffic prediction and also provid an optimal solution to the problem. Simulation is conducted for both artificially generated and real-world data, and the results validate the effectiveness of the proposed semi-persistent scheme.

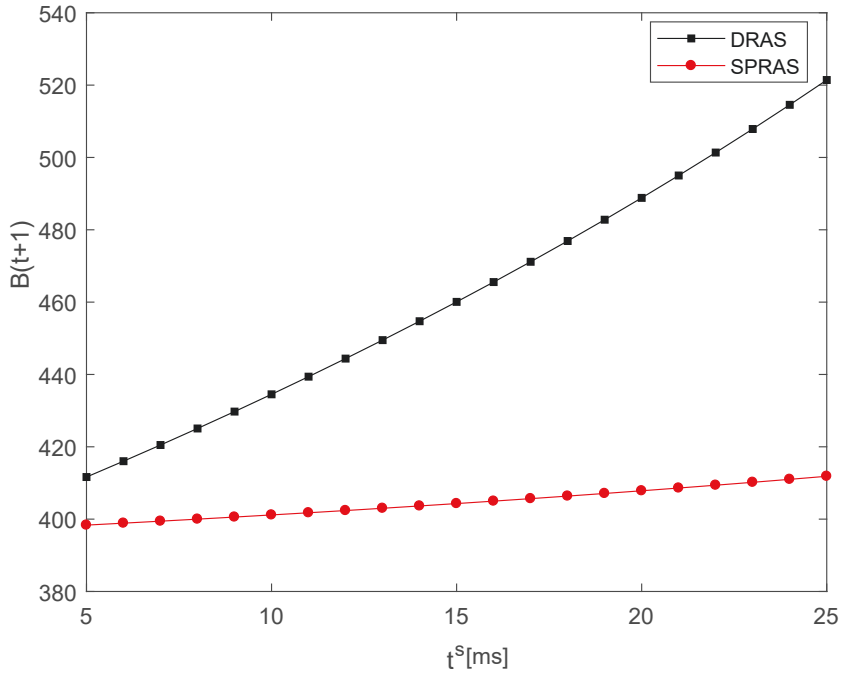

Figure 3.20 : Total bandwidth versus signalling latency t^s for DS and SPS with the real vehicle density data; $\theta = 0.89$.

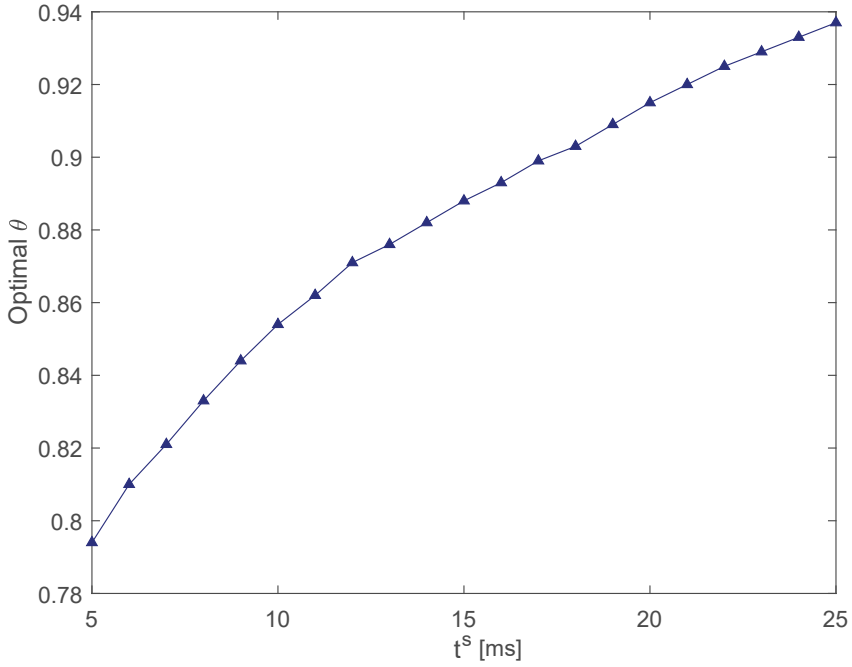

Figure 3.21 : Optimal θ versus signalling latency t^s.

Chapter 4

V-D2D Mode Selection Underlaying Two-tier Cellular Networks

In this chapter, we consider two-tier heterogeneous cellular networks. To simplify our modeling, we assume that there is one small cell formed by RSU in a macro cell and both of them operate according to a dynamic TDD scheme that natively supports multi-cell D2D-based V2V mode selection and resource allocation. The V-D2D communication pair can reuse the resource of cellular users to improve spectrum efficiency; however, that will cause a new interference (BS-to-BS) with dynamic TDD scheme. In this case, we use the character of dynamic TDD to minimize the energy consumption of the network system by adjusting UL and DL time configurations. The joint time allocation, mode selection, power control and resource allocation scheme are developed. From Shannon's capacity formula, we can know that the transmission energy per bit decreases with the transmission time [105]. Through the derivation, it shows that the joint mode selection and resource allocation problem can be formulated as a convex optimization problem. We can find the optimal time allocation and transmission mode, then we demonstrate the mode selection threshold when V-D2D communication is preferable. Finally, we give a geometrical interpretation of an energy-optimal mode selection scheme. Results show that V-D2D communication plays an important role both in the macro cell and small cell for energy consumption minimization. There is a large portion for V-D2D communication mode in the cell. Moreover, cell-edge vehicular users also benefit from V-D2D communication.

The rest of this chapter is structured as follows. Section 4.1 describes the sys-

tem model and assumptions. Then we calculate the energy consumption of three communication scenarios, present a convex optimization formulations and optimal threshold conditions for energy-efficient mode selection in section 4.2. In section 4.3, we give a geometrical interpretation of the deduced results which is supported by simulations. Section 4.4 finally concludes this part of our study and suggestions for further work.

4.1 System Overview and Problem Formulation

The considered two-tier heterogeneous cellular network where V-D2D communication is enabled with the assistance of BS is shown in Fig. 4.1. It consists of a macro BS (MBS), two vehicles which can communicate using possible modes, a RSU and two downlink traditional cellular users; all of them are denoted by 0, 1, 2, 3, c_1 and c_2, respectively. As shown in Fig. 4.1, the transmission scheduled in the two-tier cell can be realized via one of the following transmission modes:

- Mode A (Macro cellular mode): Two users use conventional cellular transmission and communicate through the MBS, i.e. V-UE$_1$ sends data to the MBS (uplink) and then the MBS forwards the data to V-UE$_2$(downlink)
- Mode B (V-D2D mode): A direct link is set up and can be used for communication between V-UE$_1$ and V-UE$_2$.
- Mode C (RSU mode): Two users within the small cell communicate through the RSU.

The main aim of our work is to develop algorithms which can determine the communication modes selection to minimize the energy cost from the perspective of both the vehicles and the overall cellular network.

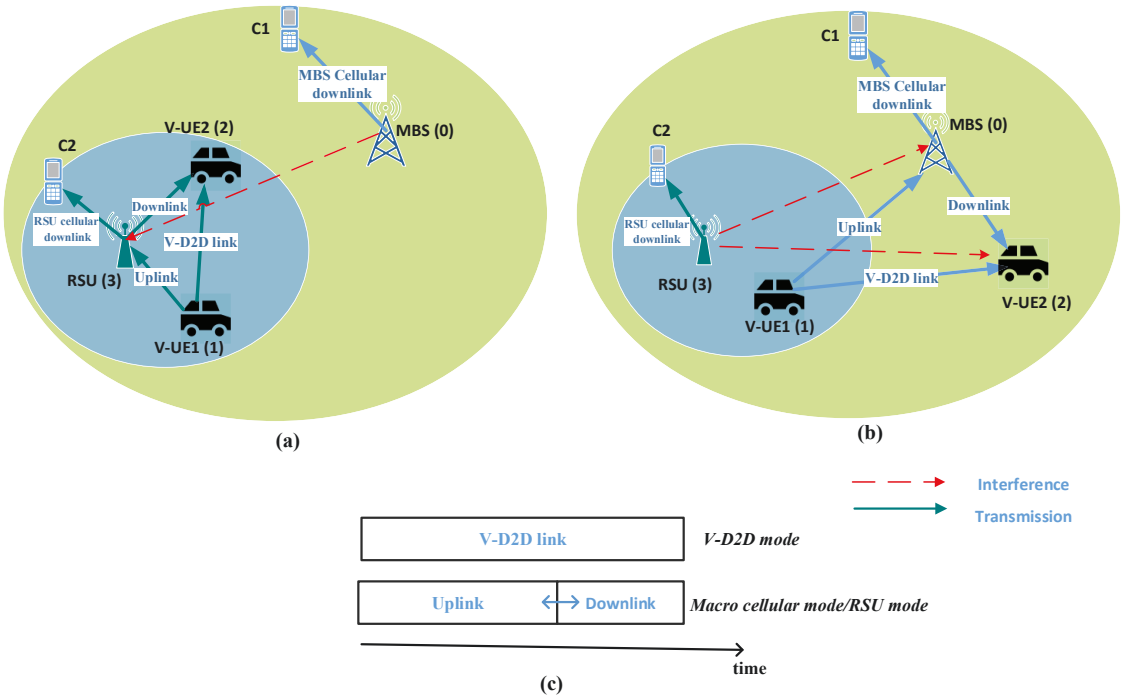

Figure 4.1 : System model for V-D2D communication underlaying two-tier heterogeneous cellular network with dynamic TDD scheme. V-UE$_1$ communicates with V-UE$_2$ via MBS, RSU or through a direct link.

In our model, we assume that the cellular base stations operate in the dynamic TDD where the uplink and downlink transmissions operate in the same bandwidth but alternate in time and time is divided into frames with duration of T seconds. In the cell, c_1 and c_2 use the orthogonal spectrum resources. As for the single communication pair (the transmitter V-UE$_1$ and the receiver V-UE$_2$), we consider a scenario of sharing downlink resource of cellular network and make the following assumptions:

- When V-UE$_1$ and V-UE$_2$ are in the coverage of the small cell, they can communicate via the RSU or communicate directly by V-D2D communication and they reuse the resource of c_1, thus V-UE$_2$ and RSU receive the interference from MBS as shown in Fig. 4.1 (a).

- When one of V-UE$_1$ and V-UE$_2$ is not in the coverage of the small cell, they can

communicate via the MBS or communicate directly by V-D2D communication. They reuse the resource of c_2, thus V-UE$_2$ and MBS receive the interference from RSU as shown in Fig. 4.1 (b).

- The two downlinks from MBS to c_1 and from RSU to c_2 keep transmitting data in the full frame time T and have the constant transmit power, p_{0c_1} and p_{3c_2} respectively. Furthermore, the positions of c_1 and c_2 are far away from the transmitters, so we don't consider the interference that they receive.

For the communication between V-UE$_1$ and V-UE$_2$, we assume that the portions of time allocated to the uplink and downlink can be adjusted dynamically. V-D2D communication can use the whole frame for its transmission, see Fig. 4.1 (c). The instantaneous rate r_{ij} between V-UE$_1$ and V-UE$_2$ based on the Shannon's capacity formula are given by

$$r_{ij}(p_{ij}, G_{ij}, I_j) = W \log(1 + \frac{p_{ij}G_{ij}}{\sigma^2 + I_j}), \tag{4.1}$$

where W denotes the channel bandwidth, and σ^2 is the noise power. G_{ij} is the channel gain between the transmitter-i and the receiver-j, p_{ij} stands for the transmit power level used for the communication from transmitter-i to receiver-j. In addition, we assume maximum transmission power level $p_{ij}^{\max}$, and denote the corresponding instantaneous rate in (4.1) by $r_{ij}^{\max}(G_{ij})$. I_j is the interference experienced from BS (MBS or RSU) at receiver-j.

We further assume that b^{req} bits must be transmitted in each time frame from V-UE$_1$ to V-UE$_2$, which translates into a minimum rate requirement of $r^{req} = b^{req}/T$. It means when the instantaneous rate r_{ij} exceeds r^{req}, the rate requirement can be satisfied by transmitting for only a fraction of the full time. Specifically, the time

t_{ij} during which the transmitter-i transmits data to receive-j can be denoted as

$$r_{ij}t_{ij} = b^{req}. \tag{4.2}$$

Obviously, when the instantaneous rate achieves the maximum value, the required transmission time achieves a lower bound, i.e., $t_{ij} \geq b^{req}/r_{ij}^{\max}$. That also means lower values of t_{ij} would make p_{ij} exceed $p_{ij}^{\max}$, leading to a power-infeasible time allocation.

By inverting the power-rate relationship (4.1), the energy cost can be derived as

$$E_{ij}(t_{ij}) = p_{ij}t_{ij} = (\exp(\frac{\ln 2b^{req}}{Wt_{ij}}) - 1)\frac{\sigma^2 + I_j}{G_{ij}}t_{ij}, \tag{4.3}$$

which has been proved to be a convex and gradually decreasing function of the transmission duration t_{ij} in paper [105]. This implies that the minimum value of E_{ij} can be obtained when t_{ij} takes the maximum value.

4.2 Optimal Mode Selection with Energy Minimization

In this section, we will solve the mode selection problem and exploit the possibility of V-D2D communication between two vehicles compared with macro cellular mode and RSU mode to reduce the transmission energy consumption. Furthermore, extending vehicular battery lifetime, reducing gasoline consumption and CO_2 emissions are vital in green transportation systems. When we are more concerned about green transportation, reducing vehicular energy cost is more important than reducing the total network one. Hence we define the following two scenarios to develop an optional mode selection policy:

- minimizing the overall network energy consumption including vehicles and BS;
- minimizing the energy consumption of vehicular transmitters.

To achieve an optional mode selection solution, we analyze the energy costs of three different modes, and further deduce and compare their minimum energy costs. The analyses show that the energy minimization problem can be formulated as a convex optimization problem, and has an optimal solution.

4.2.1 Energy Minimization based on Macro Cellular Mode

In this mode, V-UE$_1$ and V-UE$_2$ will transmit information through MBS with two time intervals, i.e., t_{10} for the uplink and t_{02} for the downlink. Note that, the sum of transmission time including uplink and downlink cannot exceed the entire frame time T. In the dynamic TDD system, the time allocation can be adjusted. Here we are interested in the minimization of energy cost by changing the transmission time:

1) Minimizing the overall energy consumption of the network. The convex optimization problem could be formulated as the summation of the cellular uplink and downlink energy consumption as following,

$$\min_{\{t_{10},t_{02}\}} \quad E_{10}(t_{10}) + E_{02}(t_{02}) + E_{0c_1} + E_{3c_2} \tag{4.4a}$$

$$\text{subject to} \quad t_{10} + t_{02} \leq T, \tag{4.4b}$$

$$t_{10} \geq \frac{b^{req}}{r_{10}^{\max}}, t_{02} \geq \frac{b^{req}}{r_{02}^{\max}}, \tag{4.4c}$$

where E_{0c_1} is the energy cost of c_1 in the time T and $E_{0c1} = p_{0c_1}T$, E_{3c_1} is the energy cost of c_2 in the frame T and $E_{3c_2} = p_{3c_2}T$. The constraint in (4.4b) ensures that the duration of the communication based on Mode A does not exceed the frame time length T, and the constraints in (4.4c) guarantee that the transmit power does not exceed the maximum value, i.e, power feasibility. To ensure the constraints (4.4b) and (4.4c) are non-empty, we deduce that b^{req} must satisfy

$$b^{req} \leq T.\frac{r_{10}^{\max} r_{02}^{\max}}{r_{10}^{\max} + r_{02}^{\max}}. \tag{4.5}$$

Since the objective function in (4.4) is monotonically decreasing in (t_{10}, t_{02}), the optimal solution is attained when $t_{10} + t_{02} = T$. Therefore, the problem (4.4) is equivalent to the following single-variable optimization problem,

$$\min_{\{t_{02}\}} \quad E_{10}(t_{10}) + E_{02}(t_{02}) + E_{0c_1} + E_{3c_2} \tag{4.6a}$$

$$\text{subject to} \quad \frac{b^{req}}{r_{02}^{\max}} \leq t_{02} \leq T - \frac{b^{req}}{r_{10}^{\max}}, \tag{4.6b}$$

which is a solvable convex optimization problem in a single variable and can be solved easily.

2) Minimizing vehicle energy consumption. When we only consider minimizing the energy consumption of vehicles (here we disregard the energy spent by the MBS and the RSU), the optimal problem changes into $\min_{t_{02}} E_{10}(T - t_{02})$ while the constraint remains the same in (4.6b). Because $E_{10}(T - t_{02})$ is monotonically increasing with t_{02} increasing, so the objective is minimized by setting t_{02} to be its minimum value $b^{req}/r_{02}^{\max}$, which means that the MBS transmits at its maximal power. The optimal time interval of uplink transmission can be obtained

$$t_{10}^* = T - t_{02} = T - \frac{b^{req}}{r_{02}^{\max}}. \tag{4.7}$$

In addition, the minimum energy cost is

$$E_{10}(t_{10}^*) = (\exp(\frac{\ln 2 b^{req}}{W t_{10}^*}) - 1)\frac{\sigma^2 + I_0}{G_{10}} t_{10}^*, \tag{4.8}$$

where I_0 stands for the interference that the RSU receives from the MBS $I_0 = p_{3c_2} G_{30}$.

4.2.2 Energy Minimization based on V-D2D Mode

In this mode, the minimum energy needed to establish a direct communication can be determined in the following scenarios.

1) Minimizing the overall energy consumption of the network: the optimization problem can be simply determined by

$$\min_{\{t_{12}\}} \quad E_{12}(t_{12}) + E_{0c_1} + E_{3c_2} \tag{4.9a}$$

$$\text{subject to} \quad \frac{b^{req}}{r_{12}^{\max}} \leq t_{12} \leq T, \tag{4.9b}$$

Similar to Mode A, the constraints (4.9b) guarantees that the communication is power feasible and its duration can not exceed the frame length. Since the objective function in (4.9) is monotonically decreasing in t_{12} , so to obtain the minimal energy consumption, t_{12} should exploit the entire frame length T. Then the minimum energy cost in Mode B can be expressed by

$$E_{\text{V-D2D}} = (\exp(\tfrac{\ln 2 b^{req}}{WT}) - 1)\tfrac{\sigma^2 + I_2}{G_{12}} T + E_{0c_1} + E_{3c_2} \ , \tag{4.10}$$

where I_2 stands for the interference that V-UE$_2$ receives from the MBS or RSU, $I_2 = p_{0c_1} G_{02}$ or $I_2 = p_{3c_2} G_{32}$.

2) Minimizing vehicle energy consumption, the optimization problem is

$$\min_{\{t_{12}\}} \quad E_{12}(t_{12}) \tag{4.11a}$$

$$\text{subject to} \quad \frac{b^{req}}{r_{12}^{\max}} \leq t_{12} \leq T, \tag{4.11b}$$

Since the objective function in (4.11) is monotonically decreasing in t_{12} , to obtain the minimal energy consumption, t_{12} should exploit the entire frame length T. Then

the minimum energy cost is

$$E_{\text{V-D2D}} = E_{12}(T) = \left(\exp\left(\frac{\ln 2 b^{req}}{WT}\right) - 1\right)\frac{\sigma^2 + I_2}{G_{12}}T. \tag{4.12}$$

4.2.3 Energy Minimization based on RSU Mode

Here, V-UE$_1$ and V-UE$_2$ will transmit information through RSU with two time intervals (t_{13}, t_{32}) , t_{13} for the uplink and t_{32} for the downlink. Here we focus on the minimization of energy cost by adjusting the transmission time, and similar to Mode A, we get the conclusion as following:

1) Minimizing the overall energy consumption: the optimization problem can be denoted as

$$\min_{\{t_{13}, t_{32}\}} \quad E_{13}(t_{13}) + E_{32}(t_{32}) + E_{0c_1} + E_{3c_2} \tag{4.13a}$$

$$\text{subject to} \quad t_{13} + t_{32} \leq T, \tag{4.13b}$$

$$t_{13} \geq \frac{b^{req}}{r_{13}^{\max}}, t_{32} \geq \frac{b^{req}}{r_{32}^{\max}}, \tag{4.13c}$$

To ensure the power feasibility, b^{req} must satisfy

$$b^{req} \leq T.\frac{r_{13}^{\max} r_{32}^{\max}}{r_{13}^{\max} + r_{32}^{\max}}. \tag{4.14}$$

2) Minimizing vehicle energy consumption: the minimum energy cost is

$$E_{13}(t_{13}^*) = \left(\exp\left(\frac{\ln 2 b^{req}}{W t_{13}^*}\right) - 1\right)\frac{\sigma^2 + I_3}{G_{13}}t_{13}^*, \tag{4.15}$$

where $t_{13}^* = T - \frac{b^{req}}{r_{32}^{\max}}$, and I_3 stands for the interference that MBS receives from the RSU, $I_3 = p_{0c_1} G_{03}$.

4.2.4 Mode Selection Scheme

We have deduced the minimum energy consumptions for three different communication modes in above, and then the optimal selection scheme is simply to use the communication mode which spends the smallest energy. There are two mode selection scenarios for the single pair V-UE$_1$ and V-UE$_2$.

i) In the small cell, there are two communication modes which can be chosen: Mode B and Mode C. The mode selection solution has the intuitive form that V-D2D mode is preferred when the direct link can be strong enough, i.e.,

$$G_{12} \geq H(G_{13}, G_{32}). \tag{4.16}$$

The threshold $H(G_{13}, G_{32})$ depends on the uplink and downlink gains of RSU, and whether we want to minimize the total system energy consumption, or only the energy cost of the vehicles.

From the overall network perspective, a direct communication should be established if $E_{\text{V-D2D}}$ in (4.10) is smaller than the minimum amount of energy needed for the Mode B, derived from the solution to problem (4.13). Let (t_{13}^*, t_{32}^*) denote the optimal time allocation in problem (4.13). Thus, when V-D2D mode (Mode B) is more energy efficient, the threshold is $H(G_{13}, G_{32}) = \frac{\left(\exp\left(\frac{\ln 2b^{req}}{WT}\right)-1\right)\left(\sigma^2+p_{0c_1}G_{02}\right)T}{E_{13}(t_{13}^*)+E_{32}(t_{32}^*)}$.

When we only care about the energy consumption by vehicles, the threshold condition that D2D communication is more efficient becomes

$$H(G_{13}, G_{32}) = n(G_{32})G_{13}, \tag{4.17}$$

where $n\left(G_{32}\right) = \frac{\left(\exp\left(\frac{\ln 2b^{req}}{WT}\right)-1\right)\left(\sigma^2+p_{0c_1}G_{02}\right)T}{E_{13}\left(T-\frac{b^{req}}{r_{32}^{\max}(G_{32})}\right)}$.

We can find that even though we neglect the energy consumption for the down-

link, G_{32} still plays a role in terms of determining mode selection.

ii) In the macro cell, there are also two communication modes which can be chosen: Mode A and Mode B. The mode selection policy form that D2D mode is preferred becomes

$$G_{12} \geq Z(G_{10}, G_{02}). \tag{4.18}$$

Similar to i), from the overall network perspective, the threshold when V-D2D mode (Mode B) is more energy efficient is $Z(G_{10}, G_{02}) = \frac{\left(\exp\left(\frac{\ln 2b^{req}}{WT}\right)-1\right)\left(\sigma^2+p_{3c_2}G_{32}\right)T}{E_{10}\left(t_{10}^*\right)+E_{02}\left(t_{02}^*\right)}$.

From the vehicular device perspective, the threshold condition that V-D2D communication is more efficient becomes

$$Z(G_{10}, G_{02}) = g(G_{02})G_{10}, \tag{4.19}$$

where $g\left(G_{02}\right) = \frac{\left(\exp\left(\frac{\ln 2b^{req}}{WT}\right)-1\right)\left(\sigma^2+p_{3c_2}G_{32}\right)T}{E_{10}\left(T-\frac{b^{req}}{r_{02}^{\max}(G_{02})}\right)}$. The G_{02} also effects the energy cost of the vehicle even though we neglect the energy consumption of the downlink.

4.3 Analysis and Simulation Results

4.3.1 Simulation Setup

This section shows the simulation results to demonstrate the geometrical interpretation about the optimal mode selection scheme. We consider two-tier heterogeneous cell with a MBS, a RSU, two cellular users, and one V2V pair. We assume that the channel gains follow a conventional path-loss model $G_{ij} = G_0 D_{ij}^{-\alpha}$, where D_{ij} is the distance between vehicular user-i and vehicular user-j. G_0 is the path gain per meter, and α is the path-loss exponent, normally in the range of 2 to 6. For simplicity, we focus on the vehicle energy consumption, and re-write (4.17) and

Table 4.1 : Simulation parameters.

Parameter	**Value**
Carrier Frequency	1 GHz
Macro Cell Radius	500 m
Small Cell Radius	200 m
Channel Bandwidth (W)	6 MHz
Noise power spectral density	-174 dBm/Hz
Path-Loss exponent (α)	4
Path gain at reference distance of 1 m	$5.7 \cdot 10^{-4}$
Max transmit power for macro BS	40 W
Max transmit power for small cell BS	8 W
Max transmit power for V-UE$_1$	0.25 W
Transmit power of Downlink c_1 (p_{0c_1})	10 W
Transmit power of Downlink c_2 (p_{3c_2})	2 W
Time frame duration T	1 time unit

(4.19) in terms of distance as

$$\begin{cases} D_{12} \leq \bar{n}(D_{32})D_{13}, & \text{(4.20a)} \\ D_{12} \leq \bar{g}(D_{02})D_{10}, & \text{(4.20b)} \end{cases}$$

where $\bar{n}(D_{32}) \triangleq \left[n(G_0 D_{32}^{-\alpha})^{-(1/\alpha)}\right]$ and $\bar{g}(D_{02}) \triangleq \left[g(G_0 D_{02}^{-\alpha})^{-(1/\alpha)}\right]$. To characterize the region where V-D2D mode and RSU mode are preferable, we fix the position of V-UE$_1$ in the small cell, hence, D_{10} and D_{13} are fixed. Meanwhile, we vary the position of V-UE$_2$ along a circle centered at the small cell base station and macro base station respectively. Conditions (4.20) state that V-D2D mode is preferable when V-UE$_2$ is located at the intersection of this circle and disc centered at the position of V-UE$_1$ (with radius $\bar{n}(D_{32})D_{13}$ or $\bar{g}(D_{02})D_{10}$).

4.3.2 Results

Now, we present the simulation results obtained with the practical system parameters summarized in Table I. The data requirement b^{req} is set to guarantee power feasibility for the mode A and mode B; we set $b^{req} = kT\frac{r_{10}^{\max} r_{02}^{\max}}{r_{10}^{\max}+r_{02}^{\max}}$ and

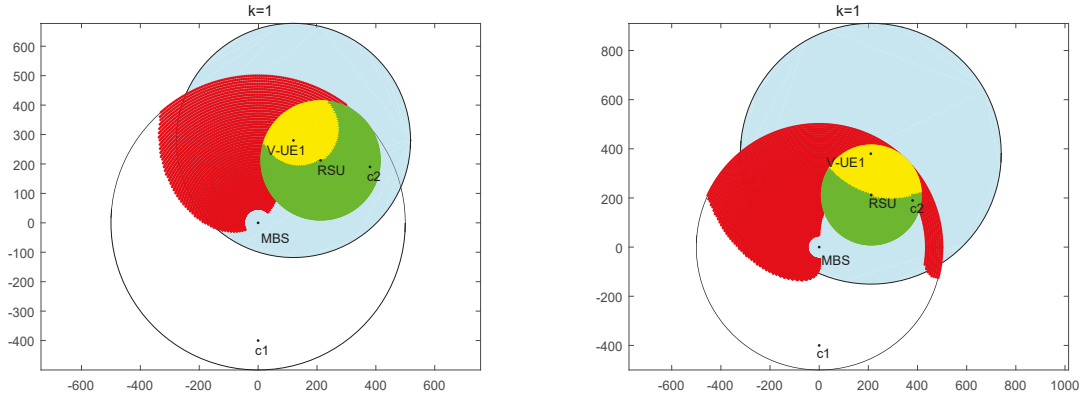

(a) (b)

Figure 4.2 : V-D2D mode and RSU mode optimality area when minimizing the vehicles energy cost.

$b^{req} = kT\frac{r_{13}^{\max} r_{32}^{\max}}{r_{13}^{\max}+r_{32}^{\max}}$, where $k \in [0,1]$, and we choose the smaller one of b^{req} when V-UE$_1$ and V-UE$_2$ communicate in the small cell.

In the presented figure, the blue area represents V-D2D power feasibility area within which V-UE$_1$ can fulfill the rate requirement in V-D2D mode with $p_{12} \leq p_{12}^{\max}$. The red area represents the V-D2D optimality area in which V-D2D mode is more energy efficient than the macro cellular mode, and the yellow area stands for the V-D2D optimality area in which V-D2D mode is more energy efficient than the RSU mode. Hence, intersection of the two areas represents the location of V-UE$_2$ where V-D2D mode is both power feasible and energy-optimal. We also gain the green area in which RSU mode is more energy efficient.

Fig. 4.2 shows the V-D2D optimality area when the vehicle energy is the primary concern. We consider two different locations of V-UE$_1$ and $k = 1$. When V-UE$_1$ stays in the edge of the macro cell and small cell, we can see that the portion of D2D optimality area increases. It is worth noting that cell-edge users can benefit from V-D2D communication, achieving the required session rate with much lower energy cost.

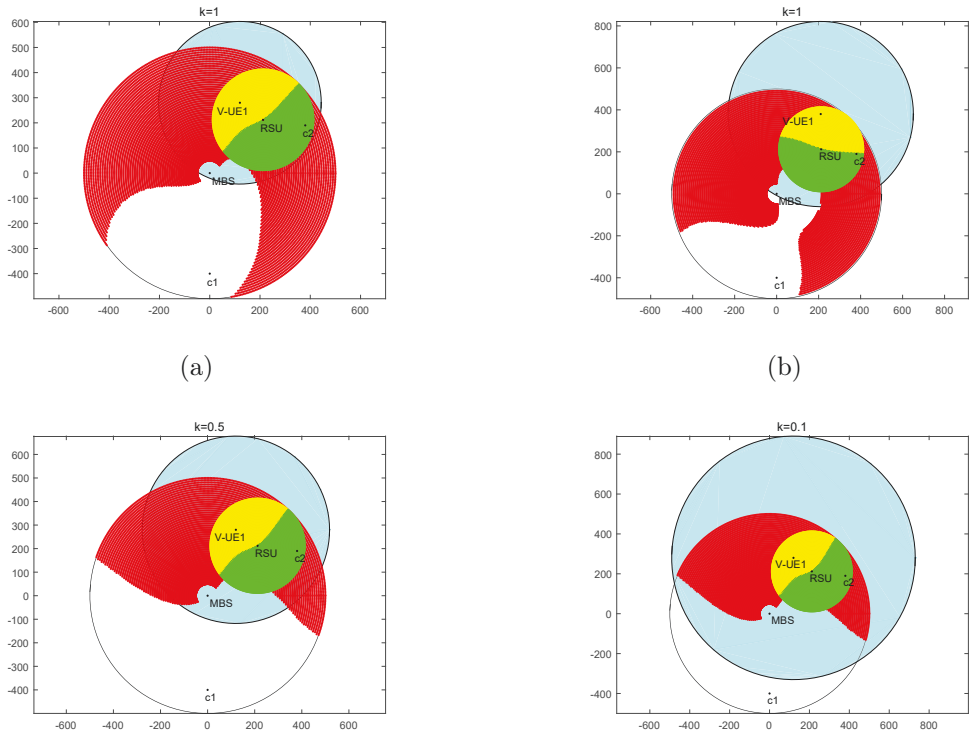

Figure 4.3 : V-D2D mode and RSU mode optimality area when minimizing the overall network energy cost.

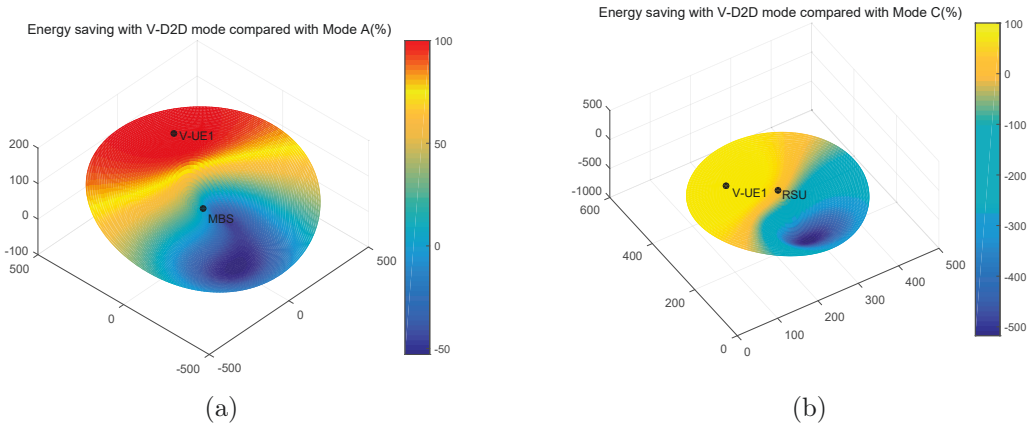

Figure 4.4 : Percentage of energy saved in V-D2D mode compared with Mode A and Mode C.

Fig. 4.3 (a) and (b) represent the V-D2D optimality area when the overall network energy cost is the primary concern. Interestingly, V-D2D communication is preferable in a large percentage of macro cell and small cell, almost close to half the cell. Fig. 4.4 (a) and (b) show the reduction of energy in V-D2D mode compared with Mode A and Mode C. When V-UE_1 and UE_2 are closer, the energy saving is significant. Fig. 4.3 (a), (c) and (d) show the impact of rate requirement on the V-D2D optimality area for the overall network energy saving problem. We fix the position of V-UE_1, and consider three different values of the target rate by choosing $k = 1$, $k = 0.5$, $k = 0.1$. This shows that the V-D2D feasibility area clearly increases as b^{req} reduces, the corresponding V-D2D optimality area decreases.

4.4 Summary

In this chapter, we have studied the optimal mode selection with energy consumption minimization for V-D2D communication underlaying a two-tier heterogeneous cellular network, considering a dynamic TDD scheme. In particular, we have discussed the problem with two objectives: minimizing the energy consumption of the overall network and the vehicles energy only. Simulation results show that the D2D optimality area is strongly affected by the network parameters. In some cases, V-D2D communication is preferable in a large portion of the macro cell and small cell.

Chapter 5

Interference Characterization and Power Optimization for Automotive Radar with Directional Antenna

In this chapter, applying the stochastic geometry model, we develop a signal and interference power analysis framework for automotive radars, by considering both front-mounted (FR) and side-mounted radars (SR), and directional antenna radiation patterns. We first study a two-lane scenario and then extend the work to a multi-lane one. Using the stochastic geometry model to formulate the vehicular location distribution in a road segment, we derive the expressions for the mean power of effective echo signals and the interference, taking into consideration the frequency reuse factor, vehicle density, and radiation patterns for FR and SR. Assuming a Gaussian waveform for the antenna radiation pattern, we provide closed-form expressions for their mean interference power. We then investigate how to minimize the total transmission power while guaranteeing an average SINR for radar sensing. Extensive simulation results are provided and found to match analytical results very well.

The remainder of this chapter is organized as follows. Section 5.1 introduces the system and stochastic geometric model, and formulates the echo and interference signals. In Section 5.2.1, considering a two-lane scenario, we present the analytical framework for mean interference characterization, and present closed-form expressions with Gaussian approximation. Section 5.2.2 extends the results to a multi-lane scenario. In Section 5.3, we present the power minimization algorithm. Finally, simulation results are provided in Section 5.4, and Section 5.5 concludes the chapter.

5.1 System and Signal Models

In this section, we adopt stochastic geometry methods to construct the system model and emulate geometric distribution of vehicles on a two-lane road and the radio propagation of associated radars. Without loss of generality, we consider a vehicle located at the origin of one lane and call it the *typical vehicle*, and assume that its statistical behaviour is typical and representative of all other vehicles. We consider a temporal snapshot of the road traffic during which the vehicles can be considered as stationary, preserving the geometric statistics of the traffic. We note that these statistics are indeed not constant over a long period. However, they are of a slow kinetic nature and can be safely regarded as static for a given segment of a road over a reasonable observation period.

5.1.1 Geometrical Model

Automotive radar is used to locate objects in the vicinity of the hosting vehicle. A modern vehicle could be equipped with more than one radar. Automotive radars can be categorized into three types based on detection capabilities: long range radar (LRR) which is used for measuring the relative speed and distance of other vehicles, medium range radar (MRR) which is used for detecting objects in a wider field of view (e.g., for cross traffic alert systems), and short range radar (SRR) which is used for sensing in the vicinity of the car (e.g., for parking aid or obstacle detection). The LRR, as well as MRR, are mounted on the front of the vehicle, and SRR, as well as MRR, are mounted on the sides and back of the vehicle. Different field of views (FoVs) are demanded for these three types of automotive radars.

Here, we consider the setup where a vehicle is equipped with one FR for adaptive cruise control and two SRs for side impact. Generally, automotive radars are equipped with directional antennas which generate directional beams with main and side lobes. The beamwidth of different radars is generally different. We assume that

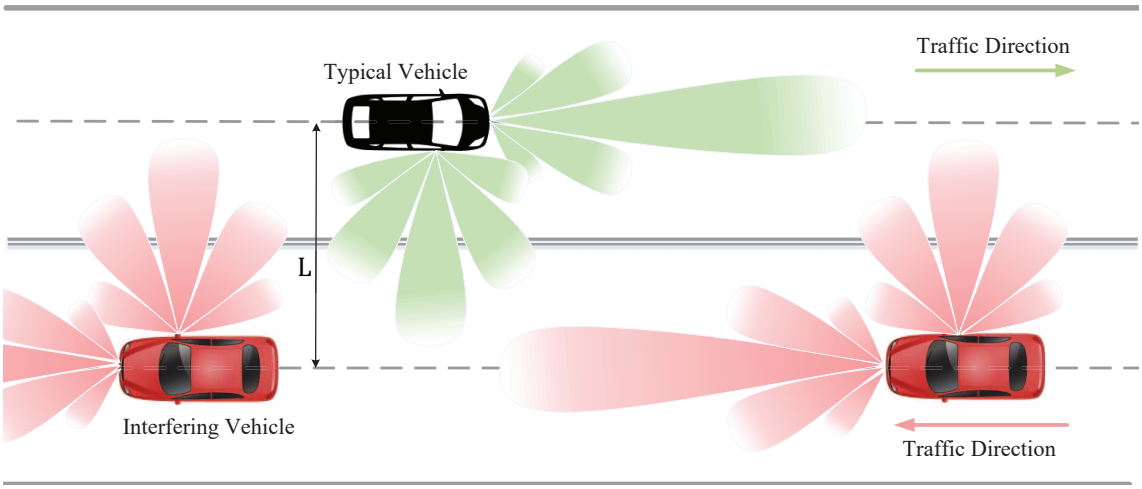

Figure 5.1 : The interference between automotive radars. (Red vehicles stand the interfering ones.)

all vehicles are equipped with the same types of FR and SR.

We consider a two-way road with one lane in each direction. Assume that the lanes are of equal width, L, and vehicles travel in the middle of the lane. We assume that there is no coordination between the frequency band that a radar uses. A radar just randomly selects its frequency band. When radars use the same frequency band, interference can be potentially generated. Fig. 5.1 illustrates a simplified layout of the interfering FR/SR radars. Only the beam from one SR is plotted for each vehicle, as the other one causes negligible interference to other radars in the setup. We assume that the interference to a FR and SR is mainly from the FR and SR of vehicles travelling in the opposite direction.

We capture the randomness of vehicle location using the popular geometrical distribution of PPP. In each lane, the locations of vehicles follow a unidimensional PPP [106] in $\mathbb{R}^1$ with a homogeneous linear density ρ measured in vehicles per unit length. We denote the set of vehicles in one lane as Φ_{PPP}. Let ξ denote the probability that a vehicle in the opposing lane uses the same frequency as the typical vehicle. Considering the interference from other vehicles to the typical one, we can

describe the interferers by applying a random marking as

$$\Theta_{\mathrm{PPP}} = \{i : i \in \Phi_{\mathrm{PPP}}, \mathcal{M}(i) = 1\}, \tag{5.1}$$

where the mark $\mathcal{M}(i)$ is defined for different interfering scenarios as follows:

- From FR to FR or from FR to SR,

$$\mathcal{M}(i) = \begin{cases} 0, & \ell_i \leq 0, \\ \boldsymbol{B}(\xi), & \ell_i > 0, \end{cases} \tag{5.2}$$

  where ℓ_i denotes the location of vehicle i, the interference between FR and FR is zero for $\ell \leq 0$, and $\boldsymbol{B}(\xi)$ is a Bernoulli random variable with selection probability ξ; and

- Between SR and SR,

$$\mathcal{M}(i) = \boldsymbol{B}(\xi), \ i \in \Phi_{\mathrm{PPP}}. \tag{5.3}$$

5.1.2 Radar Reception

Each radar may receive two types of impacting signals including *radar echo signal* and *interference signals*. The echo signal is transmitted by the typical vehicle and the reflected signal is used for object localization. The interference signals are from other radars using the same frequency band as the typical vehicle. For interference signals, we use the inverse square law of the distance for signal attenuation analysis. For the effective power of echo signals, we only take into consideration directly reflected paths from targets. For interference analysis, we consider an additional gain factor corresponding to a statistical fading process, to account for multipath propagations.

Here, we only consider signals coming from the horizontal plane, and hence a

two-dimension model is adopted for signal and interference analysis. The ideas presented in this chapter can be extended to three-dimension models.

We assume effective echo signals are coming from the direction corresponding to the maximum antenna gain, and hence the results serve as upper bounds for other target directions.

Radar Echo-Signal

The power of received echo-signal is well characterized, for example, in [107]. For FR, it can be represented as

$$\begin{aligned} S_r^f &= \frac{P_f G_f}{4\pi R_f^{-2}} \times \frac{\sigma_c^f}{4\pi R_f^{-2}} A_e^f \\ &= \underbrace{\underbrace{\frac{P_f G_f}{4\pi R_f^{-2}}}_{\text{Incident power density}} \times \frac{\sigma_c^f}{4\pi R_f^{-2}}}_{\text{Reflected power density}} \times \underbrace{\frac{G_f \lambda_f^2}{4\pi}}_{\text{Effective area of receiving antenna}} \\ &= \varepsilon_1^f \varepsilon_2^f \varepsilon_3^f P_f R_f^{-4}, \end{aligned} \tag{5.4}$$

where P_f is the FR transmission power, R is the distance between radar and target, G_f and A_e^f are the maximum antenna gain and the effective area of receiving antenna, respectively, and σ_c^f is the cross-section area (RCS) of the target. The parameters ε_1^f, ε_2^f and ε_3^f are given by

$$\varepsilon_1^f = \frac{G_f}{4\pi}, \varepsilon_2^f = \frac{\sigma_c^f}{4\pi} \text{ and } \varepsilon_3^f = \frac{G_f \lambda_f^2}{4\pi} = \frac{G_f}{4\pi}\left(\frac{c}{f_f}\right)^2, \tag{5.5}$$

where f_f is the central operating frequency and c is the speed of light.

Similarly, the received power of echo-signal for SR can be written as

$$S_r^s = \frac{P_s G_s}{4\pi R_s^{-2}} \times \frac{\sigma_c^s}{4\pi R_s^{-2}} A_e^s = \varepsilon_1^s \varepsilon_2^s \varepsilon_3^s P_s {R_s}^{-4}, \tag{5.6}$$

where P_s is the SR transmission power, and

$$\varepsilon_1^s = \frac{G_s}{4\pi}, \varepsilon_2^s = \frac{\sigma_c^s}{4\pi} \text{ and } \varepsilon_3^s = \frac{G_s {\lambda_s}^2}{4\pi} = \frac{G_s}{4\pi}\left(\frac{c}{f_s}\right)^2. \tag{5.7}$$

Symbols with subscript s are defined for SR accordingly.

Interference Signals

We introduce a random vector $\mathbf{H}_i$, where i refers to the i-th interfering vehicle, to account for the statistical channel fading for interfering signals. This randomness is caused by multipath propagation due to reflections from buildings, vegetation, and other vehicles. We assume that the elements of this random vector are identically and independently distributed (i.i.d.), because of the homogeneous fading environment.

The interference power from FR and SR of vehicle i to the FR of the typical one can be expressed by

$$\begin{aligned} I_i^f &= I_i^{ff} + I_i^{sf} \\ &= (\underbrace{\varepsilon_1^f\ P_f\ g^f(\beta_i)}_{\text{(a) FR Interference power.}} + \underbrace{\varepsilon_1^s\ P_s\ g^s(\pi/2-\beta_i)}_{\text{(b) SR Interference power.}}) \cdot \underbrace{\varepsilon_3^f\ g^f(\beta_i)}_{\text{(c) Rx antenna gain of FR.}} \mathbf{H}_i \|r_i\|^{-2} \end{aligned} \tag{5.8}$$

where I_i^{ff} and I_i^{sf} denote the interference power from FR and SR to FR, respectively, $\|r_i\|$ is the distance between the typical and interfering vehicles, β_i is the angle between the moving direction and the line connecting the two vehicles, $g^f(\beta_i)$ and $g^s(\beta_i)$ denote the normalized antenna radiation pattern (or antenna gain) as a function of signal incoming direction β, with a maximum of 1, for FR and SR, respectively. As shown in Fig. 5.2, β_i can be expressed as $\beta_i = \arcsin(L/r_i)$. In (5.8), part (a) and (b) denote the power of interference signals transmitted in the direction of β_i from FR and SR, respectively, and part (c) denotes the receiver antenna gain

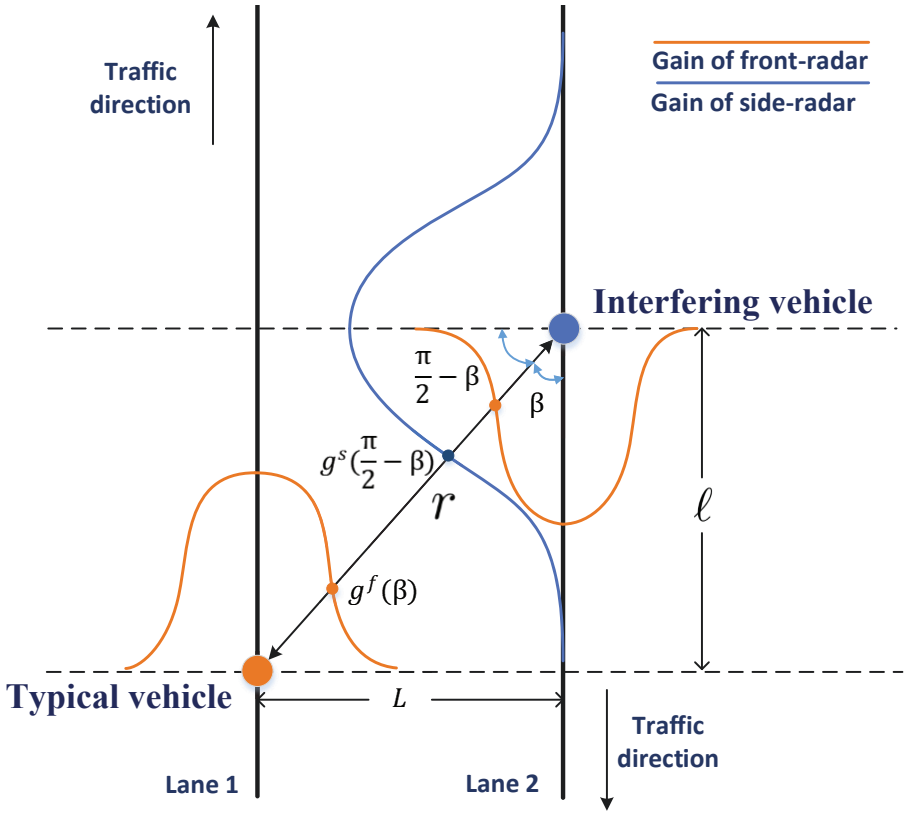

Figure 5.2 : Illustration of the signal strength and interference between automotive radars in different directions.

in the direction of β_i.

Similarly, we can represent the interference to SR as

$$I_i^s = I_i^{fs} + I_i^{ss}$$
$$= \Big(\underbrace{\varepsilon_1^f P_f \; g^f(\beta_i)}_{\text{(a) FR Interference power.}} + \underbrace{\varepsilon_1^s P_s \; g^s(\pi/2-\beta_i)}_{\text{(b) SR Interference power.}} \Big) \cdot \underbrace{\varepsilon_3^s \; g^s(\pi/2-\beta_i)}_{\text{(c) Rx antenna gain of SR.}} \mathbf{H}_i \|r_i\|^{-2}. \tag{5.9}$$

5.2 Interference Characterization

In this section, we first derive general expressions for mean interference power in order to get a general sense of the main parameters that affect the interference value and then derive closed-form expressions by using a specific Gaussian waveform to

approximate the antenna radiation pattern. The results here are also applicable to vehicles in the most left and right lanes in a multi-lane scenario. Then, we extend the analysis to multiple lanes.

5.2.1 Interference Characterization in Two-line Scenarios

General Expressions

Assume that the interference signals from vehicles are statistically independent. The total interference power received at the typical vehicle can be written as

$$\begin{aligned} \boldsymbol{I}^f &= \sum_{i\in\Theta_{\text{PPP}}} I_i^f \\ &= \sum_{i\in\Theta_{\text{PPP}}} \Big[\big(\varepsilon_1^f P_f g^f(\beta_i) + \varepsilon_1^s P_s g^s(\pi/2-\beta_i)\big)\cdot \varepsilon_3^f g^f(\beta_i)\mathbf{H}_i \|r_i\|^{-2}\Big], \text{ and} \end{aligned} \tag{5.10}$$

$$\begin{aligned} \boldsymbol{I}^s &= \sum_{i\in\Theta_{\text{PPP}}} I_i^s \\ &= \sum_{i\in\Theta_{\text{PPP}}} \Big[\big(\varepsilon_1^f P_f g^f(\beta_i) + \varepsilon_1^s P_s g^s(\pi/2-\beta_i)\big)\cdot \varepsilon_3^s g^s(\pi/2-\beta_i)\mathbf{H}_i \|r_i\|^{-2}\Big], \end{aligned} \tag{5.11}$$

for FR and SR, respectively, where Θ_{PPP} denotes the set of interfering vehicles characterized by PPP.

According to the Campbell theorem [108] [page 281], we can calculate the statistical mean of the interference power at FR as follows, as shown in the next page.

In (5.12), $\mathbb{E}_H[\cdot]$ denotes the expectation over the statistical fading channel, $\mathbb{E}_{\Theta_{\text{PPP}}}$ is the expectation over all interfering vehicles with numbers and their locations following PPP, ρ_I is the density of interfering vehicles measured in [cars/unit length] and $\rho_I = \xi\rho$, and $r(\ell) = \sqrt{(L^2+\ell^2)}$. The step (e) follows the assumption that individual propagation channels are i.i.d, and are uncorrelated to the geometrical

point process. The final step uses the assumption that the average channel gain is normalized to unity i.e., $\mathbb{E}_H[H] \triangleq u_H = 1$.

Similarly, we can obtain the mean power of the interference at SR and present it in (5.13).

From (5.12) and (5.13), we can have the following observations:

- The mean interference from FR and SR of interfering vehicles are a linearly and monotonically increasing function of their transmission power, respectively. However, the total interference to each of FR and SR is a weighted sum of their transmission power and hence is not a linear function of it any more;
- The interference power is linearly proportional to the effective density of the interfering vehicles ρ_I, as expected.

In the next section, we consider two special functions for g^f and g^s to get compact results, which provide more insights into the interference.

$$
\begin{aligned}
&\overline{I^f} = \mathbb{E}\left[\boldsymbol{I}^f\right] = \overline{I^{ff}} + \overline{I^{sf}} \\
&= \underbrace{\mathbb{E}_H\left[\mathbb{E}_{\Theta_{\mathrm{PPP}}}\left[\sum_{i\in\Theta_{\mathrm{PPP}}} \varepsilon_1^f P_f g^f(\beta_i)\varepsilon_3^f g^f(\beta_i)\|r_i\|^{-2}\right]\right]}_{\text{Mean interference from FR to FR}} + \\
&\underbrace{\mathbb{E}_H\left[\mathbb{E}_{\Theta_{\mathrm{PPP}}}\left[\sum_{i\in\Theta_{\mathrm{PPP}}} \varepsilon_1^s P_s g^s\left(\frac{\pi}{2}-\beta_i\right)\varepsilon_3^f g^f(\beta_i)\|r_i\|^{-2}\right]\right]}_{\text{Mean interference from SR to FR}} \\
&\overset{\mathrm{e}}{=} \mathbb{E}_H[H]\left\{\rho_I\varepsilon_1^f\varepsilon_3^f P_f\int_0^{+\infty}\left[g^f\left(\arcsin\frac{L}{r(\ell)}\right)\right]^2 r(\ell)^{-2}d\ell + \right. \\
&\left.\rho_I\varepsilon_1^s\varepsilon_3^f P_s\int_0^{+\infty} g^s(\frac{\pi}{2}-\arcsin\frac{L}{r(\ell)})g^f(\arcsin\frac{L}{r(\ell)})r(\ell)^{-2}d\ell\right\} \\
&= \rho_I\left\{\varepsilon_1^f\varepsilon_3^f P_f\int_0^{+\infty}\left[g^f(\arcsin\frac{L}{r(\ell)})\right]^2 r(\ell)^{-2}d\ell + \right. \\
&\left.\varepsilon_1^s\varepsilon_3^f P_s\int_0^{+\infty} g^s(\frac{\pi}{2}-\arcsin\frac{L}{r(\ell)})g^f(\arcsin\frac{L}{r(\ell)})r(\ell)^{-2}d\ell\right\}. \qquad (5.12)
\end{aligned}
$$

$$
\begin{aligned}
&\overline{I^s} = \overline{I^{fs}} + \overline{I^{ss}} \\
&= \underbrace{\mathbb{E}_H\left[\mathbb{E}_{\Theta_{\text{PPP}}}\left[\sum_{i\in\Theta_{\text{PPP}}} \varepsilon_1^f P_f g^f(\beta_i)\varepsilon_3^s g^s\left(\frac{\pi}{2}-\beta_i\right)\|r_i\|^{-2}\right]\right]}_{\text{Mean Interference from FR to SR}} + \\
&\underbrace{\mathbb{E}_H\left[\mathbb{E}_{\Theta_{\text{PPP}}}\left[\sum_{i\in\Theta_{\text{PPP}}} \varepsilon_1^s P_s g^s\left(\frac{\pi}{2}-\beta_i\right)\varepsilon_3^s g^s(\frac{\pi}{2}-\beta_i)\|r_i\|^{-2}\right]\right]}_{\text{Mean Interference from SR to SR}} \\
&\overset{\text{e}}{=} \left\{\rho_I\varepsilon_1^f\varepsilon_3^s P_f\int_0^{+\infty} g^f(\arcsin\frac{L}{r(\ell)})g^s(\frac{\pi}{2}-\arcsin\frac{L}{r(\ell)})r(\ell)^{-2}d\ell\right. \\
&\left.+2\rho_I\varepsilon_1^s\varepsilon_3^s P_s\int_0^{+\infty}\left[g^s\left(\frac{\pi}{2}-\arcsin\frac{L}{r(\ell)}\right)\right]^2 r(\ell)^{-2}d\ell\right\}\mathbb{E}_H\left[H\right] \\
&= \rho_I\left\{\varepsilon_1^f\varepsilon_3^s P_f\int_0^{+\infty} g^f(\arcsin\frac{L}{r(\ell)})g^s(\frac{\pi}{2}-\arcsin\frac{L}{r(\ell)})r(\ell)^{-2}d\ell\right. \\
&\left.+2\varepsilon_1^s\varepsilon_3^s P_s\int_0^{+\infty}\left[g^s\left(\frac{\pi}{2}-\arcsin\frac{L}{r(\ell)}\right)\right]^2 r(\ell)^{-2}d\ell\right\}. \qquad (5.13)
\end{aligned}
$$

Interference with Gaussian Directional Radiation Pattern

Here, we consider a special example for the antenna radiation pattern ($g^f(\cdot)$ and $g^s(\cdot)$), which can be represented by a normalized Gaussian function. There are two reasons for considering a beam pattern of Gaussian function: (1) It can lead to compact and closed-form expressions; and (2) it provides a good approximation to actual beam patterns as will be shown in Section 3.1.4. The gain function $g^f(\beta)$ and $g^s(\beta)$ are given by

$$
\begin{cases}
g^f(\beta) = \exp(-\dfrac{\beta^2}{2\sigma_f^2}), \beta\in[-\dfrac{\pi}{2},\dfrac{\pi}{2}], \\
g^s(\beta) = \exp(-\dfrac{\beta^2}{2\sigma_s^2}), \beta\in[-\dfrac{\pi}{2},\dfrac{\pi}{2}],
\end{cases} \qquad (5.14)
$$

where σ_f^2 and σ_s^2 are the parameters of the Gaussian function and are adjustable. From Fig. 5.2, we have $\ell = L/\tan(\beta)$. For the directional antenna, applying (5.14)

to (5.12) and (5.13), we can obtain

$$\begin{aligned}
\overline{I^f} &= \overline{I^{ff}} + \overline{I^{sf}} \\
&= \frac{\rho_I \varepsilon_1^f \varepsilon_3^f P_f}{L} \int_0^{\frac{\pi}{2}} \exp\left(-\frac{\beta^2}{\sigma_f^2}\right) d\beta + \frac{\rho_I \varepsilon_1^s \varepsilon_3^f P_s}{L} \int_0^{\frac{\pi}{2}} \exp\left(-\frac{\left(\frac{\pi}{2}-\beta\right)^2}{2\sigma_s^2} - \frac{\beta^2}{2\sigma_f^2}\right) d\beta \\
&= \frac{\sqrt{\pi}}{2L} \xi\rho \left(u_{\sigma_f} \varepsilon_1^f \varepsilon_3^f P_f + u_{\sigma_{f,s}} \varepsilon_1^s \varepsilon_3^f P_s\right), \qquad (5.15)
\end{aligned}$$

and

$$\begin{aligned}
\overline{I^s} &= \overline{I^{fs}} + \overline{I^{ss}} \\
&= \frac{\rho_I \varepsilon_1^f \varepsilon_3^s P_f}{L} \int_0^{\frac{\pi}{2}} \exp\left(-\frac{\beta^2}{2\sigma_f^2} - \frac{\left(\frac{\pi}{2}-\beta\right)^2}{2\sigma_s^2}\right) d\beta + \frac{2\rho_I \varepsilon_1^s \varepsilon_3^s P_s}{L} \int_0^{\frac{\pi}{2}} \exp\left(-\frac{\left(\frac{\pi}{2}-\beta\right)^2}{\sigma_s^2}\right) d\beta \\
&= \frac{\sqrt{\pi}}{2L} \xi\rho \left(u_{\sigma_{f,s}} \varepsilon_1^f \varepsilon_3^s P_f + 2u_{\sigma_s} \varepsilon_1^s \varepsilon_3^s P_s\right), \qquad (5.16)
\end{aligned}$$

where $\mathrm{erf}(x)$ is the Gaussian error function, and

$$\begin{cases}
u_{\sigma_f} \triangleq \sigma_f \,\mathrm{erf}(\dfrac{\pi}{2\sigma_f}), \\
u_{\sigma_s} \triangleq \sigma_s \,\mathrm{erf}(\dfrac{\pi}{2\sigma_s}), \\
u_{\sigma_{f,s}} \triangleq \exp\left(-\dfrac{\pi^2}{8\left(\sigma_f^2+\sigma_s^2\right)}\right) \left[\mathrm{erf}\left(\dfrac{\pi\sigma_f}{2\sqrt{2}\sigma_s\sqrt{\sigma_f^2+\sigma_s^2}}\right)\right. \\
\qquad\qquad \left. + \mathrm{erf}\left(\dfrac{\pi\sigma_s}{2\sqrt{2}\sigma_f\sqrt{\sigma_f^2+\sigma_s^2}}\right)\right] \dfrac{\sqrt{2}\sigma_f\sigma_s}{\sqrt{\sigma_f^2+\sigma_s^2}}.
\end{cases} \qquad (5.17)$$

From (5.15) and (5.16), we can get the following observations in addition to those obtained from (5.12) and (5.13):

- The mean interference power is linearly proportional to both the frequency reuse factor ξ and the effective density of interfering vehicles $\xi\rho$;

- It is interesting to see that, when the same radar and transmission power is used for FR and SR, $\overline{I^{sf}}$ and $\overline{I^{fs}}$ are largely the same;

- When FR and SR are the same, we can get $\overline{I^{sf}} = \overline{I^{fs}}$ and $\overline{I^{ss}} = 2\overline{I^{ff}}$, and the ratio of total interference between FR and SR is 2/3. This is because SR and FR see interference from 0 to 180 degrees and 0 to 90 degrees, respectively. Note that this only applies to the two-lane case.

5.2.2 Extension to Multiple-lane Scenarios

Now, we extend the analysis to multiple lanes, as shown in Fig. 5.3, where there are m lanes in the same direction and n lanes in the opposite direction. We assume that the vehicles in the lanes of each direction follow independent PPP geometrical distribution with density ρ_i and ρ_j, $(i \in 1, ..., m$ and $j \in 1, ..., n)$, respectively. Assume that the typical vehicle is at a non-edge lane i. Referring to Fig. 5.3, the radar interfering scenarios can be described as follows:

1) *Interference to FR from SRs and FRs:* The interfering SRs include the SR1s on vehicles from the lanes $1, ..., i-1$ and $1, ..., n$, and the SR2s on vehicles from the lanes $i+1, .., m$. The interfering FRs are on vehicles from the lanes $1, ..., n$;

2) *Interference to SR1 from SRs and FRs:* The interfering SRs include the SR2s on vehicles from the lanes $i+1, ..., m$ and the SR1s from the lanes $1, ..., n$. The interfering FRs are on vehicles from the lanes $i+1, ..., m$ and $1, ..., n$;

3) Interference to SR2 from SR1s and FRs on vehicles in the lanes $1, ..., i-1$.

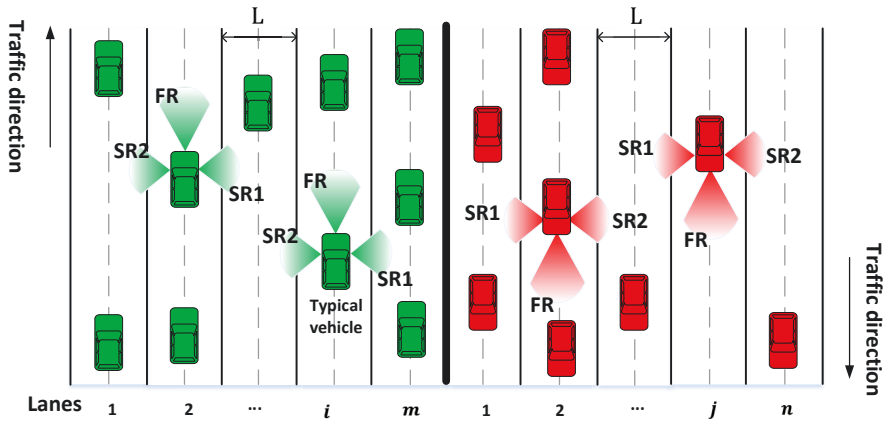

Figure 5.3 : Illustration of the interference in multiple lanes.

Mean Interference to FR

The mean interference received at the FR on the typical vehicle is given by

$$\overline{I^f} = \overline{I^{ff}} + \overline{I^{s_1 f}} + \overline{I^{s_2 f}}, \tag{5.18}$$

where $\overline{I^{s_1 f}}$ and $\overline{I^{s_2 f}}$ denote the mean interference from SR1 and SR2 to the FR, respectively. Similar to the analytical method in Section 5.2.1, we can get the following results with the Gaussian radiation pattern function:

$$\overline{I^{ff}} = \frac{\sqrt{\pi}}{2L} \sum_{j=1}^{n} \frac{1}{m-i+j} u_{\sigma_f} \xi_j \rho_j \varepsilon_1^f \varepsilon_3^f P_f, \tag{5.19}$$

$$\overline{I^{s_1 f}} = \frac{\sqrt{\pi}}{2L} \left[\sum_{j=1}^{n} \frac{\xi_j \rho_j}{m-i+j} + \sum_{k=1}^{i-1} \frac{\xi_k \rho_k}{i-k} \right] u_{\sigma_{f,s}} \varepsilon_1^s \varepsilon_3^f P_{s_1}, \tag{5.20}$$

and

$$\overline{I^{s_2 f}} = \frac{\sqrt{\pi}}{2L} \sum_{k=i+1}^{m} \frac{\xi_k \rho_k}{k-i} u_{\sigma_{f,s}} \varepsilon_1^s \varepsilon_3^f P_{s_2}, \tag{5.21}$$

where P_{s_1} and P_{s_2} denote the transmission power of SR1 and SR2, respectively, and ξ_k and ξ_j represent the frequency reusing probabilities.

Mean Interference to SR1

The mean interference to SR1 is given by

$$\overline{I^{s_1}} = \overline{I^{fs_1}} + \overline{I^{s_2s_1}} + \overline{I^{s_1s_1}}, \tag{5.22}$$

where $\overline{I^{fs_1}}$, $\overline{I^{s_2s_1}}$ and $\overline{I^{s_1s_1}}$ denote the mean interference power from FR to SR1, from SR2 to SR1, and from SR1 to SR1, respectively.

Referring to Section 5.2.1, we can derive the following results,

$$\overline{I^{fs_1}} = \frac{\sqrt{\pi}}{2L}\left[\sum_{k=i+1}^{m}\frac{\xi_k\rho_k}{k-i} + \sum_{j=1}^{n}\frac{\xi_j\rho_j}{m-i+j}\right] u_{\sigma_{f,s}}\varepsilon_1^f\varepsilon_3^s P_f, \tag{5.23}$$

$$\overline{I^{s_2s_1}} = \frac{\sqrt{\pi}}{L}\sum_{k=i+1}^{m}\frac{\xi_k\rho_k}{k-i}u_{\sigma_s}\varepsilon_1^s\varepsilon_3^s P_{s_2}, \tag{5.24}$$

and

$$\overline{I^{s_1s_1}} = \frac{\sqrt{\pi}}{L}\sum_{j=1}^{n}\frac{\xi_j\rho_j}{m-i+j}u_{\sigma_s}\varepsilon_1^s\varepsilon_3^s P_{s_1}. \tag{5.25}$$

Mean Interference to SR2

The mean interference to SR2 is given by

$$\overline{I^{s_2}} = \overline{I^{fs_2}} + \overline{I^{s_1s_2}}, \tag{5.26}$$

where $\overline{I^{fs_2}}$ and $\overline{I^{s_1s_2}}$ denote the mean interference power from FR to SR2 and from SR1 to the SR2, respectively. We can obtain the following results,

$$\overline{I^{fs_2}} = \frac{\sqrt{\pi}}{2L} \sum_{k=i}^{i-1} \frac{\xi_k \rho_k}{i-k} u_{\sigma_{f,s}} \varepsilon_1^f \varepsilon_3^s P_f, \tag{5.27}$$

and

$$\overline{I^{s_1s_2}} = \frac{\sqrt{\pi}}{L} \sum_{k=1}^{i-1} \frac{\xi_k \rho_k}{i-k} u_{\sigma_s} \varepsilon_1^s \varepsilon_3^s P_{s_1}. \tag{5.28}$$

5.3 Minimization of Radar Transmission Power

The SINR is an important parameter that determines the detection performance of vehicular radar. In this section, we study how to minimize the total radar transmission power of the typical vehicle when some low thresholds of the mean SINR are to be met. We start with the two-lane scenario and then extend it to multiple lanes.

5.3.1 Optimization in Two-lane Scenarios

The mean SINRs for FR and SR can be represented as

$$\begin{cases} \overline{\gamma_f} = \dfrac{S_r^f}{\overline{I^f} + \sigma_{\eta_f}^2}, & \text{(5.29a)} \\ \overline{\gamma_s} = \dfrac{S_r^s}{\overline{I^s} + \sigma_{\eta_s}^2}, & \text{(5.29b)} \end{cases}$$

where S_r^f and S_r^s are the reflected signal power from the target as described in (5.4) and (5.6), and $\sigma_{\eta_f}^2$ and $\sigma_{\eta_s}^2$ are the variance of the additive white Gaussian noise (AWGN) in radar.

Let $\gamma_{f,0}$ and $\gamma_{s,0}$ be the lower threshold of the desired SINR at FR and SR, respectively. Targeting at minimizing the total radar transmission power, we formulate

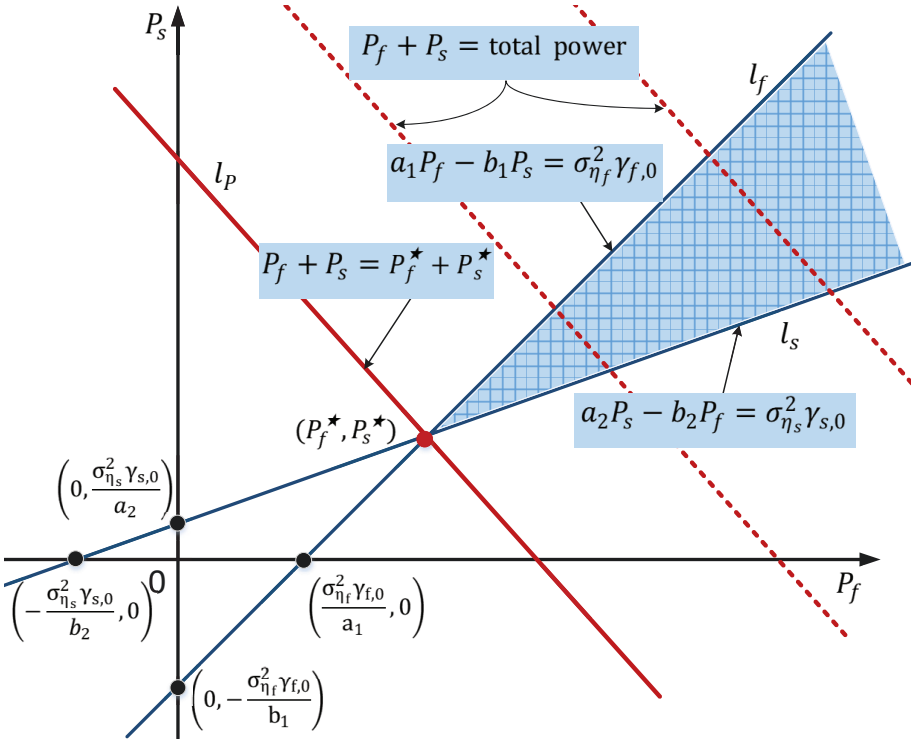

Figure 5.4 : Illustration of the optimal solution.

the following optimization problem,

$$\min_{\{P_f, P_s\}} \quad P_f + P_s \tag{5.30a}$$

$$\text{subject to} \quad P_f > 0, \tag{5.30b}$$

$$P_s > 0, \tag{5.30c}$$

$$\overline{\gamma_f} \geq \gamma_{f,0}, \tag{5.30d}$$

$$\overline{\gamma_s} \geq \gamma_{s,0}, \tag{5.30e}$$

The optimization in (5.30) is a linear programming problem which can be solved by the linear programming (LP) method. As shown in Fig. (5.4), the optimal solution can be obtained at the intersection of the two lines, where $\overline{\gamma_f} = \gamma_{f,0}$ and $\overline{\gamma_s} = \gamma_{s,0}$.

In order to get the optimal solution, we firstly rewrite (5.30d) and (5.30e) with equality as

$$\begin{cases} a_1 P_f - b_1 P_s = \sigma_{\eta_f}^2 \gamma_{f,0}, & \text{(5.31a)} \\ a_2 P_s - b_2 P_f = \sigma_{\eta_s}^2 \gamma_{s,0}, & \text{(5.31b)} \end{cases}$$

where a_1, b_1, a_2 and b_2 are given by

$$\begin{cases} a_1 = \varepsilon_1^f \varepsilon_2^f \varepsilon_3^f R_f^{-4} - \dfrac{\sqrt{\pi}}{2L} u_H u_{\sigma_f} \gamma_{f,0} \xi \rho \varepsilon_1^f \varepsilon_3^f, \\ b_1 = \dfrac{\sqrt{\pi}}{2L} u_H u_{\sigma_{f,s}} \gamma_{f,0} \xi \rho \varepsilon_1^s \varepsilon_3^f, \\ a_2 = \varepsilon_1^s \varepsilon_2^s \varepsilon_3^s R_s^{-4} - \dfrac{\sqrt{\pi}}{L} u_H u_{\sigma_s} \gamma_{s,0} \xi \rho \varepsilon_1^s \varepsilon_3^s, \\ b_2 = \dfrac{\sqrt{\pi}}{2L} u_H u_{\sigma_{f,s}} \gamma_{s,0} \xi \rho \varepsilon_1^f \varepsilon_3^s. \end{cases} \tag{5.32}$$

Existence of the optimal solution to (5.30) is under the following conditions

$$\begin{cases} a_1 > 0, & \text{(5.33a)} \\ a_2 > 0, & \text{(5.33b)} \\ a_1 a_2 - b_1 b_2 > 0. & \text{(5.33c)} \end{cases}$$

In (5.33), the constraints (5.33a) and (5.33b) guarantee the inequalities (5.30d) and (5.30e), and the constraint (5.33c) guarantees that the solution region of LP is non-empty, which means the liner inequalities (5.30d) and (5.30e) have the valid intersection, i.e., line (5.31a) has a larger slope than line (5.31b).

Therefore, we can obtain the optimal solution for the transmission power as

$$\begin{cases} P_f^\star = \dfrac{\sigma_{\eta_f}^2 \gamma_{f,0} a_2 + \sigma_{\eta_s}^2 \gamma_{s,0} b_1}{a_1 a_2 - b_1 b_2}, \\ P_s^\star = \dfrac{\sigma_{\eta_f}^2 \gamma_{f,0} b_2 + \sigma_{\eta_s}^2 \gamma_{s,0} a_1}{a_1 a_2 - b_1 b_2}. \end{cases} \tag{5.34}$$

When there is a total power constraint for each of P_f and P_s, the minimum required

SINR cannot be achieved simultaneously if either $P_f^\star$ or $P_s^\star$ exceeds the constraint. From (5.34), we can see that both $P_f^\star$ and $P_s^\star$ decrease with the resource reusing probability ξ. Hence we can reduce ξ to reduce $P_f^\star$ and $P_s^\star$.

The minimum total transmission power is thus given by

$$(P_f + P_s)_{\min} = \frac{\sigma_{\eta_f}^2 \gamma_{f,0} (a_2 + b_2) + \sigma_{\eta_s}^2 \gamma_{s,0} (a_1 + b_1)}{a_1 a_2 - b_1 b_2}. \tag{5.35}$$

Referring to Fig. 5.4 and (5.35), we can see that the minimum transmission power increases with the effective density $\xi\rho$ increasing. When $\xi\rho$ increases, the slope a_1/b_1 of line l_f decreases and the slope b_2/a_2 of line l_s increases. Consequently, the intersection of the two lines $P_f^\star$ and $P_f^\star$ increases.

5.3.2 Optimization in Multiple-lane Scenarios

In multiple-lane scenarios, considering one FR and two SRs, the optimization problem can be formulated as follows

$$\min_{\{P_f, P_s\}} \quad P_f + P_{s_1} + P_{s_2} \tag{5.36a}$$

$$\text{subject to} \quad P_f > 0, \tag{5.36b}$$

$$P_{s_1} > 0, \tag{5.36c}$$

$$P_{s_2} > 0, \tag{5.36d}$$

$$\overline{\gamma_f} \geq \gamma_{f,0}, \tag{5.36e}$$

$$\overline{\gamma_{s_1}} \geq \gamma_{s_1,0}, \tag{5.36f}$$

$$\overline{\gamma_{s_2}} \geq \gamma_{s_2,0}, \tag{5.36g}$$

where P_{s_1} and P_{s_2} denote the transmission power of radar SR1 and SR2, respectively, $\overline{\gamma_{s_1}}$ and $\overline{\gamma_{s_2}}$ represent the SINR of SR1 and SR2, respectively, and $\gamma_{s_1,0}$, $\gamma_{s_2,0}$ are the

thresholds of the mean SINR.

Similar to the process in two-lane scenarios, we can solve the optimization problem by rewriting the constraints (5.36e), (5.36f) and (5.36g) as

$$\begin{cases} a_{m,1}P_f - b_{m,1}P_{s_1} - c_{m,1}P_{s_2} \geq \sigma^2_{\eta_f}\gamma_{f,0}, & \text{(5.37a)} \\ a_{m,2}P_{s_1} - b_{m,2}P_f - c_{m,2}P_{s_2} \geq \sigma^2_{\eta_{s_1}}\gamma_{s_1,0}, & \text{(5.37b)} \\ a_{m,3}P_{s_2} - b_{m,3}P_f - c_{m,3}P_{s_1} \geq \sigma^2_{\eta_{s_2}}\gamma_{s_2,0}, & \text{(5.37c)} \end{cases}$$

where the factors are

$$\begin{cases} a_{m,1} = \varepsilon_1^f\varepsilon_2^f\varepsilon_3^f R_f^{-4} - \dfrac{\sqrt{\pi}}{2L}\displaystyle\sum_{j=1}^{n}\frac{\xi_j\rho_j}{m-i+j}u_H u_{\sigma_f}\gamma_{f,0}\varepsilon_1^f\varepsilon_3^f, \\ b_{m,1} = \dfrac{\sqrt{\pi}}{2L}\left[\displaystyle\sum_{j=1}^{n}\frac{\xi_j\rho_j}{m-i+j} + \sum_{k=1}^{i-1}\frac{\xi_k\rho_k}{i-k}\right]u_H u_{\sigma_{f,s}}\gamma_{f,0}\varepsilon_1^s\varepsilon_3^f, \\ c_{m,1} = \dfrac{\sqrt{\pi}}{2L}\displaystyle\sum_{k=i+1}^{m}\frac{\xi_k\rho_k}{k-i}u_H u_{\sigma_{f,s}}\gamma_{f,0}\varepsilon_1^s\varepsilon_3^f, \\ a_{m,2} = \varepsilon_1^s\varepsilon_2^s\varepsilon_3^s R_{s_1}^{-4} - \dfrac{\sqrt{\pi}}{L}\displaystyle\sum_{j=1}^{n}\frac{\xi_j\rho_j}{m-i+j}u_H u_{\sigma_s}\gamma_{s_1,0}\varepsilon_1^s\varepsilon_3^s, \\ b_{m,2} = \dfrac{\sqrt{\pi}}{2L}\left[\displaystyle\sum_{j=1}^{n}\frac{\xi_j\rho_j}{m-i+j} + \sum_{k=i+1}^{m}\frac{\xi_k\rho_k}{k-i}\right] \\ \qquad u_H u_{\sigma_{f,s}}\gamma_{s_1,0}\varepsilon_1^f\varepsilon_3^s, \\ c_{m,2} = \dfrac{\sqrt{\pi}}{L}\displaystyle\sum_{k=i+1}^{m}\frac{\xi_k\rho_k}{k-i}u_H u_{\sigma_s}\gamma_{s_1,0}\varepsilon_1^s\varepsilon_3^s, \\ a_{m,3} = \varepsilon_1^s\varepsilon_2^s\varepsilon_3^s R_{s_2}^{-4}, \\ b_{m,3} = \dfrac{\sqrt{\pi}}{2L}\displaystyle\sum_{k=i}^{i-1}\frac{\xi_k\rho_k}{i-k}u_H u_{\sigma_f}\gamma_{s_2,0}\varepsilon_1^f\varepsilon_3^s, \\ c_{m,3} = \displaystyle\sum_{k=1}^{i-1}\sqrt{\pi}\frac{\xi_k\rho_k}{(i-k)L}u_H u_{\sigma_s}\gamma_{s_2,0}\varepsilon_1^s\varepsilon_3^s. \end{cases} \tag{5.38}$$

Let $P_f + P_{s_1} + P_{s_2} = P_t$. Substituting $P_{s_2} = P_t - P_f - P_{s_1}$ into (5.37), we obtain

$$\begin{cases} (a_{m,1} + c_{m,1})\, P_f - (b_{m,1} - c_{m,1})\, P_{s_1} \geq \sigma^2_{\eta_f} \gamma_{f,0} + c_{m,1} P_t, & \text{(5.39a)} \\ (a_{m,2} + c_{m,2})\, P_{s_1} - (b_{m,2} - c_{m,2})\, P_f \geq \sigma^2_{\eta_{s1}} \gamma_{s_1,0} + c_{m,2} P_t, & \text{(5.39b)} \\ (a_{m,3} + b_{m,3})\, P_f + (a_{m,3} + c_{m,3})\, P_{s_1} \leq a_{m,3} P_t - \sigma^2_{\eta_{s_2}} \gamma_{s_2,0}. & \text{(5.39c)} \end{cases}$$

In order to ensure that the inequality (5.39) has a solution, the intersection $(P_f^\star, P_{s_1}^\star)$ of line (5.39a) and (5.39b) must meet the condition $\left(a_3^M + b_3^M\right) P_f^\star + \left(a_3^M + c_3^M\right) P_{s_1}^\star \leq a_3^M P_t - \sigma^2_\eta \gamma_{s_2,0}$. Therefore, we get the inequality for the total transmission power P_t as

$$P_t \geq \frac{(a_{m,3} + b_{m,3})\, P_f^\star + (a_{m,3} + c_{m,3})\, P_{s_1}^\star + \sigma^2_{\eta s2} \gamma_{s_2,0}}{a_{m,3}}, \tag{5.40}$$

The optimal solution to (5.36) is then obtained when the equality is taken in (5.40), and is given by

$$(P_t)_{min} = \frac{\sigma^2_{\eta_f} \gamma_{f,0} A_m + \sigma^2_{\eta_{s_1}} \gamma_{s_1,0} B_m + \sigma^2_{\eta_{s_2}} \gamma_{s_2,0} C_m}{D_m}. \tag{5.41}$$

where

$$\begin{cases} A_m = c_{m,2}c_{m,3} - a_{m,2}a_{m,3} - a_{m,3}b_{m,2} - b_{m,3}c_{m,2} - a_{m,2}b_{m,3} - b_{m,2}b_{m,3}, \\ B_m = b_{m,3}c_{m,1} - a_{m,1}a_{m,3} - a_{m,3}b_{m,1} - c_{m,1}c_{m,3} - a_{m,1}c_{m,3} - b_{m,1}b_{m,3}, \\ C_m = b_{m,1}b_{m,1} - a_{m,1}a_{m,1} - a_{m,1}c_{m,1} - b_{m,1}c_{m,1} - a_{m,1}c_{m,1} - b_{m,1}c_{m,1}, \\ D_m = a_{m,3}b_{m,1}b_{m,1} - a_{m,1}a_{m,1}a_{m,3} + a_{m,1}b_{m,3}c_{m,1} + a_{m,1}c_{m,1}c_{m,3} + \\ \qquad b_{m,1}b_{m,3}c_{m,1} + b_{m,1}c_{m,1}c_{m,3}. \end{cases}$$

We can see that the optimal power is obtained at the intersection of the three lines.

5.4 Simulation Results and Discussion

In this section, we present simulation results to verify the accuracy of the derived analytical expressions on radar interference, and test the optimality of our proposed power minimization scheme. Important observations are highlighted in italic in this section.

5.4.1 Simulation Setup

Referring to the simulation parameters in Table 5.1, our system setup is described as follows. We generate the number and locations of vehicles randomly following the PPP with the vehicle density paramater ρ, and allocate vehicles using the same frequency with the typical vehicle according to the frequency reuse probability ξ. The pathloss and channel fading of the effective signal and interference signals are simulated following the description in Section 5.1.2. Most of the radar parameters are similar to those used in [77, 109, 110], except for the radiation patterns of the antennas.

The directional radiation patterns of the radar antennas used in this chapter are generated as follows. Let θ_f and θ_s be the 3dB beamwidth of the main-lobe of FR and SR, respectively. From Eq. (5.14), we can obtain σ_f^2 and σ_s^2 corresponding to the 3dB beamwidth as

$$\begin{cases} \sigma_f^2 = -\dfrac{\theta_f^2}{8\ln g^f(\theta_f/2)} = \dfrac{\theta_f^2}{8\ln 2} \\ \sigma_s^2 = -\dfrac{\theta_s^2}{8\ln g^s(\theta_f/2)} = \dfrac{\theta_s^2}{8\ln 2}. \end{cases} \tag{5.42}$$

Generally, SR has wider beamwidth than FR. According to [109], the beamwidth of automotive radars is typically between 15° to 80°.

Since the maximum antenna gain is typically linked to the beamwidth and radiation pattern, we set $G_f = 1/(\sqrt{2\pi}\sigma_f)$ and $G_s = 1/(\sqrt{2\pi}\sigma_s)$, being the antenna

Table 5.1 : SYMBOLS AND THEIR VALUES USED IN THE PAPER AND SIMULATION.

Symbol	Numerical Value	Definition/Explanation
R^f	Variable [m]	Distance from FR to target
R^s	Variable [m]	Distance from SR to target
L	6 [m]	Lane spacing
P_r^f	Refer to (5.4) [mW]	Reflected signal of FR
P_r^s	Refer to (5.6) [mW]	Reflected signal of SR
ρ	Variable [cars/m]	Vehicles linear density
f_f	76.5 GHz [110]	Central frequency of FR
f_s	77.5 GHz [110]	Central frequency of SR
ξ	Variable	Spectrum reusing probability
$\gamma_{f,0}$	10 [dB] [109]	The γ threshold of FR
$\gamma_{s,0}$	10 [dB] [109]	The γ threshold of SR
G_f	as given in the paper	Maximum antenna gain of FR
G_s	as given in the paper	Maximum antenna gain of SR
σ_c	30dBsm [109]	Front-Radar cross-section
σ_c^s	30dBsm [109]	Side-Radar cross-section
$g^f(\beta)$	Refer to (5.14)	Gain in different direction (FR)
$g^s(\beta)$	Refer to (5.14)	Gain in different direction (SR)
$\mathbf{H}_i$	-	Interfering signals fading progresses
u_H	1	the mean value of $\mathbf{H}_i$
c	3e8[m/s]	Speed of light
$\varepsilon_1^f/\varepsilon_1^s$	Refer to (5.5) and (5.7)	Radar-specific transmission constant
$\varepsilon_2^f/\varepsilon_2^s$	Refer to (5.5) and (5.7)	Target-specific constant
$\varepsilon_3^f/\varepsilon_3^s$	Refer to (5.5) and (5.7)	Radar-specific received constant

gains via the Gaussian waveform for FR and SR, respectively. Note that since we only consider the gain at the horizontal plane, it is much smaller than the actual total antenna gain. Hence the values of the interference power and transmission power minimization results presented in this section are only relative, and we focus on investigating their relationship with the system parameters and verifying the accuracy of the analytical results.

5.4.2 Radar Mean Interference

In this part, we focus on studying how the interference, as well as the signal-to-interference power ratio (SIR), is affected by different system parameters in a

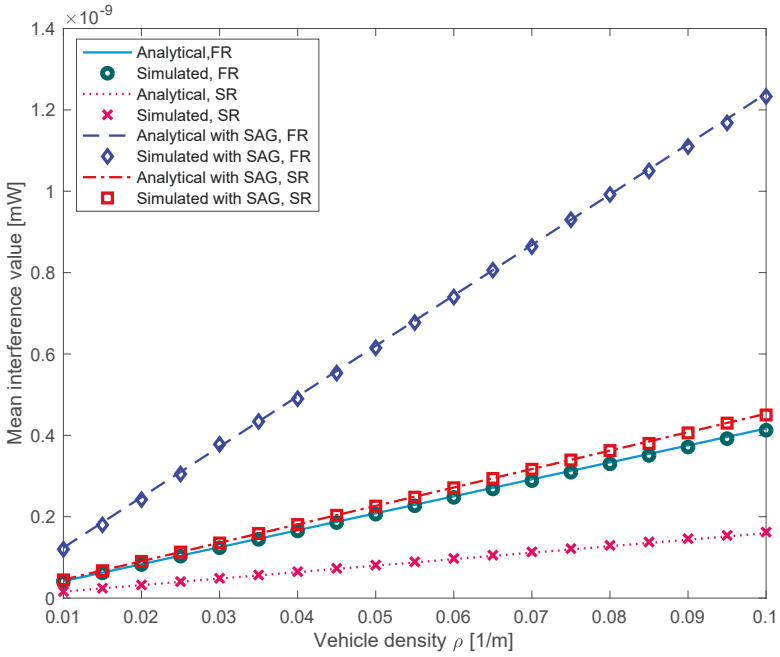

Figure 5.5 : Analytical and simulated mean interference power at SR and FR, where $\sigma_f = 0.1112, \theta_f = 15°$, and $\sigma_s = 0.5929, \theta_s = 80°$; $\xi = 4\%$.

two-lane scenario. Without considering noise, the mean SIR is defined as $\text{SIR}(\overline{I^f}) = S_r^f/\overline{I^f}$ and $\text{SIR}(\overline{I^s}) = S_r^s/\overline{I^s}$ for FR and SR, respectively. The transmission power is set as $P_f = P_s = 10$ mW.

The mean interference power at FR and SR with varying vehicle density ρ of the PPP geometrical model is shown in Fig. 5.5. We set $\theta_f = 15°$ and $\theta_s = 80°$, i.e., $\sigma_f = 0.1112$ and $\sigma_s = 0.5929$ for FR and SR, respectively. The simulated interference power is shown to be linearly proportional to vehicle density, and matches very well with the analytical one. We also compare our results with those in [77] which assumes the use of a directional antenna with the same antenna gain (SAG) over a range of directions. The mean interference for [77] is shown to be much larger than ours, which indicates that the use of directional antennas can significantly reduce the interference.

To evaluate the accuracy of approximating the directional radiation pattern of

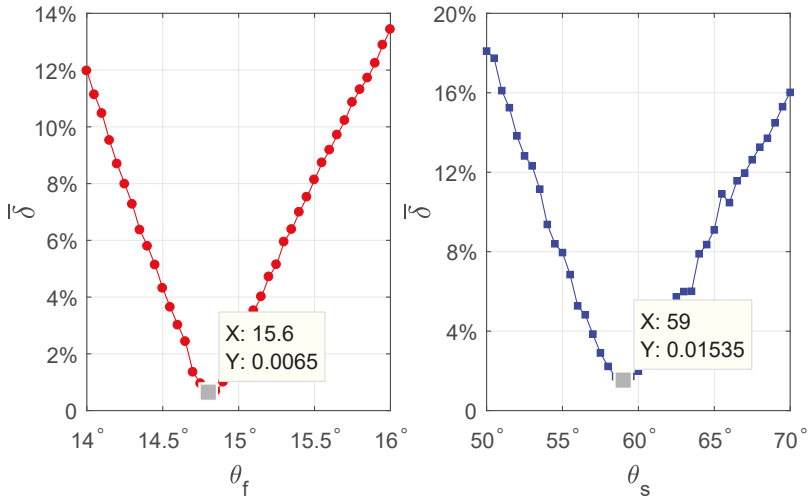

Figure 5.6 : MNAE between ULA and its Gaussian approximation for FR (left subfigure) and SR (right subfigure), with various beamwidth values.

a radar by a Gaussian function, we consider a uniform linear antenna array (ULA) here. Fig. 5.7 presents the radiation pattern for the ULAs and their Gaussian approximations for FR and SR. The beamwidth of the ULA is determined by the number of antennas in the array, where antennas are spaced at half wavelength. We introduce a metric, *mean normalized approximation error (MNAE)* $\overline{\delta}$, to evaluate the approximation accuracy for the interference. The MNAE is defined as

$$\overline{\delta} = \frac{1}{K}\left[\sum_{i=1}^{K} \frac{|\overline{I_i^{Gau}} - \overline{I_i^{ULA}}|}{\overline{I_i^{Gau}}}\right] \times 100\%, \tag{5.43}$$

where $\overline{I_i^{Gau}}$ and $\overline{I_i^{ULA}}$ denote the mean interference obtained in the i-th test for the Gaussian approximation and the actual ULA, respectively, K is the number of tests. Fig. 5.6 plots the MNAE for FR and SR with different parameters of the Gaussian approximation to the two ULA beams shown in Fig. 5.7. We obtain the minimum MNAE 0.65% when $\theta_f = 15.6°$ for FR, and 1.54% when $\theta_s = 59°$ for SR. The waveforms for the specific Gaussian approximations with these parameters are plotted in Fig. 5.7. The MNAE is very small, which means that the Gaussian

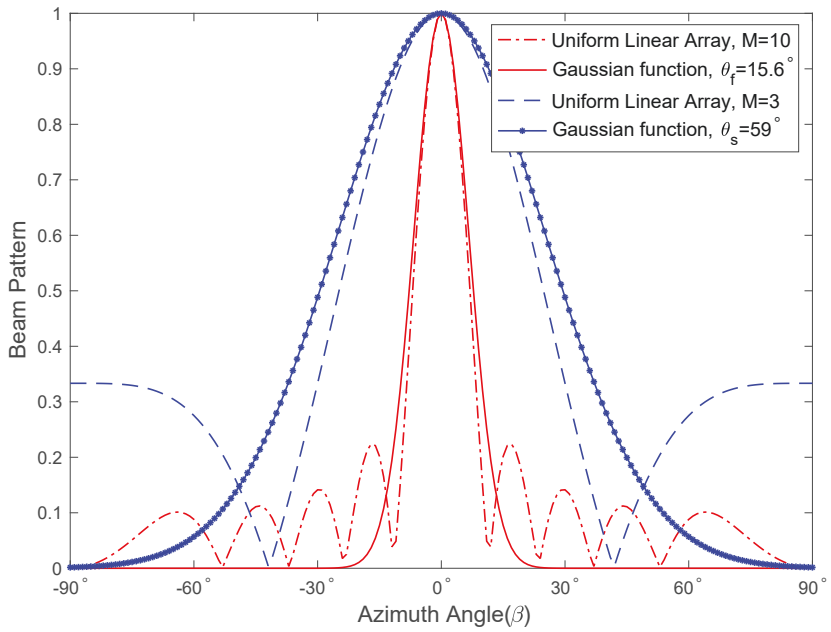

Figure 5.7 : Radiation pattern of a ULA and its Gaussian approximation for FR, where $\sigma_f = 0.1156, \theta_f = 15.6°$ and SR, where $\sigma_s = 0.4373, \theta_s = 59°$. In this specific example, the ULA has 10 and 3 antennas for the FR and SR, respectively.

function is an accurate approximation to the radiation pattern of real antenna arrays.

In Fig. 5.8, we show more details of the composition of interference. It is interesting to see that *most of the interference to one radar is from the same type of other radars*. As can be seen from Fig. 5.8 (a), more than 75% of the interference to FR is from other FRs, and the narrower the beamwidth is, the higher the proportion is. Similarly, from Fig. 5.8 (b), we can see that more than 74% of the interference is from SR-to-SR for the simulated beamwidth ranging from 40 to 80 degrees. This suggests that the cross-impact between FR and SR shall be considered differently to their respective self-impact when using resource allocation such as frequency allocation for interference mitigation.

We further study the impact of beamwidth on interference and present the results in Fig. 5.9. We can see that the mean interference power $\overline{I^f}$ decreases rapidly with θ_f increasing but increases slightly with θ_s increasing from 30° to 120°. This is

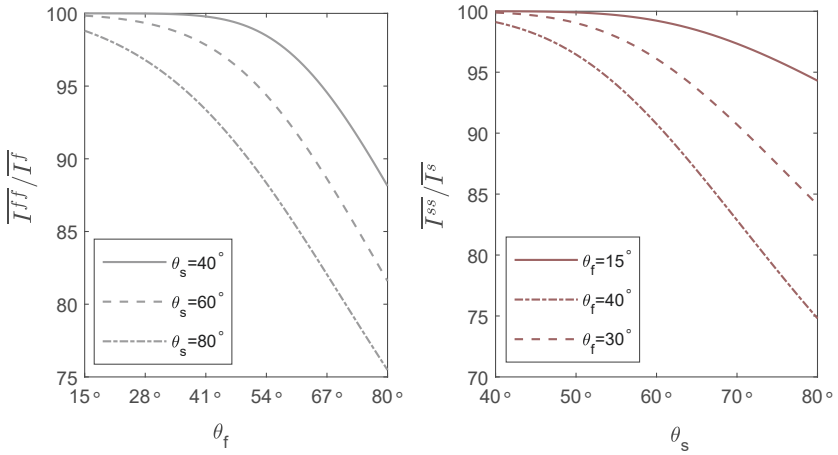

Figure 5.8 : Ratio $\overline{I^{ff}}/\overline{I^f}$ of FR (left sub-figure) and $\overline{I^{ss}}/\overline{I^s}$ of SR (right sub-figure), $\rho = 1/50$.

consistent with the results in Fig. 5.8 (a). In Fig. 5.10, we demonstrate how the mean SIR for FR is affected by beamwidth. As shown in Fig. 5.10, SIR($\overline{I^f}$) decreases with either the beamwidth θ_f or θ_s increasing. The change of SIR($\overline{I^f}$) is very small with varying θ_s, as $\overline{I^f}$ varies slowly with θ_s. Combined with the results in Fig. 5.9, we see that although the mean interference power at FR decreases, the mean SIR is reduced with θ_f increasing. This indicates that the signal power decreases faster than the interference. Therefore, *FR with a narrower beamwidth θ_f can achieve better overall sensing performance.*

We also present similar results for SR in Fig. 5.11. We can obtain similar observations to those for FR, and can conclude that using a SR with narrower beamwidth can generate overall better performance for side sensing. We can also see that *the mean interference power at SR is comparable to that at FR, even though it has a much wider beamwidth.*

Note that the above observations for FR and SR are based on the assumption that the received effective echo signal is mainly from the main beam direction. When the sensing direction deviates significantly from the centre, the conclusions may need

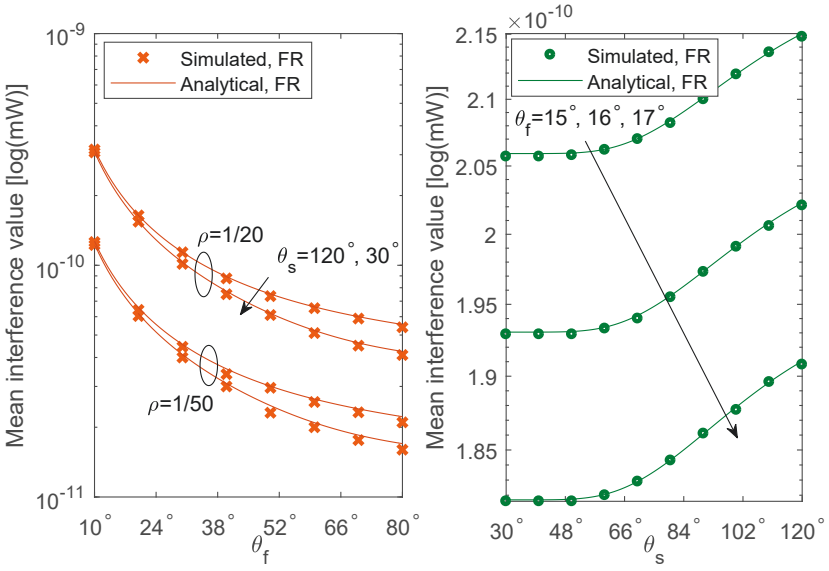

Figure 5.9 : Analytical and simulated results for the mean interference power at FR with varying beamwidth. In the right sub-figure, $\rho = 1/20$; $\xi = 4\%$.

to be further revisited.

5.4.3 Power Minimization Results

For power minimization, we need to set the noise power in the radar receiver. Since our antenna gain is relative, we cannot directly set up the receiver noise floor according to, for example, the thermal noise and device bandwidth. Instead, we determine a noise floor relative to the antenna gain, to make the simulation results close to practical realizations. This is achieved by setting a desired received SNR for targeted sensing distances. As an example, we consider the sensing distances $R_f = 25$m and $R_s = 15$m, the transmission power 10 mW, and the desired received SNR 15 dB. For radar beamwidth $\theta_f = 15°$ and $\theta_s = 60°$, without considering interference, we can work out the equivalent variance of AWGN for FR and SR as $\sigma^2_{\eta_f} = 4.0392 \times 10^{-11}$mW and $\sigma^2_{\eta_s} = 1.5076 \times 10^{-11}$mW, respectively.

We first present results for two-lanes (from Figs. 5.12 to 5.14) and then for multi-lanes. For multi-lanes, we set the numbers of lanes m and n as $m = n = 3$

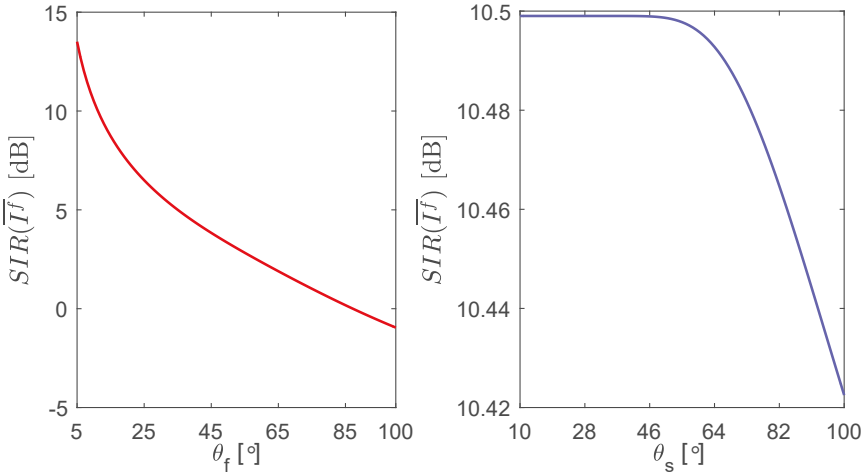

Figure 5.10 : Variation of the SIR for FR with beamwidth, where $R_f = 30$m, $\theta_s = 60°$ (left) and $\theta_f = 10°$ (right), $\rho = 1/50$; $\xi = 4\%$.

and assume that the typical vehicle located in the middle lane. Similar parameters are used in two-lane and multi-lane scenarios.

In Fig. 5.12, we demonstrate how the minimized transmission power is affected by the vehicle density ρ. The figure shows that the minimum power $P_f^* + P_s^*$ increases almost linearly with ρ increasing, particularly when ξ, the resource reusing probability, is small. As expected, it also increases with ξ increasing, as interference also grows. For comparison, the results for [77] are also presented. Its optimized transmission power is shown to be significantly larger than ours. The comparison shows clearly the great impact of using a directional antenna in reducing the required transmission power. In Fig. 5.13, we show the zone of different combinations of the transmission power from FR and SR that can meet the required minimum SINR. We can see that the optimized analytical solution indeed achieves the minimum transmission power.

In Fig. 5.14, we illustrate the relationship between the minimized transmission power and beamwidth θ_f and θ_s. In the left sub-figure, when θ_s is fixed to 60°, both $P_f^* + P_s^*$ and P_f^* increase with θ_f increasing, and P_s^* almost remains unchanged.

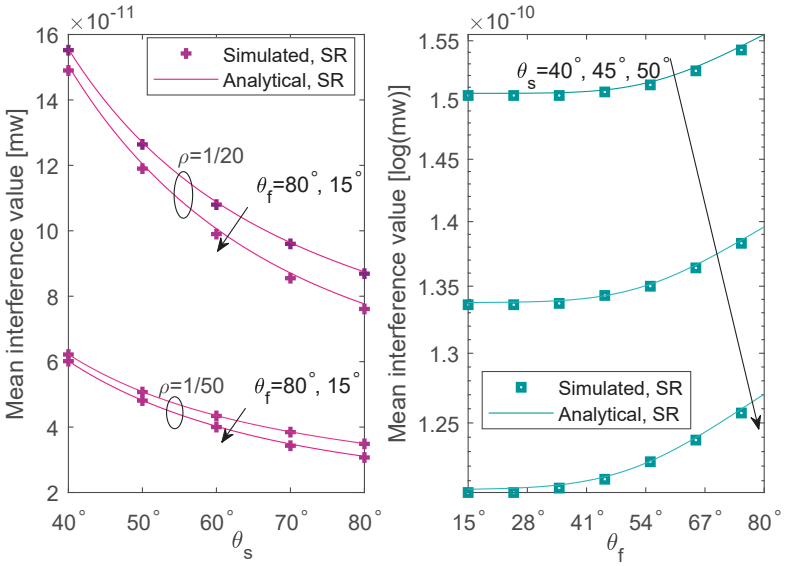

Figure 5.11 : Analytical and simulated results for the mean interference power of SR with varying beamwidth. In the right sub-figure, $\rho = 1/20$; $\xi = 4\%$.

This is because the mean interference power of SR only varies insignificantly with θ_f. In the right sub-figure, when θ_f is fixed to 15°, both $P_f^* + P_s^*$ and P_s^* increase with θ_s increasing, and P_f^* almost remains unchanged.

In Fig. 5.15, we show that similar to the two-lane case, the minimum transmission power in a multi-lane scenario increases almost linearly with the vehicle density ρ increasing. Comparing Fig. 5.15 with 5.12, we can see the averaged power per radar increases in the multi-lane case.

In Fig. 5.16, we demonstrate how the minimized transmission power changes with varying beamwidth in the three-lane case. In the left sub-figure, we note that the optimized transmission power $(P_{s_1})_{min}$ and $(P_{s_2})_{min}$ remain nearly constant with θ_f increasing, while $(P_f)_{min}$ increases rapidly with θ_f increasing. This is because the mean interference power of SR1 and SR2 only changes slightly with the beamwidth θ_f of FR, as can be seen from Fig.5.11. We also note that compared to the two-lane case, $(P_{s_2})_{min}$ remains almost unchanged and $(P_f)_{min}$ only slightly increases, benefiting from the narrow beamwidth; however, $(P_{s_1})_{min}$ is much larger than $(P_{s_2})_{min}$

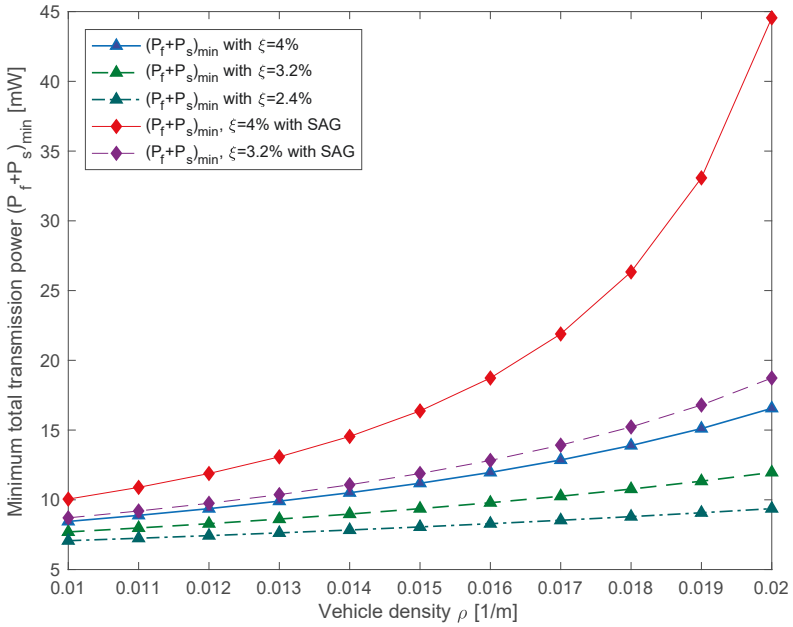

Figure 5.12 : Total minimized transmission power with a Gaussian beam for varying vehicle densities in a two-lane scenario.

because the SR on the right side of the typical vehicle sees more interference. We can have similar observations for SR from the right subfigure of Fig. 5.16.

5.5 Summary

In this chapter, we introduced a stochastic geometry method to model the location and density of vehicles and hence automotive radars. We considered both front- and side-mounted radars with directional antennas, and developed a framework for analytically calculating the mean interference power seen by each radar. Approximating the antenna radiation pattern with a Gaussian function, we derived closed-form expressions for the mean interference power. Based on the interference analysis, we then formulated the cost function for minimizing the total transmission power of radars on each vehicle. With the SINR constraints for each radar, we derived optimal solutions that minimize the total transmission power. Linking the antenna gain to the main parameter in the Gaussian function, we demonstrated how

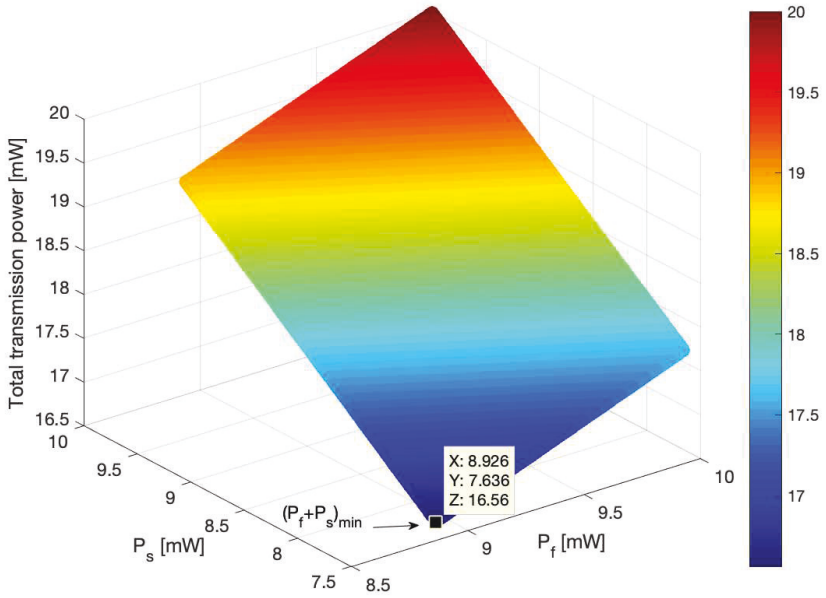

Figure 5.13 : Optimal total transmission power based on simulated results in two-lane case, where $\theta_f = 15°$, $\theta_s = 60°$, $\xi = 4\%$ and $\rho = 0.02$.

the interference and the SIR vary with the beamwidth of both radars.

Some of the important insights obtained from this study are summarized below:

- The side-mounted radar sees interference comparable to the front-mounted radar, although it has a much larger beamwidth;
- In general, narrower beamwidth leads to larger interference but higher SIR for both radars, and overall, both FR and SR with a narrower beamwidth can achieve better overall sensing performance;
- Interference power is shown to be linearly proportional to vehicle density;
- Most of the interference to one radar is from the same type of other radars, which should be an important factor to be considered by resource allocation;
- The optimized transmission power for different radars changes differently from the two-lane to three-lane cases: the power for SRs facing more lanes is much

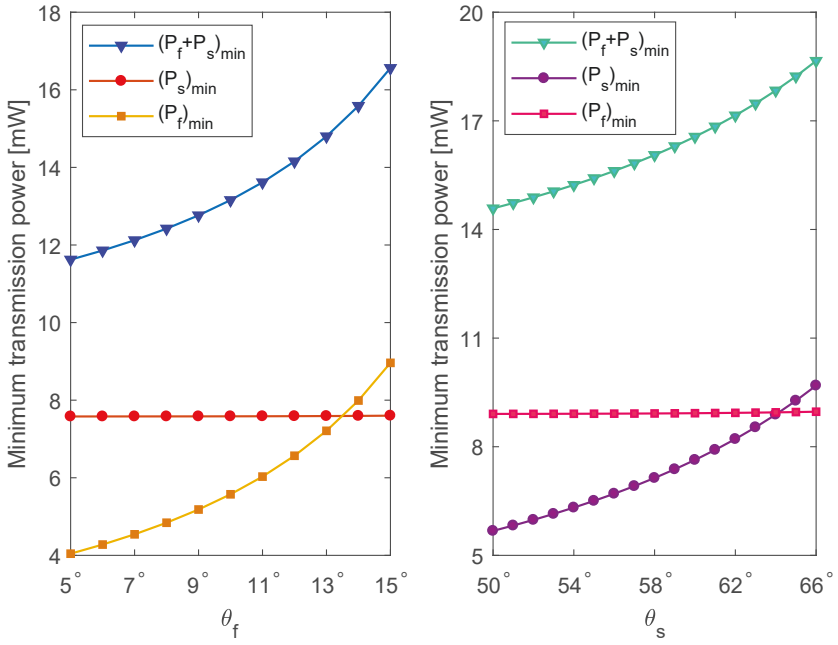

Figure 5.14 : Minimum transmission power with varying θ_f and θ_s in a two-lane scenario, where $\rho = 1/50$ and $\xi = 4\%$, $\theta_s = 60°$ (left), and $\theta_f = 15°$ (right).

larger than those facing less lanes, while the power of FR is only slightly increased due to the narrow beamwidth.

Our results provide important guidance for developing ad-hoc automotive radar networks and optimizing their frequency resource access and allocation. Our work in this study can be extended to provide more accurate characterization for radar interference, by considering actual radar operations, such as partially-overlapped frequency band of chirp waveforms due to asynchronous operation of FMCW radars, and the repetition length and period of chirp waveforms.

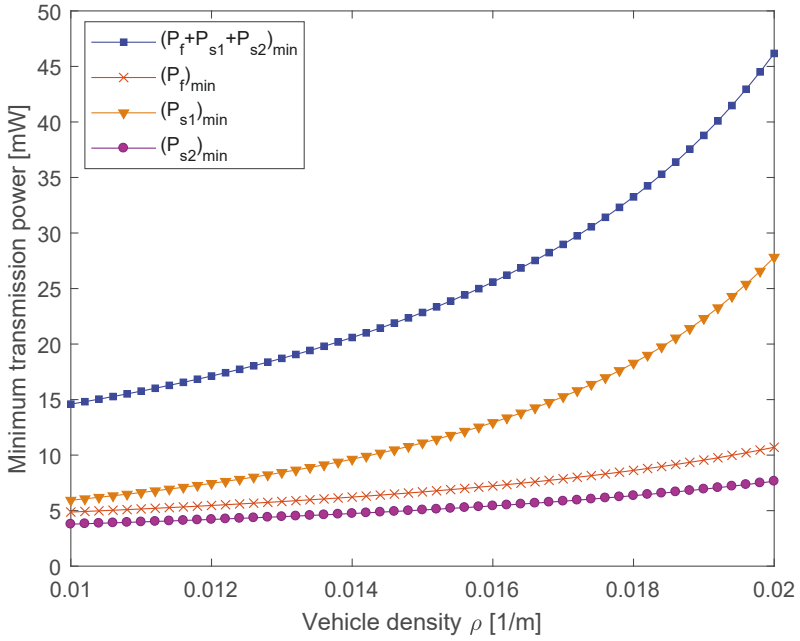

Figure 5.15 : Variation of minimum transmission power with vehicle density in a multi-lane scenario, where $\xi = 4\%$.

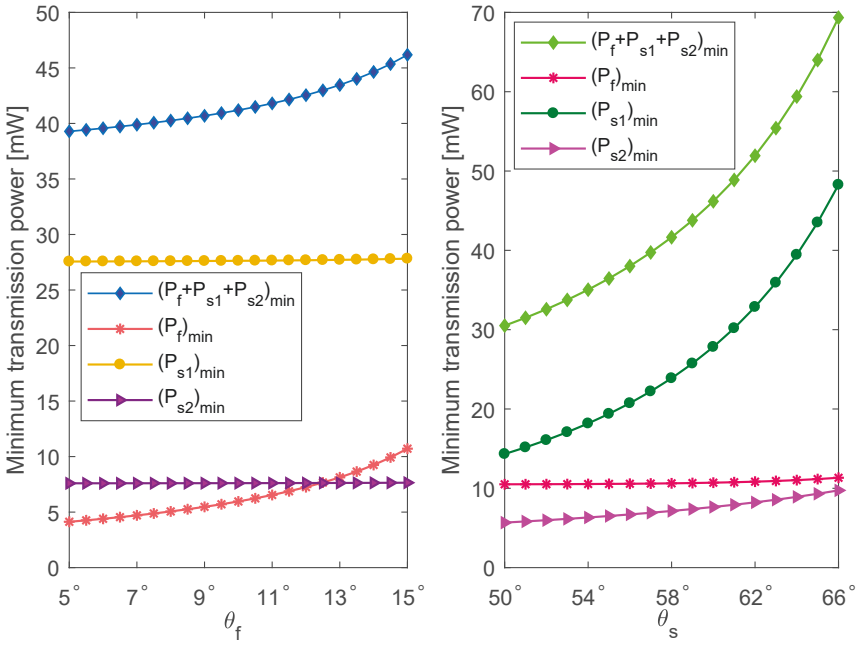

Figure 5.16 : Minimum transmission power with varying θ_f and θ_s, where $\theta_s = \theta_{s_1} = \theta_{s_2}$, $\rho = 1/50$ and $\xi = 4\%$. In the left subfigure, $\theta_{s_1} = \theta_{s_2} = 60°$, and in the right sub-figure, $\theta_f = 15°$.

Chapter 6

Conclusions

6.1 Summary

This thesis studied resource optimization for both communication and automotive radar sensing in vehicular networks, including investigating a novel semi-persistent resource allocation scheme for cellular V2X communications to minimize the latency requirement, a mode selection scheme for cellular V-D2D communications to minimize energy cost of vehicles or networks and a power optimization scheme based on a developed interference analysis framework for automotive radars. The relevant literature review can be found in Chapter 2 and the innovative research results achieved in this thesis are summarised below:

In Chapters 3 and 4, we mainly investigated two classes of optimization problems for cellular V2X in two-tier heterogeneous networks: 1) optimizing the relative latency and bandwidth efficiency for cellular V2X based on traffic prediction; 2) optimizing the energy consumption based on V2X mode selection.

In Chapter 3, considering the strict requirements and limited frequency resources of vehicular communications, we proposed a semi-persistent resource allocation scheme which is based on traffic prediction in two-tier heterogeneous cellular networks. Based on the proposed framework, we studied two optimization cases which are 1) minimizing relative latency under the constraint of total bandwidth or 2) minimizing total bandwidth resources with the constraints of latency, and we provided different solutions and algorithms in each case.

Next, in Chapter 4, considering different communication modes for cellular V2X

(e.g., V2I or V2V), we investigated a two-tier heterogeneous cellular network where the macro tier and small cell tier operate according to a dynamic TDD. Based on dynamic TDD which can adjust UL and DL time configurations to accommodate to the traffic asymmetry, we proposed a mode selection scheme jointing time allocation, power control to minimize the energy consumption of the vehicles and the whole network. Finally, we gave a geometrical interpretation of an energy-optimal mode selection scheme. Results show that V-D2D communication plays an important role both in the macro cell and small cell for energy consumption minimization. There is a large portion for V-D2D communication mode in the cell. Moreover, cell-edge users also benefit from V-D2D communication.

In Chapters 5, we studied the mean power of effective echo signals and interference, by considering both front- and side- mounted radars equipped with directional antennas. We employed the stochastic geometry method to characterize the randomness of vehicles and hence radars in both two-lane and multi-lane scenarios, and derived closed-form expressions for the mean interference by approximating the radiation pattern by Gaussian waveforms. Simulation results are shown to match the analytical results very well, and insights are obtained for the impact of radar parameters on interference. Based on the interference analysis, we aim to minimize the total transmission power of each vehicle with constraints on the required signal to interference and noise ratio. An optimal solution is obtained based on linear programming techniques and corroborated by simulation results.

6.2 Future Work

The work in this thesis can be potentially enriched in, but not limited to, the following various aspects.

Firstly, our semi-persistent resource allocation scheme can potentially be extended to a more complex environment such as a dense urban area where both traditional

cellular UEs and vehicular UEs exist and share the same resources, which will generate interference between them. A challenging problem is that multiple factors should be taken into consideration (e.g., different requirements of both C-UEs and V-UEs, interference management). In addition, with rigorous network traffic models, it is also possible to derive an optimal coefficient analytically to replace the current rule-of-thumb in Chapter 3. Therefore, this is an on-going and worthwhile topic which deserves further study.

Secondly, next-generation wireless networks (i.e., 5G and beyond) will be extremely dynamic and complex due to the ultra-dense deployment of heterogeneous networks (e.g., cellular networks, WiFi, ad-hoc). In this heterogeneous situation, vehicular communication will enjoy the benefit of cooperative multi-network. Regarding the mode selection of V2X communications, another important problem is the selection of networks. Therefore, communication mode selection combined with network mode selection is also expected in future work.

Thirdly, current automotive radar systems still lack a centralized control and resource allocation mechanism which will generate serious interference between radars caused by the use of shared spectrum and the inherent lack of coordination. Therefore, a reasonable resource allocation scheme aiming to improve accurate radar detection is expected in future work. For automotive radar, the most important thing is how to improve its localization accuracy. Generally, range and velocity estimation are indicators to measure the ability of radar. In addition, the Cramér-Rao lower bound (CRLB) is a good way to point out the best range and velocity estimation performance the FMCW radar can achieve. Based on radar's requirements for these performance indicators, we can formulate the optimization problem to allocate the resources. In addition, JCRS technology is promising in autonomous vehicular networks for its appealing capability of operating both communication and radar sensing functions. How to allocate and share the resources between communication

and radar sensing is a challenging problem when radar-communication coexists. Therefore, resource allocation for JCRS deserves further study in future work.

Bibliography

[1] G. Karagiannis, O. Altintas, E. Ekici, G. Heijenk, B. Jarupan, K. Lin, and T. Weil, "Vehicular networking: A survey and tutorial on requirements, architectures, challenges, standards and solutions," *IEEE communications surveys & tutorials*, vol. 13, no. 4, pp. 584–616, 2011.

[2] H. Vahdat-Nejad, A. Ramazani, T. Mohammadi, and W. Mansoor, "A survey on context-aware vehicular network applications," *Vehicular Communications*, vol. 3, pp. 43–57, 2016.

[3] 3rd Generation Partnership Project, "Service requirements for v2x," Valbonne, France, Tech. Rep. 3GPP TS 22.185 v14.3.0, LTE, 2017.

[4] J. Qiao, X. S. Shen, J. W. Mark, Q. Shen, Y. He, and L. Lei, "Enabling device-to-device communications in millimeter-wave 5g cellular networks," *IEEE Communications Magazine*, vol. 53, no. 1, pp. 209–215, 2015.

[5] R. Tang, J. Zhao, H. Qu, and Z. Zhang, "Energy-efficient resource allocation for 5g full-duplex enabled device-to-device communication," in *2016 IEEE Globecom Workshops (GC Wkshps)*, 2016, pp. 1–7.

[6] X. Cheng, L. Yang, and X. Shen, "D2d for intelligent transportation systems: A feasibility study," *IEEE Transactions on Intelligent Transportation Systems*, vol. 16, no. 4, pp. 1784–1793, 2015.

[7] A. Khelil and D. Soldani, "On the suitability of device-to-device communications for road traffic safety," in *2014 IEEE World Forum on Internet of Things*

(WF-IoT), 2014, pp. 224–229.

[8] M. Goppelt, H.-L. Blöcher, and W. Menzel, "Automotive radar-investigation of mutual interference mechanisms." *Advances in Radio Science*, vol. 8, 2010.

[9] X. Cheng, C. Chen, W. Zhang, and Y. Yang, "5g-enabled cooperative intelligent vehicular (5genciv) framework: When benz meets marconi," *IEEE Intelligent Systems*, vol. 32, no. 3, pp. 53–59, 2017.

[10] S. Mumtaz, K. M. S. Huq, M. I. Ashraf, J. Rodriguez, V. Monteiro, and C. Politis, "Cognitive vehicular communication for 5g," *IEEE Communications Magazine*, vol. 53, no. 7, pp. 109–117, 2015.

[11] G. Araniti, C. Campolo, M. Condoluci, A. Iera, and A. Molinaro, "Lte for vehicular networking: a survey," *IEEE communications magazine*, vol. 51, no. 5, pp. 148–157, 2013.

[12] M. Hadded, P. Muhlethaler, A. Laouiti, R. Zagrouba, and L. A. Saidane, "Tdma-based mac protocols for vehicular ad hoc networks: a survey, qualitative analysis, and open research issues," *IEEE Communications Surveys & Tutorials*, vol. 17, no. 4, pp. 2461–2492, 2015.

[13] C. Chen, T. H. Luan, X. Guan, N. Lu, and Y. Liu, "Connected vehicular transportation: Data analytics and traffic-dependent networking," *IEEE Vehicular Technology Magazine*, vol. 12, no. 3, pp. 42–54, 2017.

[14] 3rd Generation Partnership Project, "Study on LTE-based V2X services," Technical Specification Group Radio Access Network, Tech. Rep. 3GPP TR 36.885 V2.0.0, 2016.

[15] H. T. Cheng, H. Shan, and W. Zhuang, "Infotainment and road safety service support in vehicular networking: From a communication perspective," *Mechanical systems and signal processing*, vol. 25, no. 6, pp. 2020–2038, 2011.

[16] P. Lytrivis, G. Thomaidis, M. Tsogas, and A. Amditis, "An advanced cooperative path prediction algorithm for safety applications in vehicular networks," *IEEE Transactions on Intelligent Transportation Systems*, vol. 12, no. 3, pp. 669–679, 2011.

[17] S. M. Bilal, C. J. Bernardos, and C. Guerrero, "Position-based routing in vehicular networks: A survey," *Journal of Network and Computer Applications*, vol. 36, no. 2, pp. 685–697, 2013.

[18] O. K. Tonguz, N. Wisitpongphan, and F. Bai, "Dv-cast: A distributed vehicular broadcast protocol for vehicular ad hoc networks," *IEEE Wireless Communications*, vol. 17, no. 2, pp. 47–57, 2010.

[19] K. Rabieh, M. M. Mahmoud, and M. Younis, "Privacy-preserving route reporting schemes for traffic management systems," *IEEE Transactions on Vehicular Technology*, vol. 66, no. 3, pp. 2703–2713, 2016.

[20] W. Sun, E. G. Ström, F. Brännström, K. C. Sou, and Y. Sui, "Radio resource management for d2d-based v2v communication," *IEEE Transactions on Vehicular Technology*, vol. 65, no. 8, pp. 6636–6650, 2015.

[21] S. A. Bitaghsir and A. Khonsari, "Coded multicasting for content dissemination in a cellular vehicular network," *IEEE Communications Letters*, vol. 21, no. 12, pp. 2694–2697, 2017.

[22] S. H. Dokhanchi, B. S. Mysore, K. V. Mishra, and B. Ottersten, "A mmwave automotive joint radar-communications system," *IEEE Transactions on Aerospace and Electronic Systems*, vol. 55, no. 3, pp. 1241–1260, 2019.

[23] I. Mavromatis, A. Tassi, R. J. Piechocki, and A. Nix, "Beam alignment for millimetre wave links with motion prediction of autonomous vehicles," 2017.

[24] R. Molina-Masegosa and J. Gozalvez, "Lte-v for sidelink 5g v2x vehicular communications: A new 5g technology for short-range vehicle-to-everything communications," *IEEE Vehicular Technology Magazine*, vol. 12, no. 4, pp. 30–39, 2017.

[25] L. Li, Y. Li, and R. Hou, "A novel mobile edge computing-based architecture for future cellular vehicular networks," in *2017 IEEE Wireless Communications and Networking Conference (WCNC)*, 2017, pp. 1–6.

[26] S. Sun, J. Hu, Y. Peng, X. Pan, L. Zhao, and J. Fang, "Support for vehicle-to-everything services based on lte," *IEEE Wireless Communications*, vol. 23, no. 3, pp. 4–8, 2016.

[27] B. Di, L. Song, Y. Li, and Z. Han, "V2x meets noma: Non-orthogonal multiple access for 5g-enabled vehicular networks," *IEEE Wireless Communications*, vol. 24, no. 6, pp. 14–21, 2017.

[28] E. Hyun, Y. Jin, and J. Lee, "Moving and stationary target detection scheme using coherent integration and subtraction for automotive fmcw radar systems," in *2017 IEEE Radar Conference (RadarConf)*, 2017, pp. 0476–0481.

[29] M. Stolz, M. Li, Z. Feng, M. Kunert, and W. Menzel, "High resolution automotive radar data clustering with novel cluster method," in *2018 IEEE Radar Conference (RadarConf18)*, 2018, pp. 0164–0168.

[30] F. Uysal and S. Sanka, "Mitigation of automotive radar interference," in *2018 IEEE Radar Conference (RadarConf18)*, 2018, pp. 0405–0410.

[31] Z. Xu, Q. Shi, J. Shi, H. Wang, M. Wei, R. Gao, Y. Shao, and H. Tao, "A novel method of mitigating the mutual interference between multiple lfmcw radars for automotive applications," in *IGARSS 2019 - 2019 IEEE International Geoscience and Remote Sensing Symposium*, 2019, pp. 2178–2181.

[32] Z. Liu, H. Lee, G. Ali, D. Pesch, P. Xiao *et al.*, "A survey on resource allocation in vehicular networks," *arXiv preprint arXiv:1909.13587*, 2019.

[33] D. Das and S. Das, "Adaptive resource allocation scheme for cognitive radio vehicular ad-hoc network in the presence of primary user emulation attack," *IET Networks*, vol. 6, no. 1, pp. 5–13, 2016.

[34] M. Ng and S. T. Waller, "A static network level model for the information propagation in vehicular ad hoc networks," *Transportation Research Part C: Emerging Technologies*, vol. 18, no. 3, pp. 393–407, 2010.

[35] M. Li, L. Zhao, and H. Liang, "An smdp-based prioritized channel allocation scheme in cognitive enabled vehicular ad hoc networks," *IEEE Transactions on Vehicular Technology*, vol. 66, no. 9, pp. 7925–7933, 2017.

[36] G. M. N. Ali, M. Noor-A-Rahim, M. A. Rahman, S. K. Samantha, P. H. J. Chong, and Y. L. Guan, "Efficient real-time coding-assisted heterogeneous data access in vehicular networks," *IEEE Internet of Things Journal*, vol. 5, no. 5, pp. 3499–3512, 2018.

[37] Z. Liu, T. Peng, S. Xiang, and W. Wang, "Mode selection for device-to-device (d2d) communication under lte-advanced networks," in *2012 IEEE International Conference on Communications (ICC)*, 2012, pp. 5563–5567.

[38] X. Lin, J. G. Andrews, and A. Ghosh, "Spectrum sharing for device-to-device communication in cellular networks," *IEEE Transactions on Wireless Communications*, vol. 13, no. 12, pp. 6727–6740, 2014.

[39] W. Sun, E. G. Ström, F. Brännström, Y. Sui, and K. C. Sou, "D2d-based v2v communications with latency and reliability constraints," in *2014 IEEE Globecom Workshops (GC Wkshps)*, 2014, pp. 1414–1419.

[40] W. Sun, D. Yuan, E. G. Ström, and F. Brännström, "Cluster-based radio resource management for d2d-supported safety-critical v2x communications," *IEEE Transactions on Wireless Communications*, vol. 15, no. 4, pp. 2756–2769, 2015.

[41] J. Mei, K. Zheng, L. Zhao, Y. Teng, and X. Wang, "A latency and reliability guaranteed resource allocation scheme for lte v2v communication systems," *IEEE Transactions on Wireless Communications*, vol. 17, no. 6, pp. 3850–3860, 2018.

[42] Q. Wei, L. Wang, Z. Feng, and Z. Ding, "Wireless resource management in lte-u driven heterogeneous v2x communication networks," *IEEE Transactions on Vehicular Technology*, vol. 67, no. 8, pp. 7508–7522, 2018.

[43] C.-Y. Wei, A. C.-S. Huang, C.-Y. Chen, and J.-Y. Chen, "Qos-aware hybrid scheduling for geographical zone-based resource allocation in cellular vehicle-to-vehicle communications," *IEEE Communications Letters*, vol. 22, no. 3, pp. 610–613, 2017.

[44] L. Liang, S. Xie, G. Y. Li, Z. Ding, and X. Yu, "Graph-based radio resource management for vehicular networks," in *2018 IEEE International Conference on Communications (ICC)*, 2018, pp. 1–6.

[45] H. Yang, L. Zhao, L. Lei, and K. Zheng, "A two-stage allocation scheme for delay-sensitive services in dense vehicular networks," in *2017 IEEE International Conference on Communications Workshops (ICC Workshops)*, 2017, pp. 1358–1363.

[46] M. I. Ashraf, M. Bennis, C. Perfecto, and W. Saad, "Dynamic proximity-aware resource allocation in vehicle-to-vehicle (v2v) communications," in *2016 IEEE Globecom Workshops (GC Wkshps)*, 2016, pp. 1–6.

[47] F. Abbas, P. Fan, and Z. Khan, "A novel low-latency v2v resource allocation scheme based on cellular v2x communications," *IEEE Transactions on Intelligent Transportation Systems*, vol. 20, no. 6, pp. 2185–2197, 2018.

[48] F. Abbas and P. Fan, "A hybrid low-latency d2d resource allocation scheme based on cellular v2x networks," in *2018 IEEE International Conference on Communications Workshops (ICC Workshops)*, 2018, pp. 1–6.

[49] X. Zhang, Y. Shang, X. Li, and J. Fang, "Research on overlay d2d resource scheduling algorithms for v2v broadcast service," in *2016 IEEE 84th Vehicular Technology Conference (VTC-Fall)*, 2016, pp. 1–5.

[50] X. Ge, H. Cheng, G. Mao, Y. Yang, and S. Tu, "Vehicular communications for 5g cooperative small-cell networks," *IEEE Transactions on Vehicular Technology*, vol. 65, no. 10, pp. 7882–7894, 2016.

[51] E. Bernal-Mor, V. Pla, J. Martinez-Bauset, and L. Guijarro, "Performance analysis of two-tier wireless networks with dynamic traffic, backhaul constraints, and terminal mobility," *IEEE Transactions on Vehicular Technology*, vol. 65, no. 1, pp. 241–250, 2015.

[52] Q. Zheng, K. Zheng, L. Sun, and V. C. Leung, "Dynamic performance analysis of uplink transmission in cluster-based heterogeneous vehicular networks," *IEEE Transactions on Vehicular Technology*, vol. 64, no. 12, pp. 5584–5595, 2015.

[53] H. He, H. Shan, A. Huang, and L. Sun, "Resource allocation for video streaming in heterogeneous cognitive vehicular networks," *IEEE Transactions on Vehicular Technology*, vol. 65, no. 10, pp. 7917–7930, 2016.

[54] Z. Xiao, X. Shen, F. Zeng, V. Havyarimana, D. Wang, W. Chen, and K. Li, "Spectrum resource sharing in heterogeneous vehicular networks: A noncoop-

erative game-theoretic approach with correlated equilibrium," *IEEE Transactions on Vehicular Technology*, vol. 67, no. 10, pp. 9449–9458, 2018.

[55] H. ElSawy, E. Hossain, and M.-S. Alouini, "Analytical modeling of mode selection and power control for underlay d2d communication in cellular networks," *IEEE Transactions on Communications*, vol. 62, no. 11, pp. 4147–4161, 2014.

[56] H. Min, W. Seo, J. Lee, S. Park, and D. Hong, "Reliability improvement using receive mode selection in the device-to-device uplink period underlaying cellular networks," *IEEE Transactions on Wireless Communications*, vol. 10, no. 2, pp. 413–418, 2010.

[57] Y. Huang, A. A. Nasir, S. Durrani, and X. Zhou, "Mode selection, resource allocation, and power control for d2d-enabled two-tier cellular network," *IEEE Transactions on communications*, vol. 64, no. 8, pp. 3534–3547, 2016.

[58] X. Zhang, M. Peng, S. Yan, and Y. Sun, "Deep reinforcement learning based mode selection and resource allocation for cellular v2x communications," *IEEE Internet of Things Journal*, 2019.

[59] M. N. Sial, Y. Deng, J. Ahmed, A. Nallanathan, and M. Dohler, "Stochastic geometry modeling of cellular v2x communication over shared channels," *IEEE Transactions on Vehicular Technology*, vol. 68, no. 12, pp. 11 873–11 887, 2019.

[60] X. Li, L. Ma, R. Shankaran, Y. Xu, and M. A. Orgun, "Joint power control and resource allocation mode selection for safety-related v2x communication," *IEEE Transactions on Vehicular Technology*, vol. 68, no. 8, pp. 7970–7986, 2019.

[61] J. Du, C. Jiang, Y. Qian, Z. Han, and Y. Ren, "Resource allocation with video traffic prediction in cloud-based space systems," *IEEE Transactions on Multimedia*, vol. 18, no. 5, pp. 820–830, 2016.

[62] P. Koutsakis, "On providing dynamic resource allocation based on multimedia traffic prediction in satellite systems," *Computer Communications*, vol. 30, no. 2, pp. 404–415, 2007.

[63] S. Oh, Y.-J. Byon, K. Jang, and H. Yeo, "Short-term travel-time prediction on highway: a review of the data-driven approach," *Transport Reviews*, vol. 35, no. 1, pp. 4–32, 2015.

[64] Y.-j. Kim, J.-s. Hong *et al.*, "Urban traffic flow prediction system using a multifactor pattern recognition model," *IEEE Transactions on Intelligent Transportation Systems*, vol. 16, no. 5, pp. 2744–2755, 2015.

[65] D. Miao, X. Qin, and W. Wang, "The periodic data traffic modeling based on multiplicative seasonal arima model," in *2014 Sixth International Conference on Wireless Communications and Signal Processing (WCSP)*. IEEE, 2014, pp. 1–5.

[66] V. Alarcon-Aquino and J. A. Barria, "Multiresolution fir neural-network-based learning algorithm applied to network traffic prediction," *IEEE Transactions on Systems, Man, and Cybernetics, Part C (Applications and Reviews)*, vol. 36, no. 2, pp. 208–220, 2006.

[67] B. Sun, W. Cheng, P. Goswami, and G. Bai, "Short-term traffic forecasting using self-adjusting k-nearest neighbours," *IET Intelligent Transport Systems*, vol. 12, no. 1, pp. 41–48, 2017.

[68] G. A. Davis and N. L. Nihan, "Nonparametric regression and short-term freeway traffic forecasting," *Journal of Transportation Engineering*, vol. 117, no. 2, pp. 178–188, 1991.

[69] L. Zhang, Q. Liu, W. Yang, N. Wei, and D. Dong, "An improved k-nearest neighbor model for short-term traffic flow prediction," *Procedia-Social and*

Behavioral Sciences, vol. 96, pp. 653–662, 2013.

[70] A. Asheralieva, J. Y. Khan, K. Mahata, and E. H. Ong, "A predictive network resource allocation technique for cognitive wireless networks," in *2010 4th International Conference on Signal Processing and Communication Systems*. IEEE, 2010, pp. 1–9.

[71] M. Ismail, A. Abdrabou, and W. Zhuang, "Cooperative decentralized resource allocation in heterogeneous wireless access medium," *IEEE Transactions on wireless communications*, vol. 12, no. 2, pp. 714–724, 2012.

[72] V. Sciancalepore, K. Samdanis, X. Costa-Perez, D. Bega, M. Gramaglia, and A. Banchs, "Mobile traffic forecasting for maximizing 5g network slicing resource utilization," in *IEEE INFOCOM 2017-IEEE Conference on Computer Communications*, 2017, pp. 1–9.

[73] X. Du, H. Zhang, H. Van Nguyen, and Z. Han, "Stacked lstm deep learning model for traffic prediction in vehicle-to-vehicle communication," in *2017 IEEE 86th Vehicular Technology Conference (VTC-Fall)*, 2017, pp. 1–5.

[74] M. Goppelt, H.-L. Blöcher, and W. Menzel, "Analytical investigation of mutual interference between automotive fmcw radar sensors," in *2011 German Microwave Conference*. IEEE, 2011, pp. 1–4.

[75] G. M. Brooker, "Mutual interference of millimeter-wave radar systems," *IEEE Transactions on Electromagnetic Compatibility*, vol. 49, no. 1, pp. 170–181, 2007.

[76] T. Schipper, S. Prophet, M. Harter, L. Zwirello, and T. Zwick, "Simulative prediction of the interference potential between radars in common road scenarios," *IEEE Transactions on Electromagnetic Compatibility*, vol. 57, no. 3, pp. 322–328, 2015.

[77] A. Al-Hourani, R. J. Evans, S. Kandeepan, B. Moran, and H. Eltom, "Stochastic geometry methods for modeling automotive radar interference," *IEEE Transactions on Intelligent Transportation Systems*, vol. 19, no. 2, pp. 333–344, 2017.

[78] C. Shi, F. Wang, M. Sellathurai, and J. Zhou, "Non-cooperative game theoretic power allocation strategy for distributed multiple-radar architecture in a spectrum sharing environment," *IEEE Access*, vol. 6, pp. 17 787–17 800, 2018.

[79] A. Deligiannis, S. Lambotharan, and J. A. Chambers, "Game theoretic analysis for mimo radars with multiple targets," *IEEE transactions on aerospace and electronic systems*, vol. 52, no. 6, pp. 2760–2774, 2016.

[80] Z. Geng, H. Deng, and B. Himed, "Adaptive radar beamforming for interference mitigation in radar-wireless spectrum sharing," *IEEE Signal Processing Letters*, vol. 22, no. 4, pp. 484–488, 2014.

[81] T.-N. Luo, C.-H. E. Wu, and Y.-J. E. Chen, "A 77-ghz cmos automotive radar transceiver with anti-interference function," *IEEE Transactions on Circuits and Systems I: Regular Papers*, vol. 60, no. 12, pp. 3247–3255, 2013.

[82] H. Godrich, A. P. Petropulu, and H. V. Poor, "Power allocation strategies for target localization in distributed multiple-radar architectures," *IEEE Transactions on Signal Processing*, vol. 59, no. 7, pp. 3226–3240, 2011.

[83] C. Shi, F. Wang, M. Sellathurai, J. Zhou, and S. Salous, "Power minimization-based robust ofdm radar waveform design for radar and communication systems in coexistence," *IEEE Transactions on Signal Processing*, vol. 66, no. 5, pp. 1316–1330, 2017.

[84] C. Shi, F. Wang, S. Salous, and J. Zhou, "Joint subcarrier assignment and power allocation strategy for integrated radar and communications system

based on power minimization," *IEEE Sensors Journal*, vol. 19, no. 23, pp. 11 167–11 179, 2019.

[85] C. Shi, F. Wang, M. Sellathurai, J. Zhou, and S. Salous, "Low probability of intercept-based optimal power allocation scheme for an integrated multistatic radar and communication system," *IEEE Systems Journal*, vol. 14, no. 1, pp. 983–994, 2020.

[86] Y. Zhou, H. Zhou, F. Zhou, Y. Wu, and V. C. Leung, "Resource allocation for a wireless powered integrated radar and communication system," *IEEE Wireless Communications Letters*, vol. 8, no. 1, pp. 253–256, 2018.

[87] M. K. Saleem, H. Vettikaladi, M. A. Alkanhal, and M. Himdi, "Lens antenna for wide angle beam scanning at 79 ghz for automotive short range radar applications," *IEEE Transactions on Antennas and Propagation*, vol. 65, no. 4, pp. 2041–2046, 2017.

[88] M. J. Farooq, H. ElSawy, and M.-S. Alouini, "A stochastic geometry model for multi-hop highway vehicular communication," *IEEE Transactions on Wireless Communications*, vol. 15, no. 3, pp. 2276–2291, 2015.

[89] Z. Tong, H. Lu, M. Haenggi, and C. Poellabauer, "A stochastic geometry approach to the modeling of dsrc for vehicular safety communication," *IEEE Transactions on Intelligent Transportation Systems*, vol. 17, no. 5, pp. 1448–1458, 2016.

[90] H. ElSawy, A. Sultan-Salem, M.-S. Alouini, and M. Z. Win, "Modeling and analysis of cellular networks using stochastic geometry: A tutorial," *IEEE Communications Surveys & Tutorials*, vol. 19, no. 1, pp. 167–203, 2016.

[91] J. Zhang and J. G. Andrews, "Distributed antenna systems with randomness," *IEEE Transactions on Wireless Communications*, vol. 7, no. 9, pp. 3636–3646,

2008.

[92] S. P. Weber, X. Yang, J. G. Andrews, and G. De Veciana, "Transmission capacity of wireless ad hoc networks with outage constraints," *IEEE transactions on information theory*, vol. 51, no. 12, pp. 4091–4102, 2005.

[93] B. Blaszczyszyn, P. Mühlethaler, and Y. Toor, "Maximizing throughput of linear vehicular ad-hoc networks (vanets)-a stochastic approach," in *2009 European Wireless Conference*. IEEE, 2009, pp. 32–36.

[94] M. Haenggi, J. G. Andrews, F. Baccelli, O. Dousse, and M. Franceschetti, "Stochastic geometry and random graphs for the analysis and design of wireless networks," *IEEE journal on selected areas in communications*, vol. 27, no. 7, pp. 1029–1046, 2009.

[95] N. Bhatia and Vandana, "Survey of nearest neighbor techniques," *International Journal of Computer Science and Information Security*, vol. 8, no. 2, 2010.

[96] P. Duan, G. Mao, C. Zhang, and S. Wang, "Starima-based traffic prediction with time-varying lags," in *2016 IEEE 19th International Conference on Intelligent Transportation Systems (ITSC)*, 2016, pp. 1610–1615.

[97] L. Yang and R. Jin, "Distance metric learning: A comprehensive survey," *Michigan State University*, vol. 2, no. 2, p. 4, 2006.

[98] X. Wang, K. An, L. Tang, and X. Chen, "Short term prediction of freeway exiting volume based on svm and knn," *International Journal of Transportation Science and Technology*, vol. 4, no. 3, pp. 337–352, 2015.

[99] F. Guo, R. Krishnan, and J. Polak, "Short-term traffic prediction under normal and incident conditions using singular spectrum analysis and the k-nearest

neighbour method," *IET and ITS Conference on Road Transport Information and Control*, 2012.

[100] P. He, L. Zhao, S. Zhou, and Z. Niu, "Water-filling: A geometric approach and its application to solve generalized radio resource allocation problems," *IEEE transactions on Wireless Communications*, vol. 12, no. 7, pp. 3637–3647, 2013.

[101] NGSIM, "Next generation simulation," *http://ngsim-community.org/*, 2010.

[102] J. S. Armstrong and F. Collopy, "Error measures for generalizing about forecasting methods: Empirical comparisons," *International journal of forecasting*, vol. 8, no. 1, pp. 69–80, 1992.

[103] J. Zhang, D. Smith, and Z. Chen, "Linear finite state markov chain predictor for channel prediction," in *Personal Indoor and Mobile Radio Communications (PIMRC), 2012 IEEE 23rd International Symposium on*, 2012, pp. 2085–2089.

[104] Y. Gao, G. He, and J. C. Hou, "On exploiting traffic predictability in active queue management," in *INFOCOM 2002. Twenty-First Annual Joint Conference of the IEEE Computer and Communications Societies. Proceedings. IEEE*, vol. 3, 2002, pp. 1630–1639.

[105] E. Uysal-Biyikoglu, B. Prabhakar, and A. El Gamal, "Energy-efficient packet transmission over a wireless link," *IEEE/ACM Transactions on Networking*, vol. 10, no. 4, pp. 487–499, 2002.

[106] M. Haenggi, "Mean interference in hard-core wireless networks," *IEEE Communications Letters*, vol. 15, no. 8, pp. 792–794, 2011.

[107] M. I. Skolnik, *Radar Handbook,3rd ed.* New York, NY, USA: McGraw-Hill, 2008.

[108] Haenggi, *Stochastic geometry for wireless networks.* Cambridge University Press, 2012.

[109] J. Hasch, E. Topak, R. Schnabel, T. Zwick, R. Weigel, and C. Waldschmidt, "Millimeter-wave technology for automotive radar sensors in the 77 ghz frequency band," *IEEE Transactions on Microwave Theory and Techniques*, vol. 60, no. 3, pp. 845–860, 2012.

[110] International Telecommunications Union (ITU), document ITU-R M.2057-0., "Systems characteristics of automotive radars operating in the frequency band 76-81 GHz for intelligent transport systems applications," 2014. [Online]. Available: https://www.itu.int/rec/R-REC-M.2057-0-201402-S/en